AXISYMMETRIC BI-PROPELLANT AIR AUGMENTED ROCKET TESTING WITH ANNULAR CAVITY MIXING ENHANCEMENT

A Thesis

presented to

the Faculty of California Polytechnic State University,

San Luis Obispo

In Partial Fulfillment

of the Requirements for the Degree

Master of Science in Aerospace Engineering

by

Allen Andrei Cristian Capatina

October 2015

COMMITTEE MEMBERSHIP

TITLE:	Axisymmetric Bi-Propellant Air Augmented Rocket Testing with Annular Cavity Mixing Enhancement
AUTHOR:	Allen Andrei Cristian Capatina
DATE SUBMITTED:	October 2015

COMMITTEE CHAIR:	Dianne DeTurris, Ph.D. Professor of Aerospace Engineering
COMMITTEE MEMBER:	Faysal Kolkailah, Ph.D. Professor of Aerospace Engineering
COMMITTEE MEMBER:	Eltahry Elghandour, Ph.D. Lecturer of Aerospace Engineering
COMMITTEE MEMBER:	Trevor J. Foster, MS Industry Advisor from Empirical Systems Aerospace Pismo Beach, California

ABSTRACT

Axisymmetric Bi-Propellant Air Augmented Rocket Testing with

Annular Cavity Mixing Enhancement

Allen Andrei Cristian Capatina

Performance characterization was undertaken for an air augmented rocket mixing duct with annular cavity configurations intended to produce thrust augmentation. Three mixing duct geometries and a fully annular cavity at the exit of the nozzle were tested to enable thrust comparisons. The rocket engine used liquid ethanol and gaseous oxygen, and was instrumented with sensors to output total thrust, mixing duct thrust, combustion chamber pressure, and propellant differential pressures across a Venturi flow measurement tube.

The rocket engine was tested to $\sim 65\ lbf$ thrust maximum, with three different mixing ducts, three major combustion pressure sets, and a nozzle exit plane annular cavity (a grooved ring). The combustion pressures tested were $\sim 400\ psi$, $\sim 550\ psi$, and $\sim 680\ psi$ allowing for a nozzle pressure ratio range of $\sim 27 - 47$ relative to $14.7\ psi$ ambient pressure. The engine operated very consistently and its mixture ratio was fuel rich throughout all the tests performed; however, pressure losses in the feed system prevented higher combustion pressures from being tested.

Three mixing ducts of the same outer diameter were tested. The short and diverging ducts were the same length ($\sim 4\ in$) and the long duct was $\sim 10\ in$ long. The short and long ducts created positive mixing duct thrust and the diverging duct created negative mixing duct thrust. The long duct case showed better performance than the no duct case when the total thrust was divided by combustion pressure and nozzle throat area. The long duct always created several times more mixing duct thrust than either the short or diverging ducts, but none of the mixing ducts created positive overall thrust augmentation in the over expanded cases tested. The mixing duct thrusts ranged between $-0.6\ lbf$ and $+3.3\ lbf$. As the combustion pressures were increased, getting closer the nozzle's optimal expansion, the mixing duct thrusts started converging, indicating a difference between nozzle operation at over expanded and under expanded.

The annular cavity had a noticeable effect on the thrust of the engine and the appearance of the plume. The total thrust of the system was decreased by a maximum of $\sim 1\ lbf$ and the plume was more sharply defined when the annular cavity was attached. Better mixing between the primary (engine exhaust) flow and the secondary (ambient air) flow was promoted by the annular cavity because it increased the shear layer's turbulence and increased the mixing duct thrust. The greater mixing also allowed for secondary combustion which made the plumes more sharply defined. The annular cavity was also seen to enhance the mixing duct thrusts for all three mixing ducts.

ACKNOWLEDGMENTS

Thank you everyone:

- Dr. Dianne DeTurris for your guidance and encouragement.
- Kyle Johnson for helping point me in the right direction.
- Joe Vanherweg for bouncing ideas back and forth.
- Damon Turner for helping placate the voices of naysayers.
- Tom Featherstone for helping look over my operating procedures.
- Aero Student Fee Committee of 2014-2015 for funding a bit of the project.
- CPConnect for funding the majority of the project costs.
- T-Slots for providing donated aluminum t-slot extrusion to make the test stand.
- Dr. Lily Laiho for providing advice for the CPConnect proposal.
- Tyler Beck for being roommates and giving me someone to talk to instead of just the walls.
- Ross Gregoriev for helping set up and reduce noise in the DAQ system.
- Steve Reiber for helping during test fires and providing chili.
- Chris Hunt for helping during test fires and providing helpful encouragement.
- George Bushnell for helping with testing and some electronics.
- Dr. Jin Tso for advice on the project, the Master's program, and life.
- Dana Capatina for being my awesome mother.
- Liviu Capatina for being my awesome father.
- Gabe Badea for chatting with me on engineering topics.
- Carmen Barsu for also chatting about engineering topics and making great food.
- Trevor Foster for giving me advice on the previous work done and being on my committee.
- Kyle Rosenow for being my Hangar buddy and helping with testing.
- Jason Daniel for helping me learn how to use ICEM and Fluent.
- Samantha Rawlins for being part of the CPConnect team.

- Sarah Horne for helping make the thesis and graduate office paperwork submission process understandable.
- Katie Gezi for helping with final formatting revisions.
- Adam Frye for being part of the CPConnect team.
- George Georgiou for being my Hangar buddy many times and supplying comic relief every so often.
- Daniel Johnson for being part of the CPConnect team.
- Cody Thompson for being a great and uber helpful member of the Aerospace staff.
- Roberto Rosila for being there to chat about rocket engines.
- Roland Morrison for providing the smallest spark plugs I have ever seen.
- Eric Pulse for being my boss and friend, giving me advice and assistance with getting materials for the test stand.
- George Leone for being my boss, friend, and support throughout the whole project.
- Dr. Eric Mehiel for helping make Dean Debra Larson's advice a possibility.
- Dean Debra Larson for providing the best safety advice ever, without her I would have finished on time and kept my respect for Cal Poly's administration.
- Adam Whitmarsh for being there for several tests and being on the CPConnect team.
- Luke Whitmarsh for being there for several tests and being on the CPConnect team.
- SLO Donut Co. for providing great donuts and a friendly place to sit/talk.
- Firestone Grill for providing tritip, French fries, BBQ sauce, and a friendly place to sit/talk.
- Dr. Eltahry Elghandour for giving me advice and being on my committee.
- Temo Cuna for being my friend and someone to talk to about the thesis.
- Sam Moss for helping with testing and being someone to bounce ideas off.

- Dr. Faysal Kolkailah for being there to talk with and give me advice.
- Steven MacLean for helping with testing and making the electrical diagram of the control box.
- Lowell Magleby for being a great co-worker and providing advice on machining everything.
- Lou Maack for giving me advice about Lockheed and putting me in contact with John Henderson.
- Richard DeLuna for helping with testing and being a friend to talk about the thesis process.
- Dave Esposto for helping with structural analysis of the engine.
- Jonathan Pickrel for showing interest in the AAR work here.
- Mark Aldecoa for helping pick out and buy Swagelok materials.
- John Newman for helping with making decisions on engine and fuel choices.
- John Henderson for helping with engine design and helping me decide to use ethanol instead of hydrogen as a fuel.
- Alex Athougies for helping with engine design and bouncing ideas off of.
- Jeff Muss for getting CEA for use in designing the engine.
- Jeff Massman for helping understand what CEA does.
- Jeff Freeman for helping with shear layer and thesis process understanding.

TABLE OF CONTENTS

Page

LIST OF TABLES xii

LIST OF FIGURES xiii

NOMENCLATURE xvii

CHAPTER

1. Introduction 1

1.1 Why Research Air Augmented Rockets 1

1.2 AAR Work and Research 3

1.3 Flow Over a Cavity 5

1.4 Objective and Intent 8

2. Engine, Mixing Ducts, and Cavity Design 11

2.1 Engine 11

2.1.1 Engine Performance Design 13

2.1.2 Nozzle Streamlining 14

2.2 Mixing Ducts 16

2.3 Cavity 19

3. Test Stand and Data Acquisition 21

3.1 Sensors and Data Collection 22

3.2 Supply Feed and Control System 23

3.3 Venturi Flow Measurement Tubes 26

3.4 Data Acquisition Testing 28

3.4.1 Thrust 29
3.4.2 Pressure and Mass Flow Rate 30
3.4.3 Error and Sanity Check 34
4. Test Results 36
4.1 Total Thrust Plots 37
4.1.1 Total Thrust: Comparing Duct Cases 37
4.1.2 Total Thrust: Comparing Ring Cases 40
4.1.3 Total Thrust: Duct Cases Divided by Combustion Pressure and Throat Area 44
4.2 Duct Thrust Plots 47
4.2.1 Duct Thrust: Comparing Duct Cases 47
4.2.2 Duct Thrust: Comparing Ring Cases 50
4.2.3 Duct Thrust: Duct Cases Divided by Combustion Pressure and Throat Area 53
4.2.4 Duct Thrust: Comparing Long and Short Ducts Divided by Internal Area 56
4.3 Primary Mass Flow Rate Plots 58
4.4 Mass Flow Rate Ratio and Pressure Ratios 60
4.5 Over-Expanded Nozzle Operation 62
4.6 Flow Interpretation 64
5. Conclusion 71
6. Future Work and Suggestions 74
BIBLIOGRAPHY 76
APPENDICES
Appendix A: Testing Procedure 78
Appendix B: Cold Flow Test Plan 78

Appendix C: Hot Fire Test Readiness Review (TRR) for More than 420 *psi* Chamber Pressure 87

Appendix D: Hot Fire Test Plan for More than 420 *psi* Chamber Pressure 89

Appendix E: Oxygen Cleaning Procedure.....90

Appendix F: Project Safety Operation Plan (SOP).....92

Appendix G: Microsoft Visual Basic Program Written by Ross Gregoriev.....96

Appendix H: Example Input File to Chemical Equilibrium Application (CEA).....97

Appendix I: Full Engine Performance and Design Calculations.....98

Appendix J: Pressure Transducers, Load Cells, and Load Cell Conditioners 99

Appendix K: CPConnect Funding Proposal.....102

Proposal.....102

Proposal Award Letter.....112

Proposal Summary and Thank You Report.....113

Appendix L: LabView Front Panel and Block Diagram 118

Appendix M: Major Purchases.....119

Appendix N: Test Matrices 129

Appendix O: AARLITE Firing 134

LIST OF TABLES

Table Page

Table 1: Planned test matrix. 10

Table 2: The set of the data generated using the CEA program. The input file also contained the "RO" keyword to make CEA perform the proper calculations. 14

Table 3: Major engine performance and design calculation results. 14

Table 4: The results of calculating the base areas of SCAARD and AARLITE. 15

Table 5: Case #1 and #10 were used by Johnson. Case #7 was used in the current research along with #1 and #10. The table was based on Smith et al. (5) (4). 16

Table 6: Mixing duct dimensions. All units are inches. 17

Table 7: Mixing duct thrust predictions using Johnson's work and scaling by engine thrust (5). All units are pound force. 19

Table 8: Venturi tube flow measurement design calculation results. 27

Table 9: Ideas for improvement and future research were categorized by two levels of complexity. 75

Table 10: Selected cold flow test data, chamber pressure approximately 100 psi. 130

Table 11: Nominally 400 psi chamber pressure test data. 131

Table 12: Nominally 550 psi chamber pressure test data. 132

Table 13: Nominally 680 psi chamber pressure test data. 133

LIST OF FIGURES

Figure Page

Figure 1: AAR configuration diagram showed the different flows and their paths (1). 2

Figure 2: Speed and efficiency of various flight options. AAR has a significantly higher efficiency than typical rockets.....3

Figure 3: Flow going over a simple 2D cavity. The top arrow shows the direction of the flow, the other arrows illustrate the depth and length dimensions of a rectangular cavity (9). 7

Figure 4: Illustration of the gas generator testing done by Yu and Schadow (10). 8

Figure 5: Partial section view of the engine's nozzle, C-ring, and diverging duct. Burgundy components were made of copper, the gray components were made of steel, and the black component is graphite. 12

Figure 6: Engine pictured in the lab. The top picture is a close up of the engine with wrenches nearby for scale and the bottom picture is of the engine attached and prepared on the test stand for firing. 13

Figure 7: SCAARD drawing on the left and AARLITE drawing on the right illustrated the greater taper on AARLITE (5). The red ellipses highlight the nozzle tapers. All dimensions are in inches.....15

Figure 8: Illustration of base area at the end of the SCAARD engine. The blue highlight shows the area which would be pulled downward by the low pressure secondary flow and reduce the system performance (4). 16

Figure 9: Section view drawings of the three ducts, from left to right the diverging, short, and long ducts. Drawings are not to scale; all units are inches. 18

Figure 10: The test stand designed and built to test the engine. 22

Figure 11: Plumbing diagram of the feed system going into the AARLITE. 26

Figure 12: Plot of the total thrust profile of the engine firing at about 400 psi chamber pressure. The red line shows the total thrust load cell output and the green line shows the average used for analysis.....29

Figure 13: Plot of the chamber pressure profile of the engine firing at about 400 psi. The

black line shows the measured chamber pressure and the green line shows the average used for analysis. 30
Figure 14: Plot of the oxygen Venturi flow tube from the engine firing at about 400 psi chamber pressure. The blue line shows the low pressure trace measured at the throat of the Venturi tube and the orange line shows the high pressure trace measured at the inlet section of the Venturi tube. 31
Figure 15: Plot of the ethanol Venturi flow tube from the engine firing at about 400 psi chamber pressure. The blue line shows the low pressure trace measured at the throat of the Venturi tube and the orange line shows the high pressure trace measured at the inlet section of the Venturi tube. 31
Figure 16: Plot of the mass flow rate of oxygen when chamber pressure was about 400 psi. The green line shows the oxygen mass flow rate calculated from the measured differential pressure and the purple line shows the average oxygen mass flow rate used for analysis. 33
Figure 17: Plot of the mass flow rate of ethanol when chamber pressure was about 400 psi. The red line shows the ethanol mass flow rate calculated from the measured differential pressure and the orange line shows the average ethanol mass flow rate used for analysis. 33
Figure 18: No ring, total thrust for different ducts at multiple combustion pressures. 38
Figure 19: Solid ring, total thrust for different ducts at multiple combustion pressures. 39
Figure 20: C-ring, total thrust for different ducts at multiple combustion pressures. 40
Figure 21: No duct, total thrust for different nozzle configurations at multiple combustion pressures. 41
Figure 22: Diverging duct, total thrust for different nozzle configurations at multiple combustion pressures. 42
Figure 23: Short duct, total thrust for different nozzle configurations at multiple combustion pressures. 43
Figure 24: Long duct, total thrust for different nozzle configurations at multiple combustion pressures. 44
Figure 25: No ring, total thrust divided by combustion pressure and nozzle throat area for

different mixing ducts at multiple combustion pressures. 45
Figure 26: Solid ring, total thrust divided by combustion pressure and nozzle throat area for different mixing ducts at multiple combustion pressures. 46
Figure 27: C- ring, total thrust divided by combustion pressure and nozzle throat area for different mixing ducts at multiple combustion pressures. 47
Figure 28: No ring, duct thrust at multiple combustion pressures. 48
Figure 29: Solid ring, duct thrust at multiple combustion pressures. 49
Figure 30: C-ring, duct thrust at multiple combustion pressures. 50
Figure 31: Diverging duct thrust for different nozzle configurations at multiple combustion pressures. 51
Figure 32: Short duct thrust for different nozzle configurations at multiple combustion pressures. 52
Figure 33: Long duct thrust for different nozzle configurations at multiple combustion pressures. 53
Figure 34: No ring, duct thrust divided by combustion pressure and nozzle throat area at multiple combustion pressures. 54
Figure 35: Solid ring, duct thrust divided by combustion pressure and nozzle throat area at multiple combustion pressures. 55
Figure 36: C-ring, duct thrust divided by combustion pressure and nozzle throat area at multiple combustion pressures. 55
Figure 37: No ring, short and long duct thrusts divided by internal surface area at multiple combustion pressures. 56
Figure 38: Solid ring, short and long duct thrusts divided by internal surface area at multiple combustion pressures. 57
Figure 39: C-ring, short and long duct thrusts divided by internal surface area at multiple combustion pressures. 57
Figure 40: Duct thrust and total propellant mass flow rate for all tests. 59
Figure 41: Total thrust and total propellant mass flow rate for all tests. 60

Figure 42: Ideal pumping curve showed the mass flow rate ratio versus the exit area to duct inlet area ratio (20). 61
Figure 43: Duct thrust and total thrust versus pressure ratio for all tests. The top plot was duct thrust and pressure ratio for all ducts, and the bottom plot was total thrust and pressure ratio for all ducts. 62
Figure 44: Screenshots of several test fires showing how the plume of the engine changes with increasing chamber pressure. 64
Figure 45: Depiction of how the plume and shear layer look with different rings. The nozzle and rings had been sectioned to see the details. 65
Figure 46: Screen captures of test #25, 26, 27 ($Pc = \sim 580$ psi) in that order from left to right. The pictures show the change in the plume between the ring conditions. The red ellipses highlight where the flow differences were the most noticeable. 67
Figure 47: Screen captures of test #40, 41, 42 ($Pc = \sim 500$ psi), in that order from left to right. The pictures show the change in the plume between the ring conditions. The red circles highlight where the flow differences were the most noticeable. 68
Figure 48: Partial section view of the engine with the three ducts and no ring, possible flow fields shown with the arrows. 70

NOMENCLATURE

A	Area	in^2
D	Diameter	in
F	Thrust Force	lbf
f	Frequency	Hz
g	Gravity Constant	$\frac{ft}{s^2}$
I_{sp}	Specific Impulse	s
K_C	Ratio of Convection Speed	-
M	Mach number	-
$\mathcal{M}$	Molar Mass	$\frac{1}{mol}$
m	Whole Number	-
$\dot{m}$	Mass Flow Rate	$\frac{slug}{s}$
P_0	Stagnation Pressure	$\frac{lbf}{in^2}$
P	Static Pressure	$\frac{lbf}{in^2}$
R	Universal Gas Constant	$\frac{lbf*ft}{mol*R}$
Re	Reynolds Number	-
T	Temperature	$°F, °R$
V	Volume	in^3
U	Velocity	$\frac{ft}{s}$
v	Velocity	$\frac{ft}{s}$

Greek

α	Empirical Phase Number	-
γ	Ratio of Specific Heats	-
μ	Absolute Viscosity	$\frac{lbm}{ft*s}$

Subscripts

amb	Ambient
c	Chamber
e	Nozzle Exit
f	Fuel
s	Secondary
ox	Oxygen
p	Primary
t	Primary Nozzle Throat
3	Mixing Duct Inlet
4	Mixing Duct Exit

1. Introduction

Research and experimentation with air augmented rockets and work on inducing large turbulence in the flow coming out of a rocket engine has been done but it pales in comparison to the efforts put into typical rocket engines. The background on air augmentation with a mixing duct and induction of turbulence into a rocket engine's exhaust is important to this current report and are thus presented. The current work focuses on testing of several mixing duct geometries, large turbulence inducing ring at the exit plane of the rocket engine's nozzle, and multiple combustion pressure groups. The augmentation mixing duct and the large induced turbulence concepts went hand in hand and were experimentally tested to show evidence of system thrust augmentation.

1.1 Why Research Air Augmented Rockets

The Air Augmented Rocket (AAR) is a mode of the Rocket Based Combined Cycle (RBCC) propulsion which has been a field of interest in the propulsion world for many years. Continued work on RBCC holds the possibility to revolutionize launch vehicle capabilities, making them more efficient, less expensive, and even reusable. AAR's have the possibility to be a very simple, easy to implement, robust, and one of the less expensive modes of RBCC. The advantages of AAR's also allow them to be implemented and experimented with by programs at the university level.

An AAR is simply a ducted rocket. The basic configuration and main components of an AAR are diagramed in Figure 1 by Gist (1). The primary flow coming out of a rocket engine exits the nozzle and forms a shear layer with the secondary flow. The shear layer forms on the primary plume boundary, where mixing and energy exchange between the primary and secondary flows occurs.

The plume coming out of the engine works to compress and accelerate the secondary, ambient air. The compression and acceleration increases the total mass flow going through the system and if the rocket engine burns fuel rich or there is secondary fuel injection, the mixing of ambient air into the primary flow allows for energy release from the unused or injected fuel. The secondary energy release, or afterburning, causes the flow to expand further and increase in velocity. Thus the thrust from the system is increased because the final velocity and mass flow rate increase. The specific impulse of the engine would be increased since the same amount of propellant would have produced more thrust.

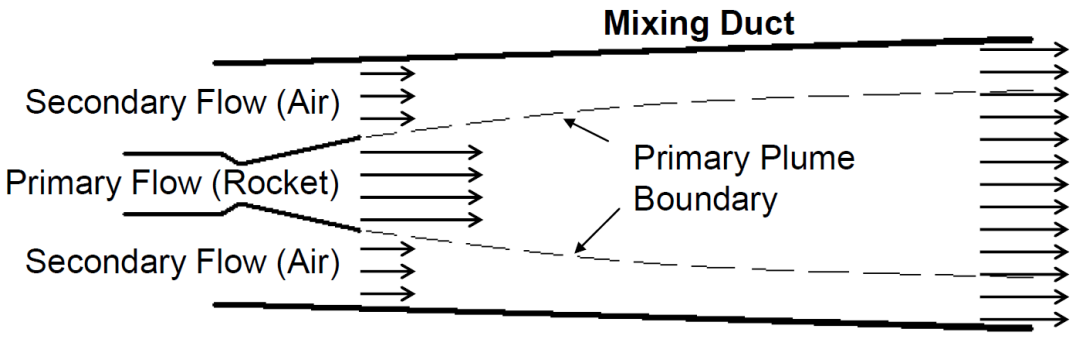

Figure 1: AAR configuration diagram showed the different flows and their paths (1).

AAR technology, if developed further, could make the dream of Single Stage to Orbit (SSTO) a reality. The idea of SSTO is something engineers have wondered about for a long time as a way to reduce costs making space travel orders of magnitude less expensive than present standard costs. Reliability would also be increased since having a one stage launch vehicle would reduce the number of possible points of failure. Increasing reliability and reducing cost SSTO, could allow the average middle class citizen access to space travel. Figure 2 presented by Foster et al. highlights the theoretical higher efficiency of the AAR mode (2). There is interest in making AAR's possible engine configurations for cheaper, better launch vehicles. Jonathan Pickrel who was an Aerospace Engineer from the NASA Dryden Flight Research Center was one such person with interest in AAR's.

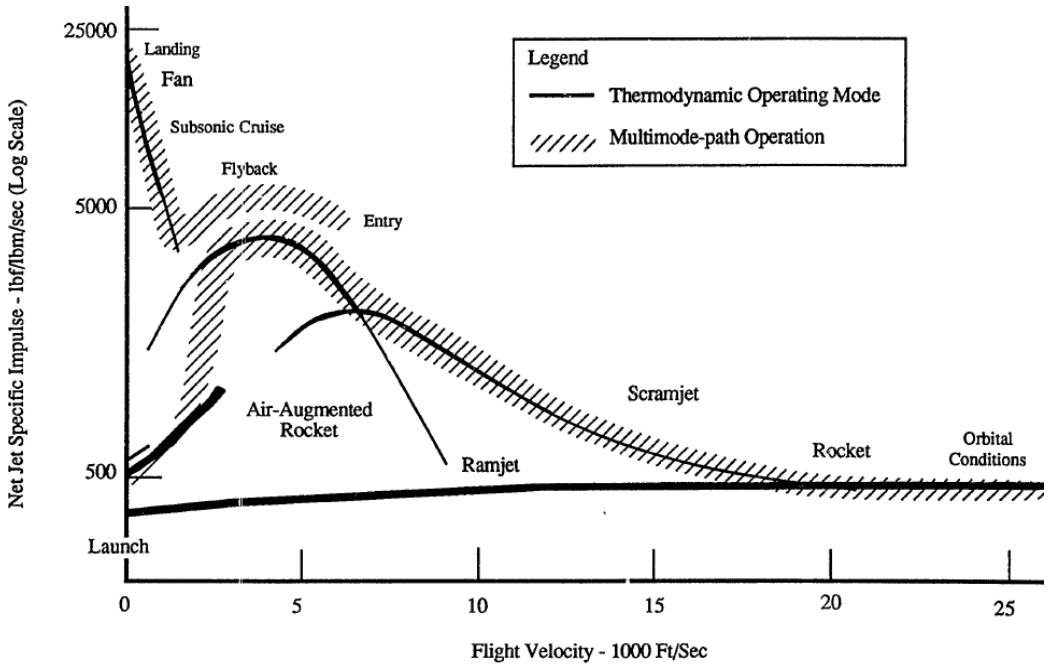

Figure 2: Speed and efficiency of various flight options. AAR has a significantly higher efficiency than typical rockets.

1.2 AAR Work and Research

Since the late 1990's there has been AAR research at Cal Poly. In addition to experimental and theoretical work that has been done at Cal Poly, several other organizations have looked into the AAR and RBCC subjects.

Foster et al. focused on analysis of past work on RBCC engine systems, the selection of five engines for more evaluation, and investigation of design approach alternatives to integrate the five engines into a launch vehicle. Engine to vehicle integration, vehicle structure and other subsystems, thermal protection systems, and crew compartment and payload integration were considered in the study of vehicle integration. Several possible designs evolved from the work and were further refined with trajectory and aerothermodynamic analysis, in support of the thermal protection system (2). The assembled report showed RBCC to be a feasible method for increasing the specific impulse of high velocity (launch) vehicles. The AAR mode of RBCC was shown to be an important and valuable area of study for increasing specific impulse.

Graduate students at Cal Poly have researched and tested 2D planar AAR's and one axisymmetric. Most notably with 2D research and testing Fabri choking and Fabri blocking were explored. Fabri choking is the name for choking of the secondary flow in an AAR. Once choked the flow supersonically expands increasing the total mass flow rate and average velocity of the mass exiting the AAR engine. Fabri blocking is similar to choking; however, it blocks the secondary flow and is a detrimental condition. Fabri blocking is analogous to stalling a jet engine. Both Fabri choking and blocking occurred at a minimum pressure ratio, first choking and then blocking. Reaching the minimum pressure ratio and Fabri choking is essential for making an AAR function.

Gist and Foster conducted extensive testing of a 2D rocket engine and air augmenting mixing duct. They tested up to $2{,}000\ psi$ combustion chamber pressure and found that past a minimum pressure ratio $\left(\frac{P_c}{P_{amb}}\right)$ the secondary flow would choke and as the ratio continued to increase the secondary flow would become blocked. The minimum pressure ratio to cause secondary flow choking was determined to be 80 (3). Further work on 2D AAR research was conducted by Josef Sanchez, Brett Morham, Trevor Montre, and Martin Popish.

Smith et al. used multiple linear regression analysis to build parametric models investigating rocket chamber pressure, rocket exit area ratio, injected secondary flow, mixing duct inlet area ratio, mixing duct area ratio, and mixing duct length to inlet diameter ratio. The models were run with a computational fluid dynamics (CFD) program to obtain a vacuum specific impulse. The specific impulses were compared and showed that increasing mixing duct area ratio and rocket area ratio increase specific impulse, while increasing mixing duct inlet area ratio and mixing duct length to diameter ratio decrease performance (4). Chamber pressure was reported to not have a significant impact on performance, however, the chamber pressure was optimally or under-expanded to the pressure of the secondary flow, never over-expanded. The investigated variables were well chosen because most of them are non-dimensional while still fully characterizing a simple duct. The non-dimensional values served as a starting point for Johnson in the design and testing of his ducts. Furthermore, the non-dimensional values complemented with Johnson's work serve as the starting point for the design and testing of this report's ducts.

Johnson continued the work done on 2D testing of AAR's and moved the testing to a 3D axisymmetric engine. Mixing duct thrust and total thrust were measured, the engine could run a nominal $20\ lbf$ of thrust for a calculated $300\ psi$ combustion chamber pressure and two different mixing duct profiles were tested (5). The engine primary mass flow rate maximum was $0.00264\ \frac{slug}{s}$. Two mixing ducts were made and tested, a straight wall and a diverging wall mixing ducts. The straight wall duct was able to achieve an average $0.97\ lbf$ and the diverging wall duct averaged about $0.18\ lbf$ of thrust. However, the addition of the duct negatively impacted the system's total thrust. The base area at the nozzle end of the engine was believed to be the main reason for this reduction in performance. The base area is the area difference between the engine's cross sectional area and the nozzle's exit area. Several other compounding factors included: the duct inlet diameter was too small because it did not account for the base area and the combustion pressure to ambient pressure ratio was too low to get near Fabri choking. The combustion pressure was never directly measured and was most likely lower than the calculated $300\ psi$.

For ease of reference the mixing ducts Johnson tested were called "diverging duct" and "short duct". The current report also uses the diverging and short duct terminology along with "long duct" to refer to a mixing duct that was designed longer than the diverging and short ducts, and "no duct" to refer to no mixing duct attached to the system.

1.3 Flow Over a Cavity

The mixing and entrainment in an AAR occurs in the shear layer between the primary and secondary flows. The shear layer is a critical key to making an AAR work. As described by Papamoschou, the shear layer and mixing are governed by the instability of the turbulent large-scale structure which is formed by the difference in physical properties and velocities of two flows (6).

To improve AAR performance the compressible shear layer growth rate and mixing of the primary and secondary flows must increase. Further work by Papamoschou together with Roshko points out that with supersonic compressible flows (as is the case in an AAR engine) the shear layer growth rate decreased as free-stream Mach number increased (7). However, Smits and Dussauge said the lower mixing rate in the shear layer when the free-stream Mach number was high is still considerable and allows the primary and

secondary flows to interact (8). If the compressible shear layer growth and mixing rates could be forced to grow faster with a small addition, an AAR system would benefit greatly.

Throughout the 1950's and 1960's there was interest in understanding what happened when a high speed flow went over a cavity. Rossiter explained the interest was directed toward understanding the pressure oscillations and vibrations excited in the bomb bays of airplanes (9). Rossiter's work along with several others including Krishnamurty and Plumblee et al. paved the way to understanding and predicting the principal excitation frequency for a cavity with a specific set of dimensions and flow properties going over said cavity. As the airspeed over a constant depth cavity increases and the length of the cavity decreases, the frequency in the cavity and acoustic radiation would increase.

For the purposes of this study, a cavity refers to a simple groove, pocket, or channel with the open face parallel to the flow direction. As the flow travels passed the cavity a resonant pressure oscillation is established in the cavity and interacts with the flow that created it. Figure 3 illustrates the basic shape of a simple rectangular cavity with the flow going parallel to the opening of the cavity. For a simple, rectangular 2D cavity if the length to depth ratio is 1 or less, the excited frequencies would have one peak in the amplitude spectra that is much larger than the other peaks and as the airspeed increases this peak frequency also increases (9). Along with pressure oscillations and corresponding acoustic radiation, the flow over a cavity is also observed to be more turbulent after passing over the cavity. The turbulent nature of the flow can be seen in the swirls which propagate across Figure 3. The greater turbulence increases the mixing rate of the flow when it encounters another fluid.

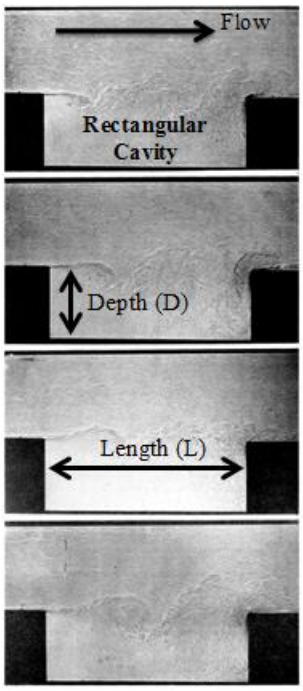

Figure 3: Flow going over a simple 2D cavity. The top arrow shows the direction of the flow, the other arrows illustrate the depth and length dimensions of a rectangular cavity (9).

In the late 1990's researchers Yu and Schadow at China Lake, California continued the research of how flow behaves over a cavity. However, they focused on flows over cavities placed at the exit of a rocket engine nozzle instead of bomb bays, and found if a flow went over a cavity and then encountered a second flow the shear layer would grow faster (10). They tested several different cavities, with different flow properties, and were able to non-dimensionalize cavity dimensions. A jet preferred mode was determined that would result in a specific frequency being radiated and the shear layer growth rate being increased to a maximum. In addition, to increasing the shear layer growth rate the cavity also caused the jet from the gas generator (i.e. rocket engine) to afterburn if the jet was fuel-rich and the frequency generated was at or above the jet preferred mode frequency. An equation that was used by Rossiter was found to be the best predictor for a jet's frequency given a simple rectangular cavity's dimensions and flow gas properties. The equation used is adapted and follows as Equation 1-1.

$$\frac{fL}{U} = \frac{m - \alpha}{M + \frac{1}{K_c}} \qquad \textbf{1-1}$$

Figure 4 is an illustration of the setup from the report written by Yu and Schadow. Straight rectangular, semi-annular and fully annular cavities were investigated. The flow excitation at the exit of a supersonic discharge is seen as large gray swirls in the Mach 2 jet after it passes over the straight rectangular cavity.

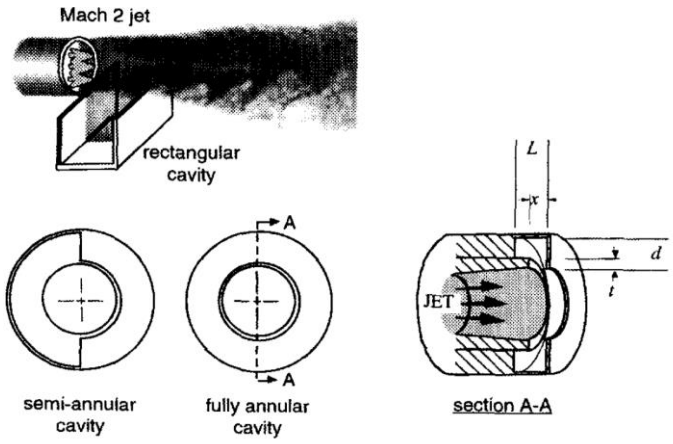

Figure 4: Illustration of the gas generator testing done by Yu and Schadow (10).

The use of a cavity to increase the shear layer growth rate and cause afterburning goes hand in hand with the use of a mixing duct to form an AAR. The cavity causes the primary flow from a fuel rich engine to have an increased shear layer growth rate and greater entrainment of secondary flow, higher mixing and afterburning releases energy, and the mix expands pushing on the mixing duct creating more thrust for the same amount of primary propellants.

1.4 Objective and Intent

The focus of the current report is to characterize the performance of the mixing duct and annular cavity configurations to serve as a baseline for future work. The major objectives were to test three mixing duct geometries and a fully annular cavity at the exit of the nozzle to produce evidence of thrust augmentation. A liquid ethanol and gaseous oxygen supplied rocket engine was designed and instrumented to output measurements of total thrust, mixing duct thrust, combustion chamber pressure, and individual propellant differential pressures across Venturi flow tubes that allow for mass flow rate calculation.

In support of the major objectives were several sub-goals. The first sub-goal was to improve the base area of the engine. The base area at the nozzle end of the SCAARD engine was large causing the lower pressure secondary flow to pull the engine downward when a mixing duct was attached (5). The base area of the

current engine was reduced as much as possible by reducing the outer diameter of the engine and increasing the exit area of the nozzle. The design combustion chamber pressure was $1{,}000\ psi$ to increase the nozzle exit area and to get closer to the minimum pressure ratio required for Fabri choking of the secondary.

Burning at or near the stoichiometric mixture ratio creates more heat than the engine can handle and cause the engine to melt. Burning oxidizer rich would be detrimental because the combustion chamber and nozzle could oxidize catastrophically. Burning fuel rich makes sense from the standpoint of engine longevity. Burning fuel rich allows for insight to be drawn from testing with the cavity since Yu and Schadow saw greater afterburning of fuel rich plumes. Thus the engine was tested while burning fuel rich.

The design of the annular cavity is explained in detail in a further section, but for reference the cavity configuration is referred to as the "ring" configuration. Furthermore, "no ring" means the nozzle has nothing attached, "solid ring" means there is a solid graphite ring with no groove (no cavity) attached to the nozzle, and "C-ring" means there is a grooved graphite ring (a cavity) attached to the nozzle.

Table 1 shows an empty test matrix intended to be used for testing and data organization. The matrix is constructed around the mixing ducts, rings, and pressure sets. The nine pressure sets are based on the combustion pressure obtained when the supply cylinder regulators are set to specific pressures before each test. The sets are intended to test the system at distinct nominal combustion pressures. When the engine is combusting, the sets are set up to test with two levels of fuel richness while the combustion pressure is still in the pressure set. The fuel richness of the mixture ratio is controlled by setting the oxygen regulator $50\ psi$ lower when a more fuel rich test is desired. Pressure sets 1 and 2 will be $\sim 400\ psi$, sets 3 and 4 will be $\sim 530\ psi$, and 5 and 6 will be $\sim 680\ psi$ combustion pressure. Sets 2, 4, and 6 are run more fuel rich than sets 1, 3, and 5. The filled cells of Table 1 show the test numbers which correlate to the tests that were done and are fully documented in the matrices in Appendix N.

Four of the tests in Table 1 were conducted as cold flow tests and are under pressure set 0. These tests were done in addition to the regular combusting test fires in the other pressure sets. The cold flow tests were conducted exactly like tests with combustion except no ethanol was in the fuel tank, only nitrogen and oxygen gas were in the feed system and fired from the engine. With no ethanol there was no combustion

and hence the term cold flow. The cold flow tests have "cold" appended to the test number and only reached $\sim 100\ psi$ in chamber pressure.

Testing above $\sim 680\ psi$ could not be done because the pressure loss across the feed system and the injector manifold assembly was about five times greater than planned. The pressure loss was designed to be $\sim 20\%$ of the combustion pressure so the feed pressure would have to be $\sim 1{,}200\ psi$. However, in reality the feed pressure would have had to be $\sim 2{,}000\ psi$ for the combustion pressure to be $1{,}000\ psi$. Preliminary tests attempting to reach $1{,}000\ psi$ combustion pressure were stopped after reaching $\sim 750\ psi$ because in the next higher pressure test the injector manifold assembly spread apart enough for ethanol to leak into the oxygen feed channel, combust in the assembly, and erode the sealing gasket. The tests for this current report were conducted to a maximum of $\sim 680\ psi$ and the nozzle was always operating over-expanded.

Table 1: Planned test matrix.

		Nozzle Expansion								
		Over							Optimally	Under
		Pressure Set (psi)								
		#0 P_c~100	#1 P_c~400	#2 P_c~400	#3 P_c~530	#4 P_c~530	#5 P_c~680	#6 P_c~680	#7 P_c~1,000	#8 P_c~1,200
No Duct	No Ring	#1cold	#1	#13	#25	#40	#55			
	Solid Ring		#2	#14	#26	#41				
	C-Ring		#6	#18	#27	#42				
Diverging Duct	No Ring		#10	#22	#34	#39				
	Solid Ring		#4	#15	#31	#46				
	C-Ring		#8	#19	#28	#43				
Short Duct	No Ring		#11	#23	#35	#38				
	Solid Ring		#3	#16	#32	#47				
	C-Ring		#7	#20	#29	#44				
Long Duct	No Ring	#12cold	#12	#24	#36	#37	#53	#54		
	Solid Ring	#6cold	#5	#17	#33	#48	#51	#50		
	C-Ring	#7cold	#9	#21	#30	#45	#52	#49		

2. Engine, Mixing Ducts, and Cavity Design

The ethanol and oxygen fed engine was designed specifically for this current report's testing. The engine previously used by Johnson was not adequate enough but was used as a point of insight. The ducts and cavity were also designed alongside the new engine.

2.1 Engine

The engine was designed using several resources including Johnson, Huzel, Sutton, Young, John, and Muss (5) (11) (12) (13) (14) (15). The goals for the engine design and construction were $100\ lbf$ of thrust, $1{,}000\ psi$ combustion pressure, integrated spark plug ignition, combustion chamber pressure measurement, smaller outer diameter (OD) relative to the SCAARD engine, and gradually tapered the OD of the engine to the exit diameter of the nozzle. The new engine from here further is referred to as the Air Augmented Rocket Large Induced Turbulence Engine or AARLITE for short.

The final engine design was rendered in SolidWorks. Figure 5 shows a rendering with the diverging duct and C-ring attached. The mixing duct, C-ring, and part of the nozzle are sectioned to show how the secondary flow enters the duct. The callouts in the figure point out the major components. The inlet plane to the mixing duct coincides with the exit plane of the nozzle when no ring is attached. However the configuration in Figure 5 shows that when a ring is attached the mixing duct inlet plane coincides with the exit plane of the ring. The machining of all the parts was done by Allen Capatina, George Georgiou, Joe Vanherweg, and Kyle Rosenow in the Cal Poly Mechanical Engineering Student Machine Shops, the Hangar and Mustang '60.

Figure 6 shows a close up picture of the finished engine with several wrenches for scale reference. The middle open end wrench is a $3/4\ \ in$. The second picture in the figure shows the assembled engine attached to the test stand ready to fire.

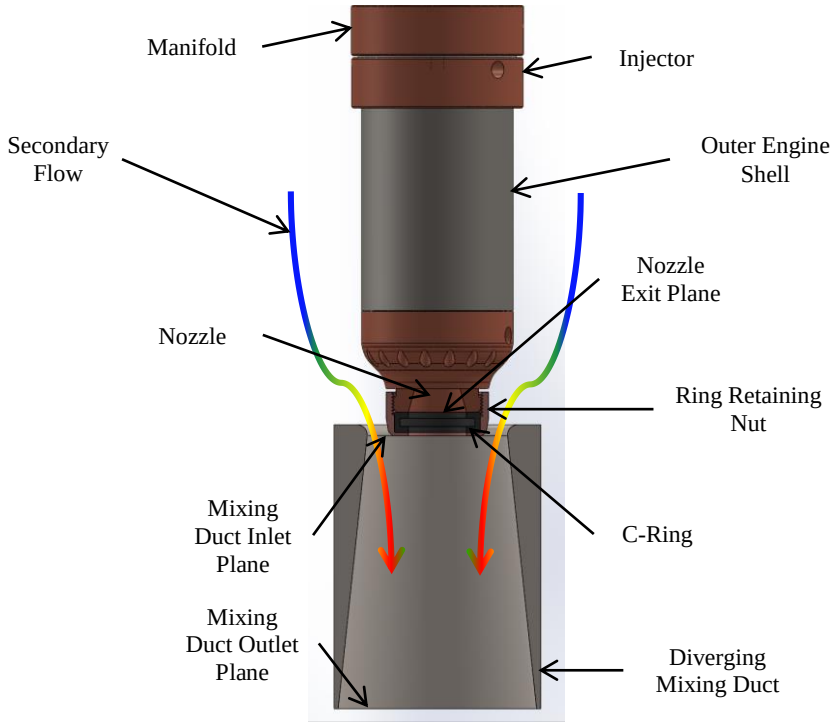

Figure 5: Partial section view of the engine's nozzle, C-ring, and diverging duct. Burgundy components were made of copper, the gray components were made of steel, and the black component is graphite.

Figure 6: Engine pictured in the lab. The top picture is a close up of the engine with wrenches nearby for scale and the bottom picture is of the engine attached and prepared on the test stand for firing.

2.1.1 Engine Performance Design

The remaining engine parameters were identified after the propellants, the combustion pressure, and the thrust were chosen. Liquid ethanol and gaseous oxygen were chosen as the design propellants because they are easy to obtain. The design combustion pressure is 1,000 psi with 100 lbf thrust.

The properties of the combustion process were found thanks to help from Muss of Sierra Engineering Inc. (15). He allowed the use of a program called Combustion Equilibrium Application (CEA) to predict the

combustion temperature and gas properties given the fuel and oxidizer pressure and mixture ratio. A set of inputs and outputs are displayed in Table 2 and a full input file can be seen in Appendix H. The input files are simply text files with an ".inp" suffix which the CEA terminal window takes in for input and the puts out the calculated data to an ".out" suffix text file.

Table 2: The set of the data generated using the CEA program. The input file also contained the "RO" keyword to make CEA perform the proper calculations.

Input file parameters			Output file parameters		
Combustion Pressure $(psi; Pa)$	Propellants	Mixture Ratio $(unitless)$	Combustion Temperature $(K;\ °R)$	Molar Mass of Products $\left(\frac{1}{mol}\right)$	Ratio of Specific Heats $(unitless)$
1,000; 6.89×10^6	Oxygen; Ethanol	2.1	3490; 6282	24.8	1.19

The results from CEA were used to calculate the rocket engine performance values and are presented in Table 3. The full calculations for the results are presented in Appendix I and were made possible thanks to work published by Huzel, Sutton, and John (11) (12) (14). The final dimensions of the engine were obtained after calculating the structural margins with methods published by Huzel and by Young (11) (13). The thermal margins required for safe and reliable operation and orifice sizing of the injector were also analyzed with help from Huzel and from Sutton (11) (12).

Table 3: Major engine performance and design calculation results.

Nozzle Exit Velocity: $V_e = 8776 \frac{ft}{s}$	Nozzle Exit Mach Number: $M_e = 3.18\ Mach$
Nozzle Throat Area: $A_t = 0.0625\ in^2$	Nozzle Throat Radius: $R_t = 0.141\ in$
Nozzle Expansion Ratio: $\varepsilon = 8.95$	Nozzle Exit Radius: $R_e = 0.422\ in$
Total Primary Mass Flow Rate: $\dot{m}_{tot} = 0.0114 \frac{slug}{s}$	Oxygen Mass Flow Rate: $\dot{m}_{Ox} = 0.00767 \frac{slug}{s}$
Fuel Mass Flow Rate: $\dot{m}_{Fuel} = 0.00366 \frac{slug}{s}$	Engine Specific Impulse: $I_{sp} = 273\ s$

2.1.2 Nozzle Streamlining

The outer diameter of AARLITE was designed $0.1\ in$ smaller than the outer diameter of the SCAARD engine. The AARLITE engine has an outer diameter which measures $2.2\ in$ and the nozzle exit diameter is $0.9\ in$. Reducing the outer diameter of the engine reduced the base area which was detrimental to performance (5). Table 4 illustrates how the design of AARLITE reduces the base area at the nozzle end of the engine relative to the SCAARD. A 20% reduction in base area was achieved.

Table 4: The results of calculating the base areas of SCAARD and AARLITE.

	SCAARD	AARLITE
Total Engine Cross Sectional Area:	$A_o = 4.15\ in^2$	$A_o = 3.80\ in^2$
Nozzle Exit Area:	$A_e = 0.196\ in^2$	$A_e = 0.636\ in^2$
Base Area:	$A_{base} = A_o - A_e = 3.95\ in^2$	$A_{base} = A_o - A_e = 3.16\ in^2$

Area Reduction:	$\frac{3.95 - 3.16}{3.95} * 100 = 20\%$

In addition to the base area improvement, the new engine's nozzle has a greater taper compared to the SCAARD engine. The improved taper reduces the area exposed to the entrained secondary flow as the flow gets closer of the mixing duct and decreases in pressure. Figure 7 shows the SCAARD and AARLITE engines drawn side by side to show the differences in length, diameter, and taper. The drawings are not fully defined, the dimensions shown for reference.

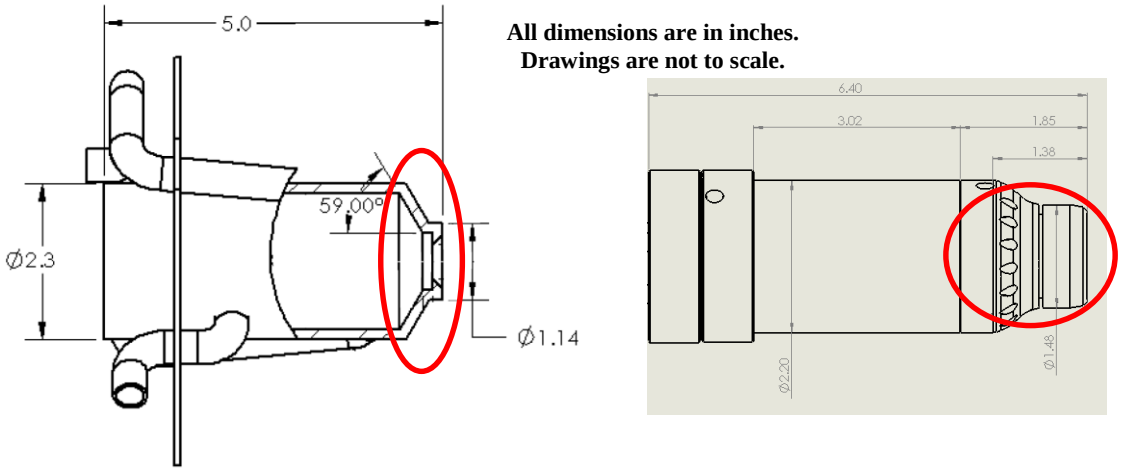

Figure 7: SCAARD drawing on the left and AARLITE drawing on the right illustrated the greater taper on AARLITE (5). The red ellipses highlight the nozzle tapers. All dimensions are in inches.

The improved base area and taper were intended to reduce the negative impact the low pressure secondary flow had on the system. Figure 8 illustrates the base area on the SCAARD and the low pressure region which caused the system performance to be decreased when the addition of the duct was made (5).

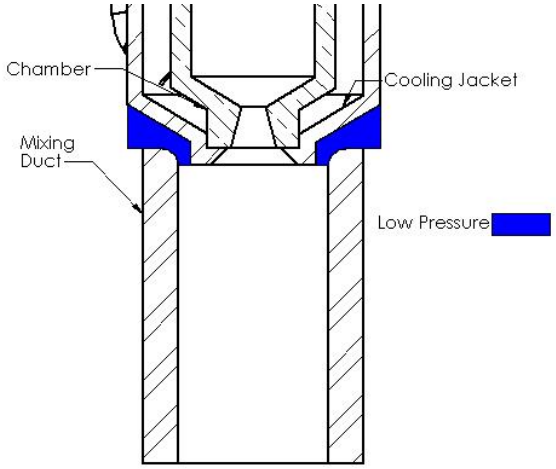

Figure 8: Illustration of base area at the end of the SCAARD engine. The blue highlight shows the area which would be pulled downward by the low pressure secondary flow and reduce the system performance (4).

2.2 Mixing Ducts

Johnson used cases #1 and #10 in Table 5 and for ease of reference are called diverging duct and short duct, respectively. The case numbers in Table 5 correlate to the numbers used by Smith et al. and Johnson. The table is based on the work by Smith et al. and the two cases were chosen by Johnson as a starting point for the cases he tested because they were feasible and modeled at 300 psi chamber pressure (4) (5). The short and diverging duct cases' mixing duct inlet area ratio, length to diameter ratio, mixing duct area ratio, and rocket area ratio along with those of case #7 were used for the design and testing in the current research. For ease of reference, case #7 is called the long duct case. The other cases Smith et al. investigated were determined to be unfeasible for the current study.

Table 5: Case #1 and #10 were used by Johnson. Case #7 was used in the current research along with #1 and #10. The table was based on Smith et al. (5) (4).

Case	Chamber Pressure (psi)	Mixing Duct Inlet Area Ratio $\left(\frac{A_3}{A_t}\right)$	Length to Diameter Ratio $\left(\frac{L}{D_3}\right)$	Mixing Duct Area Ratio $\left(\frac{A_4}{A_3}\right)$	Rocket Area Ratio $\left(\frac{A_e}{A_t}\right)$
1	300	40	2	2	4
7	1200	40	5	1	4
10	300	40	2	1	4

Once the throat and exit areas of the engine's nozzle were settled upon, the mixing ducts were directly calculated using the ratios in Table 5. For all three cases #1, #7, and #10 the mixing duct inlet area ratio, which was the ratio of mixing duct inlet area to rocket engine throat area, are the same ratio forty to one.

However, using the ratio directly and going from the engine throat area to mixing duct inlet area is the ideal case where the nozzle lip thickness (base area) is assumed zero. To account for the base area of the nozzle at the inlet plane of the mixing duct, the base area was added to the mixing duct inlet area. Johnson presented the design idea of accounting for the base area at the mixing duct inlet plane (16).

The throat area was $A_t = 0.0625\ in^2$, multiplied by forty, adding in the base area, lead to the real mixing duct inlet area: $A_3 = 3.26\ in^2$. For manufacturing purposes the diameter was calculated: $D_3 = 2.036\ in$. All three cases had the same mixing duct inlet area since the engine's throat stayed the same between all the cases.

For cases #7 and #10 the mixing duct area ratio, which was the ratio of mixing duct outlet area to mixing duct inlet area, are the same ratio one to one. The two cases' outlet areas are equal to their inlet areas, they are straight walled. Case #1 has a mixing duct area ratio of two to one so the outlet area was twice that of the inlet area and the outlet diameter is root two times large than the inlet diameter. Case #1 has a diverging wall profile. Cases #1 and #10 have a length to inlet diameter ratio of two to one, while case #10 has a five to one ratio. All the dimensions calculated are displayed in Table 6 and a drawing of each ducts' revolved profile is in Figure 9. The outer diameter, which was 3 in on all the mixing ducts, was kept the same and straight. Also the inlets were all made with a $0.150\ in$ radius fillet to stay consistent with Johnson, be machinable and have a smooth entrance.

Table 6: Mixing duct dimensions. All units are inches.

	Diverging (case #1)	Short (case #10)	Long (case #7)
Inlet diameter (in)	2.036	2.036	2.036
Outlet diameter (in)	2.879	2.036	2.036
Inlet to outlet length (in)	4.072	4.072	10.18

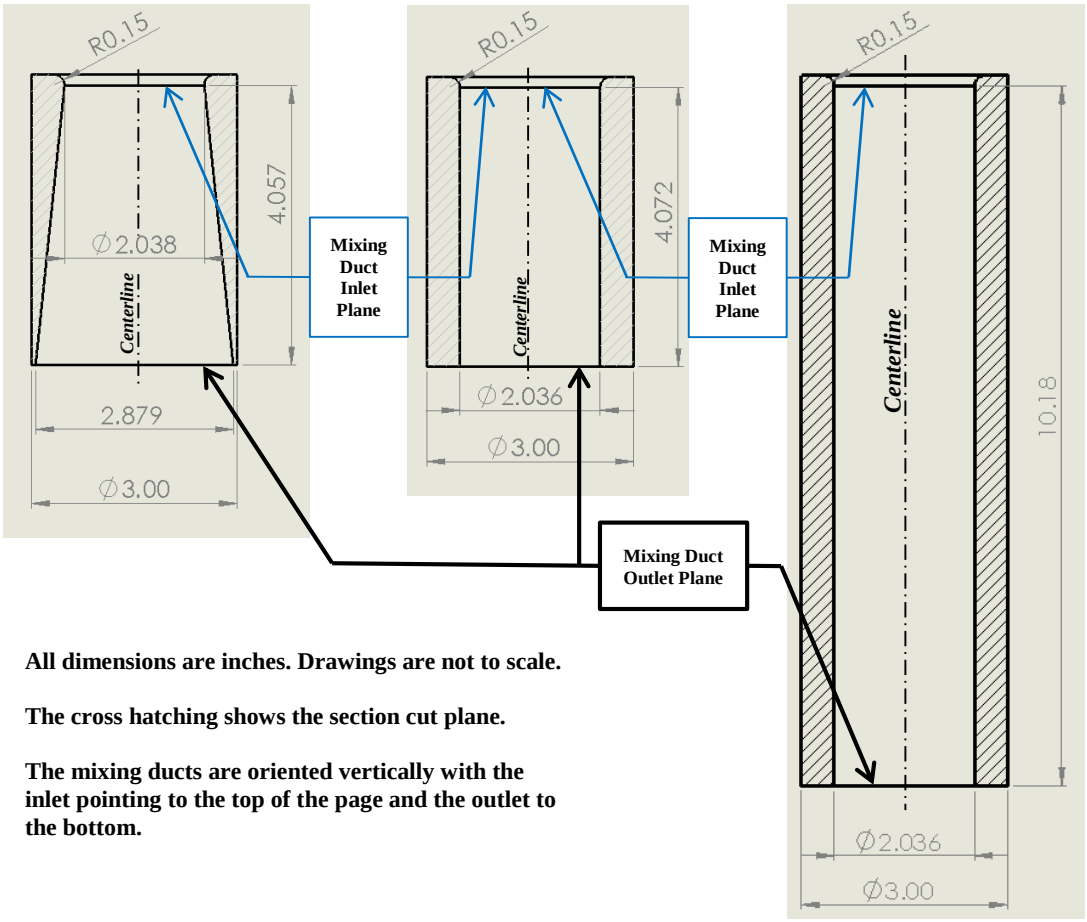

Figure 9: Section view drawings of the three ducts, from left to right the diverging, short, and long ducts. Drawings are not to scale; all units are inches.

Estimation of the performance of the new mixing ducts was done by scaling the results Johnson had. Thrust estimation for the long mixing duct was not feasible, but expected to produce less thrust than the short duct since the length to diameter ratio is higher (8).

Table 7 displays the predicted mixing duct thrusts assuming AARLITE produces 100 lbf. Mixing duct thrust was scaled using engine thrust. The diverging duct is predicted to produce 1.7 lbf and the short duct is predicted to produce 7.3 lbf. It is interesting that Smith et al. found that increasing mixing duct area ratio increases performance while Johnson's tests showed the opposite (4) (5).

Table 7: Mixing duct thrust predictions using Johnson's work and scaling by engine thrust (5). All units are pound force.

	SCAARD	AARLITE
Engine thrust (lbf)	15	100
Short mixing duct thrust (lbf)	1.1	7.3
Diverging mixing duct thrust (lbf)	0.26	1.7

2.3 Cavity

Early studies into the resonant structures and frequencies created inside cavities with high velocity flows across their open side were conducted around the 1960's. A specific interest in studying the phenomenon was for bomb bays in aircraft and how the pressure fluctuations would impact the structural modes of the aircraft. The interest in studying the phenomenon with respect to air augmented rockets is to increase the shear layer growth rate leading to greater mixing between the primary and secondary flows over a shorter distance and time.

Yu and Schadow took the cavity research further and applied it to cavities at the exit of a gas generator and found large turbulent structures formed, they are important for fine-scale mixing, and the plume's afterburning luminosity was significantly reduced for relatively long wavelength structures while it was increased for short wavelength structures. The transition from suppressing the luminosity to enhancing the luminosity occurred at the jet preferred mode frequency (10). In order to get afterburning, a high coherent structure frequency is chosen.

Another report by Hirahara et al. on the subject provides some necessary insight on the Strouhal number which is what Rossiter also used (17). The Strouhal number is defined as

$$St = \frac{fL}{U} = \frac{m - \alpha}{M + \frac{1}{K_c}} \qquad \textbf{2-1}$$

and is the same equation presented in section 1.3 but now it is called the Strouhal number. In Equation 2-1 $\alpha = 0.25$, $K_c = 0.57$, and $m = 1, 2, 3, etc.$ are unitless (17). From the engine design performance in Table 3: $M_e = 3.18$ and $U = U_e = 8776\frac{ft}{s}$. The design frequency is chosen to be $f = 135{,}000\ Hz$ because anything lower would make the cavity much larger than is feasible to manufacture and fit inside the mixing ducts without physically blocking the secondary flow. The frequency is much higher than the frequencies

Yu and Schadow tested but since it is higher than the jet preferred mode frequency $(13 - 14\ kHz)$ it should increase afterburning capability which is what is required (10). Solving Equation 2-2 for the length of the cavity:

$$L = \frac{U}{f} * \frac{m - \alpha}{M + \frac{1}{K_c}} = \frac{8776}{135000} * \frac{1 - 0.25}{3.18 + \frac{1}{0.57}} = 0.00988\ ft$$
$$= 0.119\ in \qquad \textbf{2-2}$$

Hirahara also provided an improved version for Rossiter's equation which lead to $\mathrm{L} = 0.1275\ in$. The final dimension chosen was $0.123\ in$ for both length and depth to be one-to-one ratio and for manufacturability.

The nozzle was designed such that the $0.123\ in$ square cavity was machined into a graphite ring of $0.3\ in$ thickness, $1.244\ in$ outer diameter (OD), and $0.844\ in$ inner diameter (ID). The graphite was attached with a threaded retaining nut to the exit plane of the nozzle. To have control, another graphite ring was machined but with no cavity, so that a ring of graphite with the dimensions given would also be attached to the exit plane of the nozzle with the same threaded nut for testing.

Configurations when the graphite ring with a cavity was attached to the nozzle with the retaining nut were referred to as "C-ring" configurations, the graphite ring with no cavity were called "solid ring" configurations, and the nozzle alone with no ring and no retaining nut were called the "no ring" configurations.

3. Test Stand and Data Acquisition

The test stand holds the rocket engine which was attached by three $3/8\ in$ hexagonal shafts to a support rail that was attached to the total thrust $(200\ lbf)$ load cell. The load cell $(25\ lbf)$ for the mixing duct clamp frame was attached to the support rail and interlaced between the three hexagonal shafts that held the engine. The support rail had linear bearings where it was attached to the test stand's two $7\ foot$ vertical columns. The support rail could be identified by its horizontal orientation and central location on the stand. Above the support rail there was another horizontal fixed beam which held the two $12\ V$ sealed lead acid (SLA) batteries, the actuated supply ball valves, and the Venturi tubes. The stand was designed to hold well over $100\ lbf$ of thrust from the engine; the weakest link on the stand was the $200\ lbf$ load cell.

Figure 10 shows a picture taken of the test stand ready for test firing. It was primarily built using 1.5 Series aluminum T-slot extrusions and hardware, a steel engine plume deflector plate, chains for securing nitrogen and oxygen cylinders, chains for securing the stand to the lab foundation, and various wiring, tubing, and fittings for supply/control of propellant and data acquisition. The test stand was equipped with two load cells, two load cell signal conditioners, and five pressure internally conditioned transducers for collecting data.

Figure 10: The test stand designed and built to test the engine.

3.1 Sensors and Data Collection

A 200 lbf load cell made by AmCell and purchased from Tacuna Systems was used to measure the thrust from the engine and mixing duct together. A 25 lbf load cell made by AmCell and purchased from Tacuna Systems was used to measure the thrust of the mixing duct alone. The engine thrust was calculated by subtracting the mixing duct (25 lbf load cell) measurements from the measurements made by the 200 lbf load cell. Equation 3-1 shows the variables explained.

$$F_{eng} = F_{tot} - F_{duct} \quad \textbf{3-1}$$

Each load cell had its own signal conditioner which was made and sold by Tacuna Systems. Both load cells had a maximum error of $\pm 1.0\%$ of full scale reading. The pressure measurements were done using five Wika Type A-10 pressure transducers rated for a maximum $3{,}000\ psi$ and had a maximum error of $\pm 0.5\%$ of full scale reading. One pressure transducer was connected to the engine's combustion chamber through a pressure snubber/filter to measure the combustion pressure. Two pressure transducers were connected to the oxygen Venturi flow measurement tube and two pressure transducers were connected to the ethanol Venturi flow measurement tube. The transducers on the Venturi flow measurement tubes were attached to pressure taps which see pressure differentials that are used to calculate the mass flow of ethanol and oxygen into the engine. More details on the sensors and the signal conditioners were attached in Appendix J.

All the sensors were powered using two $12\ V$ SLA batteries which were connected together in series to supply the pressure transducers with $24\ V$. The Tacuna conditioners used only $12\ V$ from one of the two SLA batteries. The signals from all the sensors were sent along shielded cables to a simple resistor-capacitor low pass filter (a $1{,}000\ \Omega$ resistor connected with a $0.1\ \mu F$ capacitor for a cutoff frequency of about $f_c = 1.6\ kHz$) connected to a National Instruments (NI) USB-6210 Data Acquisition (DAQ). The output from the DAQ was connected to a computer running National Instruments LabView program which recorded the data to a Microsoft Excel file. The LabView program was set to collect data at a sampling rate of $1\ kHz$.

3.2 Supply Feed and Control System

The engine was supplied with fuel, oxygen, high voltage ignition power, and water in order to function properly. These supplies were provided by the test stand.

The $120\ VAC$ power from the control box was brought out to the test stand along shielded cables from the control box. All commands from the control box were power signals which turned the various solenoids and other devices on the test stand on and off. Other than the two $12\ V$ SLA batteries on the test stand, all electrical power was routed through the control box which had a 1Amp circuit breaker in case of an over current event, a keyed power switch to assure only trained personnel who have access to the key could use the box and a secondary power switch as second point which had to be turned on in order for any power to

flow. The box itself was a large plastic conduit box and all metal components which were exposed were grounded. The test stand was grounded to mains ground through the control box and through a secondary cable inside the firing room.

Water was used as the coolant for the engine and was transported to and from the test stand through two garden hoses. The water sink in the Propulsion Laboratory was equipped with a hose spigot to supply the test stand. The water used was at the temperature of the supply, it was not cooled with ice or other method. On the stand, an analog pressure and two temperature gauges monitored the inlet pressure and inlet and outlet temperatures of the water. After the inlet pressure and temperature gauges, the water was controlled by a $120\ VAC$ diaphragm solenoid valve. A pair of clear vinyl tubes took the supply of water from the solenoid valve to the engine's nozzle. The water traveled around the nozzle at the plane of the throat in a machined channel, then up the combustion chamber copper liner, and the water exited through the injector and manifold assembly. A second pair of clear vinyl tubes returned the water to a manifold which held the second temperature gauge and finally went through another garden hose to the sink.

Dry compressed air regulated to $90\ psi$ was supplied to the test stand for actuation of Swagelok ball valve actuators which control the flow of ethanol and oxygen to the engine. The laboratory had air hookups which were accessed using an air hose with quick disconnect fittings.

A cylinder of compressed nitrogen gas was secured to the test stand using a top and bottom chain. The nitrogen was used to pressurize the ethanol fuel and push it into the engine. The high cylinder pressure was regulated using a Victor 0781-1448 SR4J-580 regulator and attached to the fuel tank with a flexible high pressure hose.

A cylinder of compressed oxygen gas was attached to the test stand and used to supply the engine with oxygen to combust the ethanol. To balance the test stand and to follow standard oxygen/fuel practices, the oxygen cylinder was chained on the opposite side of the nitrogen cylinder and ethanol tank. The oxygen cylinder was also secured with a top and bottom chain. The high cylinder pressure was regulated using a Victor 0781-1445 SR4J-540 regulator and attached to the oxygen control valve with a flexible, high pressure, oxygen service cleaned hose.

A 300 cm^3, 5,000 psi rated sample cylinder was used as the fuel tank to hold ethanol fuel during testing. During testing the ethanol was loaded into the top of the tank using a 150 cm^3 graduated plastic syringe through a high pressure ball valve, the valves was then closed, and the system was pressurized using the nitrogen gas. To drain the ethanol tank the nitrogen cylinder's valve was closed and the high pressure needle drain valve located at the lowest point in the system, at the bottom of the ethanol tank, was opened.

Oxygen and ethanol supply copper tubing pigtails were made and used to attach the supply control ball valves to the engine. Pigtails were used for this purpose because a flexible, compact, and inexpensive method was required; other options such as flexible hoses were too expensive or too large.

All the tubes, hoses, cylinders, tanks, valves, actuators, regulators, Venturi flow measurement tubes, pressure transducers, and miscellaneous fittings were selected to have higher service pressures than the pressure required to supply the engine for nominal 1,000 psi combustion chamber pressure. All the plumbing on the oxygen side of the feed system was either purchased cleaned for oxygen service or was cleaned using the procedure in Appendix E. A schematic drawing of the plumbing feed system was drawn and shown in Figure 11.

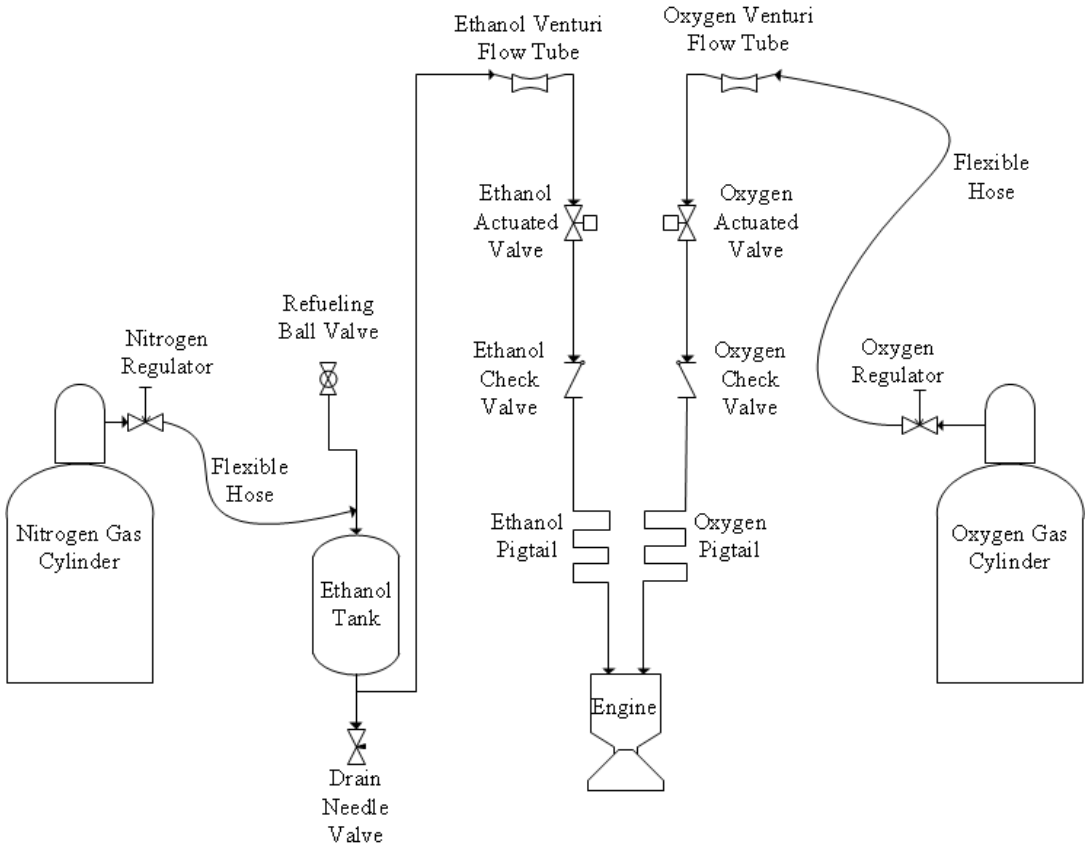

Figure 11: Plumbing diagram of the feed system going into the AARLITE.

3.3 Venturi Flow Measurement Tubes

Measuring the mass flow rates of ethanol and oxygen going into the engine was important. There were several options available for the measurements including Coriolis meters, orifice plates, sonic nozzles, Venturi tubes, and Venturi nozzles. Of the options considered, the Venturi tube was chosen for use measuring both propellants because it was the cheapest, easiest to manufacture, most adaptable, and produced the least head loss. Several design standards were used as points of insight into how to design the Venturi tubes. The standards are published by the American Society of Mechanical Engineers (ASME) and International Organization for Standards (ISO) and were available over the internet (18) (19).

Using the ASME and ISO standards directly was not possible because they were written for Venturi tubes which were at least $\sim 2\ in$ or larger internal diameter (ID). The Venturi tubes required for this research had to be on the order of $0.25\ in$ because of the flow rate required by the engine and the error associated with

the Wika pressure transducers. Two Wika transducers were used and a minimum pressure differential of $30\ psi$ was chosen based on the $\pm 0.5\%$ error of full rated pressure of each $3{,}000\ psi$ transducer. However, the standards were used a guidelines and provided enough details to allow for the design of the Venturi tubes.

The assumed mass flow rate of ethanol was $0.00366 \frac{slug}{s}$ and the mass flow rate of oxygen was $0.00767 \frac{slug}{s}$. Using Bernoulli's equation (assuming no significant height differences) and the mass flow rate relation in Equation 3-2 where $\dot{m}$ is mass flow rate, v is velocity, ρ is density, and A is area:

$$\dot{m} = v\rho A \qquad \textbf{3-2}$$

the entrance and throat diameters of the Venturi tubes were calculated to meet the minimum differential pressure of $30\ psi$ and to be machinable. For ethanol the density was assumed to be constant and for oxygen the density was calculated based on assumed room temperature and feed pressure.

The entrance diameters on both Venturi tubes were designed and machined to $0.248\ in$ because of the $30°$ countersink used. The ethanol throat diameter was $0.070\ in$ and the oxygen throat diameter was $0.125\ in$, resulting in pressure differentials of $42\ psi$ and $125\ psi$ respectively. These critical dimensions and values are summarized in Table 8. The size and position of the pressure taps was based on the ASME and ISO guidelines and what was machinable. The tubes were made of cartridge brass round stock and machined using a lathe and mill. These features were carefully machined and checked using pin gauges, calipers, and/or micrometers. The entrance and exit angles were made using a $30°$ countersink assumed to create the $15°$ entrance half angle dictated by the guidelines.

Table 8: Venturi tube flow measurement design calculation results.

	Oxygen	Ethanol
Mass flow rate $\left(\frac{slug}{s}\right)$	0.00767	0.00366
Entrance diameter (in)	0.248	0.248
Throat diameter (in)	0.125	0.070
Design differential pressure (psi)	125	42

The velocity of the fluids going through the Venturi tubes was checked to make sure the incompressible flow assumption (Mach < 0.3) made by Bernoulli's equation was valid at the throat of the Venturi tubes. The Reynolds numbers at the entrance and throat of the tubes were also checked to make sure the flows were turbulent and in the range suggested by the guidelines.

3.4 Data Acquisition Testing

A series of almost 70 tests were conducted with the engine and feed system to investigate air augmentation. One of the first tests, with no mixing duct and no ring, was presented to show the behavior of the engine during a test fire. The oxygen cylinder regulator was set to $\sim 820\ psi$ and the nitrogen cylinder regulator was set to $\sim 870\ psi$ which resulted in $\sim 400\ psi$ in the combustion chamber. Test #1 in Table 11 was used to make Figure 12 through Figure 17. Plots of the thrust, combustion pressure, differential pressures, and calculated mass flow rates with respect to time were useful in understanding how the system behaves at startup, during steady state, and at shut down. The method of data analysis from the recorded measurements taken by LabView was reviewed and several sanity checks were performed on the data to make sure the values calculated make sense. The data collected using LabView was processed using Microsoft Excel and Matlab.

The data values saved by LabView to Excel were filtered and consolidated using a program written by Ross Gregoriev; the code was inserted in Appendix G for reference. The steady state region of the engine's combustion was the region of interest and was determined by looking at consecutive data points which did not change by more than $5\ psi$ relative to the last data points. Limiting the change between data points to $5\ psi$ was a good method for limiting the standard deviation and getting a good representation of the pertinent data. The phases of the engine's operation were highlighted using the logical comparison method given by equation 3-3. The equation operated using the combustion pressure which was stored in column "M" in the Excel file. The idle/off, startup, steady state, and shut down phases of the engine's operation were highlighted by iteration the logic statement through all of the combustion pressure data. The corresponding ethanol Venturi pressures, oxygen Venturi pressures, thrust, and time data were determined by using the highlighted rows of combustion pressure. The ethanol and oxygen Venturi data points were recorded by sensors which were several feet away from the combustion chamber and for the ethanol

Venturi that was especially important because the ethanol would run through the Venturi and transition to nitrogen before the engine would shut down. To handle change in fluid, the Venturi pressure data region of interest was shifted up about three rows.

$$= IF(ABS(M3 - M2) > 5, M2, "0") \quad \textbf{3-3}$$

Following the data analysis procedure yielded ~ 0.6 to $\sim 1\ s$ of steady state combustion data throughout all the tests. The mean and standard deviation were then calculated for the highlighted steady state regions. The standard deviation was used as a measure of the error for each corresponding mean value.

3.4.1 Thrust

The total thrust results are shown in Figure 12 versus time (in this case there was no duct so the values are just the engine's thrust). The average thrust was plotted on top of the actual thrust curve in order to show how the two compare.

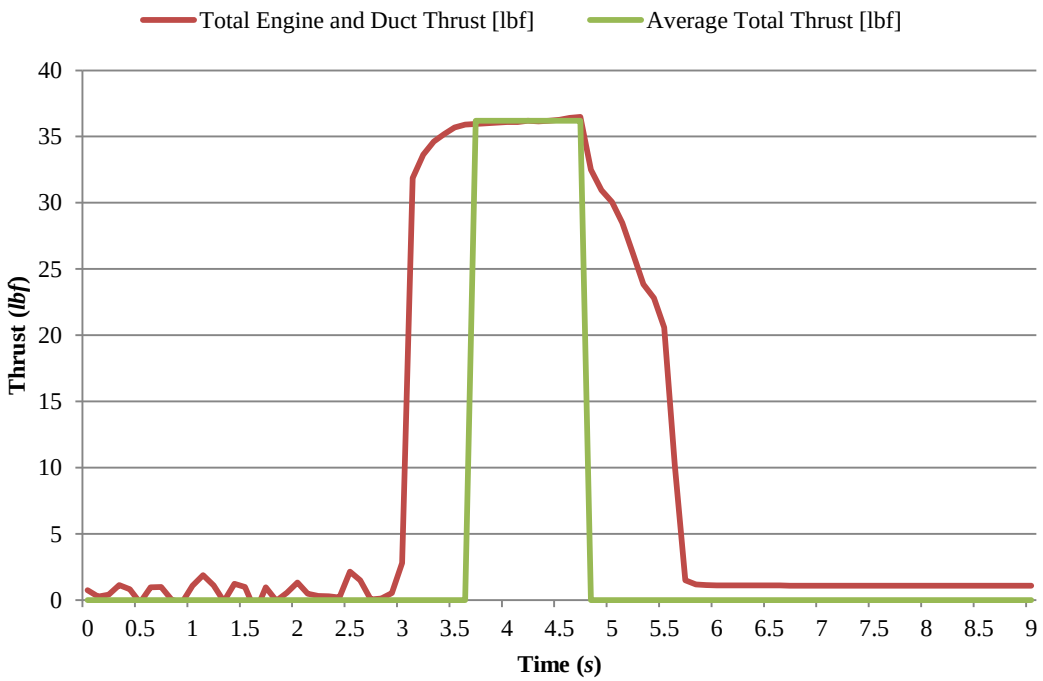

Figure 12: Plot of the total thrust profile of the engine firing at about $400\ psi$ chamber pressure. The red line shows the total thrust load cell output and the green line shows the average used for analysis.

3.4.2 Pressure and Mass Flow Rate

The pressure transducers placed throughout the feed system and attached to the combustion chamber read the static pressures of the various fluids. The pressure profiles for the same test as the thrust profile in Figure 12 are presented.

The chamber pressure transducer functioned well. The chamber pressure results for the engine were displayed in Figure 13. The average chamber pressure and standard deviation were calculated by looking at the chamber pressure curve and considering the data points which were in the steady state region of the curve. The average pressure was plotted on top of the actual pressure curve in order to show how the two compare.

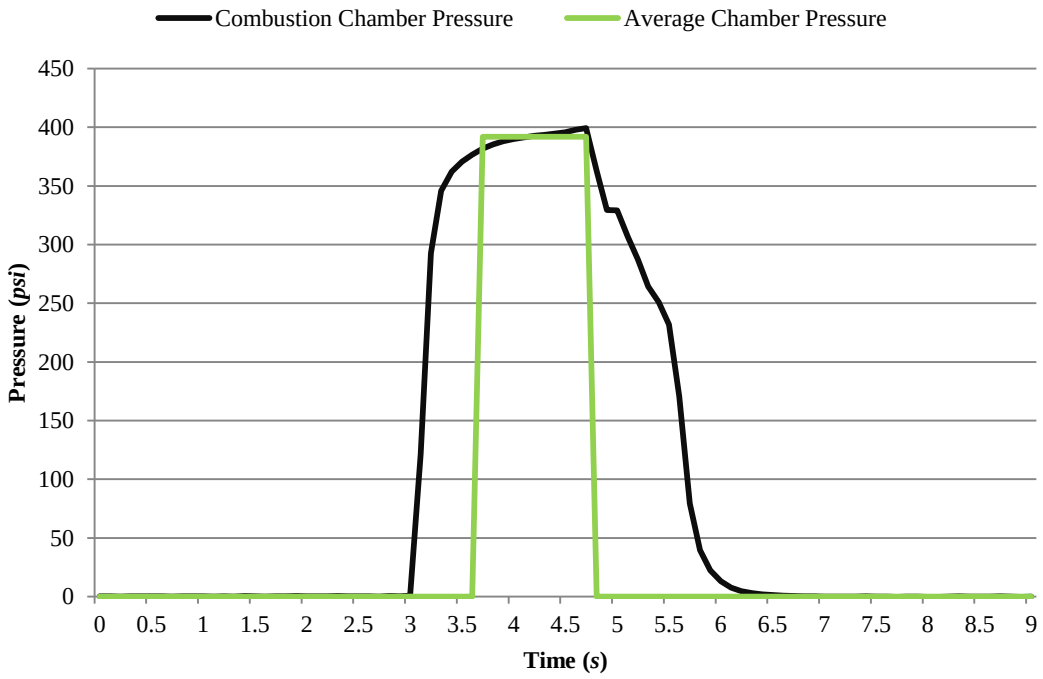

Figure 13: Plot of the chamber pressure profile of the engine firing at about $400\ psi$. The black line shows the measured chamber pressure and the green line shows the average used for analysis.

The oxygen Venturi tube pressure transducers functioned perfectly. The pressure results were displayed in Figure 14. The differential pressure was calculated by subtracting the lower pressure reading from the higher pressure reading, and this differential was then used to calculate the mass flow rate of oxygen.

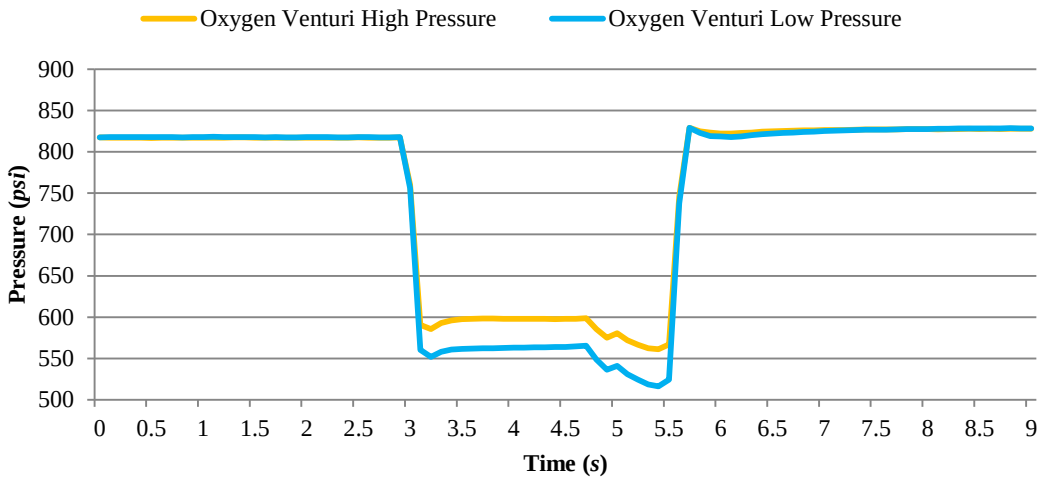

Figure 14: Plot of the oxygen Venturi flow tube from the engine firing at about $400\,psi$ chamber pressure. The blue line shows the low pressure trace measured at the throat of the Venturi tube and the orange line shows the high pressure trace measured at the inlet section of the Venturi tube.

The ethanol Venturi tube pressure transducers functioned perfectly. The pressure results were displayed in Figure 15. The differential pressure was calculated by subtracting the lower pressure reading from the higher pressure reading, and this differential was then used to calculate the mass flow rate of ethanol or of nitrogen when the system was cold flow testing.

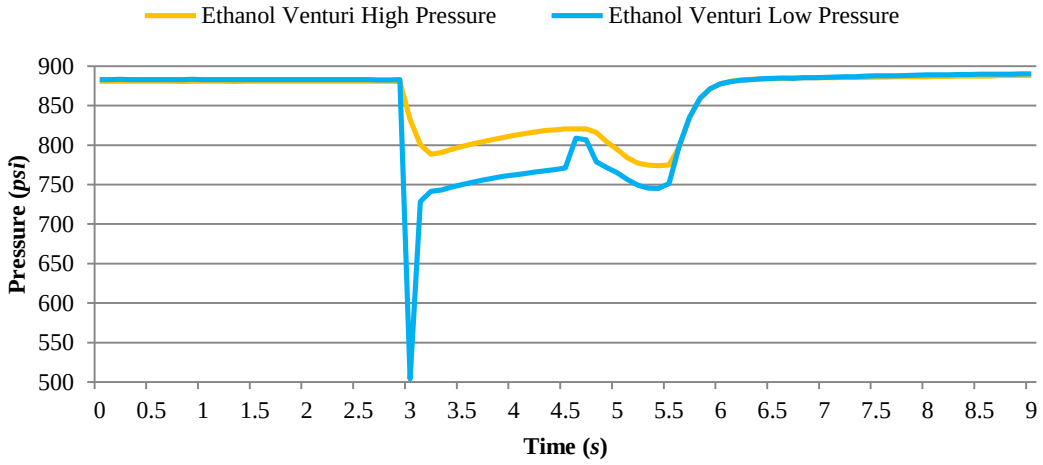

Figure 15: Plot of the ethanol Venturi flow tube from the engine firing at about $400\,psi$ chamber pressure. The blue line shows the low pressure trace measured at the throat of the Venturi tube and the orange line shows the high pressure trace measured at the inlet section of the Venturi tube.

The pressure profiles shown in Figure 14 and Figure 15 were used to calculate the respective mass flow rates of the propellants and are shown in Figure 16 and Figure 17. Using Bernoulli's equation assuming incompressible fluids, and assuming the vertical change in the flow was negligible the mass flow rate was calculated. For oxygen and during cold flow testing for nitrogen, the density of the gases was calculated using the higher pressure measurement from the Venturi tubes and assumed the gases were at the same temperature as the ambient environment. The density of ethanol was assumed to be constant $0.789 \frac{kg}{L}$.

The mass flow rates calculated from the differential pressure do not go all the way to zero because after the transducers were calibrated and zeroed using LabView, they drifted a little bit over time and they did not output exactly the same signal when pressurized to the same initial pressure. Thus the mass flow rates did not go to zero, but when the engine was not firing and the valves were shut the mass flow was obviously zero, so the lines showing the average mass flow were set to zero.

The average mass flow rates and the respective standard deviations were found by looking at the chamber pressure curve and considering the data points which were in the steady state region of the curve. The average mass flow rates were plotted on top of the actual mass flow rate curves in order to show how the two compare.

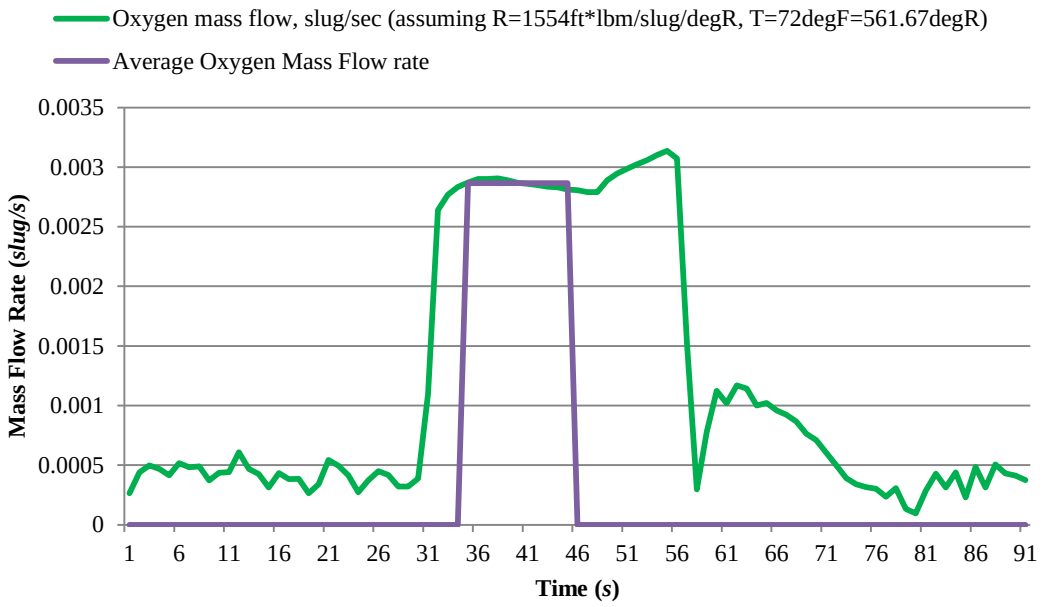

Figure 16: Plot of the mass flow rate of oxygen when chamber pressure was about 400 *psi*. The green line shows the oxygen mass flow rate calculated from the measured differential pressure and the purple line shows the average oxygen mass flow rate used for analysis.

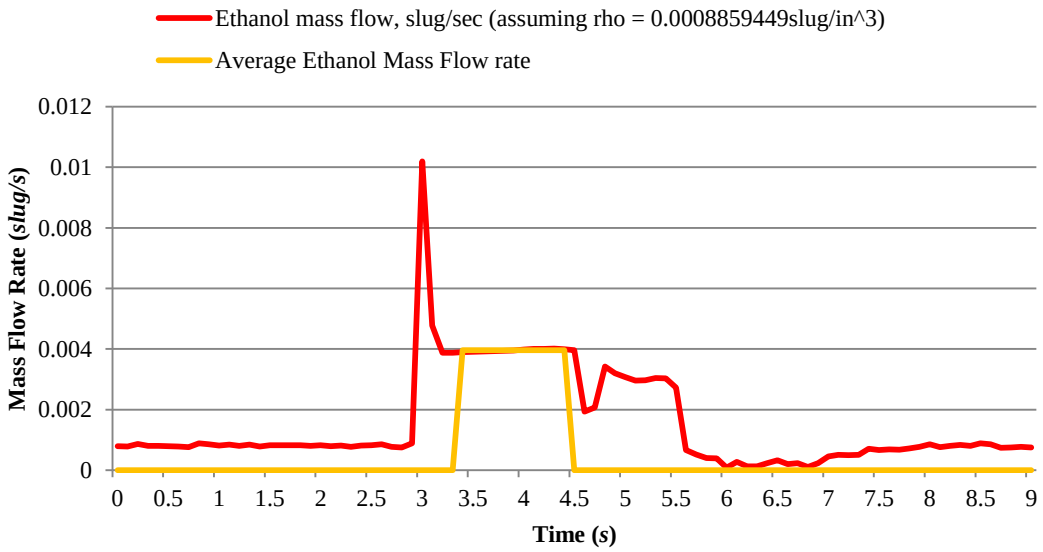

Figure 17: Plot of the mass flow rate of ethanol when chamber pressure was about 400 *psi*. The red line shows the ethanol mass flow rate calculated from the measured differential pressure and the orange line shows the average ethanol mass flow rate used for analysis.

3.4.3 Error and Sanity Check

The thrust profile and pressure profiles shown in Figure 12 through Figure 17 are reasonable and agree with each other. Furthermore, the thrust and pressure profiles behaved in similar fashions for the test displayed and all the tests not shown.

A check of the agreement between all the sensors and theoretical analysis was conducted using test #43 in Table 12. The thrust of the engine during the test was $51.7\ lbf$. The measured combustion pressure was used to calculate a theoretical engine thrust which was $52.6\ lbf$. The percent difference was a reasonable 1.34%.

The majority of test fires were video recorded and the footage from one test was used to get an approximate burn time. The burn time was then used to get an average ethanol mass flow rate and check against the average mass flow rate calculated using the differential pressure measured with the Venturi flow tube. The time found using the video footage was not accurate since it involved guessing when the ethanol started to flow and when it stopped. Thus this was a sanity check to make sure the differential pressure measurement yields mass flow rates which are in the proper range.

Each run used $150mL$ of ethanol in the fuel tank and the density of ethanol is $0.789\frac{kg}{L}$. Equation 3-3 calculates the mass of ethanol:

$$0.150L * 0.789\frac{kg}{L} = 0.118\ kg \qquad \textbf{3-4}$$

Footage from test #1 while the engine had ethanol in the combustion chamber and was combusting properly, showed the plume for about $2.57\ s$. Equation 3-5 calculates the average mass flow rate from the video footage:

$$\frac{0.118\ kg}{2.57s} = 0.0461\frac{kg}{s} = 0.00316\frac{slug}{s} \qquad \textbf{3-5}$$

The average differential pressure calculated mass flow rate of ethanol during steady state combustion for that test was $0.00396\frac{slug}{s}$. There is approximately 20% difference between $0.00396\frac{slug}{s}$ and $0.00316\frac{slug}{s}$. The percent difference is reasonable and means the differential pressure calculated mass flow rate of

ethanol is in the correct range of values and no significant errors exist. Furthermore, since the Venturi tubes were designed using the same process the oxygen Venturi mass flow rate calculations inspired more confidence as well.

4. Test Results

Plots of the thrust and mass flow rate were made to help interpret the data. The plots are organized by total thrust, mixing duct thrust, primary mass flow rate, and mass flow rate ratio and pressure ratios. The total thrust and mixing duct thrust sections are divided into several subsections comparing mixing duct results while holding the rings constant, comparing rings while holding mixing ducts constant, and comparing mixing ducts while holding rings constant and dividing thrust by combustion pressure. The mixing duct sections has an additional subsection which compares the short and long duct thrusts divided by the internal area of the ducts. The majority of plots have thrust in pound force on the vertical axis and pressure sets on the horizontal axis. The pressure sets were assembled based on the pressures the supply cylinder regulators were set to before each test. Some inconsistencies existed with the regulators' function, but for all the plots showing pressure sets on the horizontal axis the test cases are organized so that the combustion pressure generally increases with set number. The pressure sets 1 and 2 are $\sim 400\ psi$, $3 \sim 500\ psi$, $4 \sim 550\ psi$, and 5 and $6 \sim 680\ psi$.

For the tests around $680\ psi$ only the long duct and ring configurations were used. The diverging and short ducts were not used and only one test was performed with no mixing duct and no ring. Preliminary analysis of the lower pressure tests showed the long duct was the one to focus on. If all the possible cases were tested the engine may have malfunctioned and become unusable. Thus for several of the figures in this section the last two pressure sets will only show the long duct cases and/or the no duct, no ring case.

The tests with mixing ducts performed worse than the tests with no mixing duct and the engine was consistent across all the tests. The mixing ducts were the only significant differences which caused the lower performance. However the mixing duct load cell registered positive thrust from the short and long ducts, which means that there must be another factor to account for the lower performance. Put simply the addition of the mixing ducts created drag on the engine which pulled it downward. Equation 4-1 is a modified version of Equation 3-1. The D_{duct} term represents the drag created on the engine when the mixing ducts are attached and why the total thrust is less in the ducted cases even though the short and long ducts produce positive thrust.

$$F_{tot} = F_{eng} + F_{duct} + D_{duct} \quad \text{4-1}$$

4.1 Total Thrust Plots

For each test, the total thrust was the physical summation of the engine and mixing duct thrusts. The total thrust was recorded directly using the $200\ lbf$ AmCell load cell and the results are plotted with using multiple methods to help explain the tests. Based on the preliminary tests, the engine was expected to produce between $\sim 40 - 70\ lbf$ of thrust depending on the combustion pressure between $\sim 400 - 700\ psi$. In theory when the nozzle is equipped with the C-ring and the diverging duct is attached, the system is expected to produce the greatest total thrust because the C-ring will cause increased entrainment and afterburning, and the diverging duct will expand the two high speed flows.

4.1.1 Total Thrust: Comparing Duct Cases

Figure 18, Figure 19, and Figure 20 show plots of the total thrust of the system at six different combustion pressure sets. The respective combustion pressure sets were based on how the oxygen and nitrogen cylinder regulators were set (if the regulators were set to be equal or $\sim 50\ psi$ lower on the oxygen regulator). Depending on how full the cylinders were, the combustion pressures were affected. Some test cases may not fit well in the respective pressure set, but they were grouped in this fashion because it was a simple way to know the regulators' pressures. The plots show the thrust of the system with each of the four duct configurations and each separate plot shows the results of the three different ring configurations. The test number and combustion pressures were noted either above or on the respective bars of the graph.

The important thing to note about Figure 18, Figure 19, and Figure 20 was that they show how the total thrust behaves with respect to changing duct configuration. It seemed that the total thrust was generally best with no duct, but the long duct case was closest to the performance of the engine without a duct. The short duct was not as good as the long duct and the diverging duct consistently produced the least total thrust.

Figure 18 shows that for each of the pressure sets the non-ducted configuration produced more thrust or the same thrust as some of the long duct cases. The diverging duct case (test #10) produced a total thrust of $34.45\ lbf$, the short duct case (test #11) produced $34.93\ lbf$, and the long duct case (test #12) produced $35.53\ lbf$. The no duct case (test #1) was tested to the same conditions as tests #10, #11, and #12, but

produced 36.18 lbf of total thrust. Pressure set 3 shows that the long duct case did better than the no duct case; however the combustion pressure difference was large such that it could account for the difference in total thrust. The small error bars plotted on each bar represent one standard deviation of the data during the steady state region of the thrust curve.

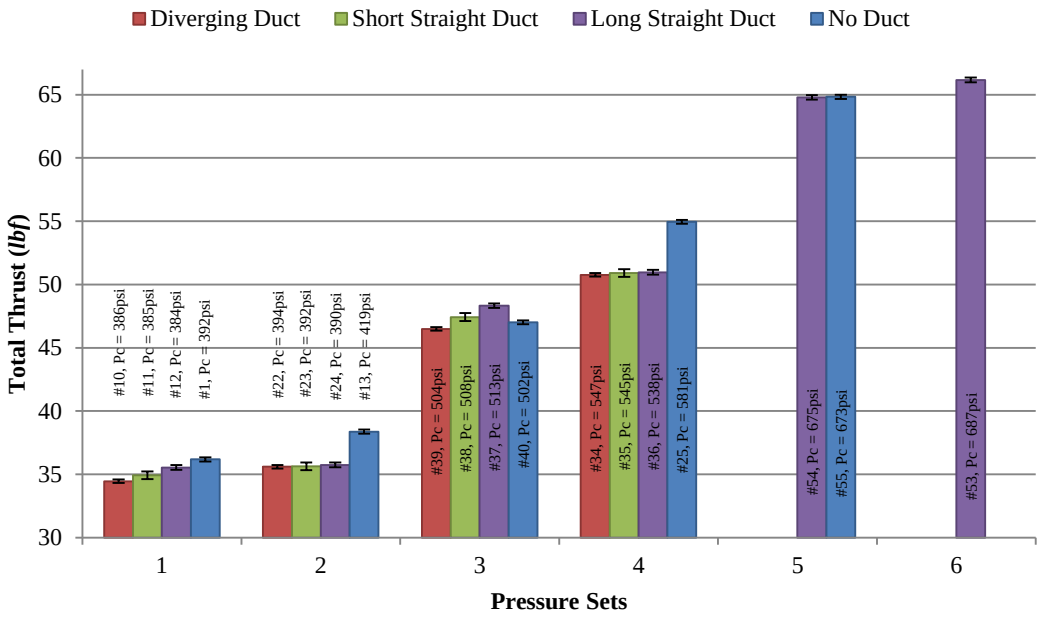

Figure 18: No ring, total thrust for different ducts at multiple combustion pressures.

Figure 19 shows similar values as Figure 18, however it was for the solid ring configuration. At the low 420 psi combustion pressure sets the no duct cases performed better, but as the combustion pressure grew the differences in total thrust diminished. The high differences in combustion pressure could account for the significant total thrust differences in pressure sets 3 and 4.

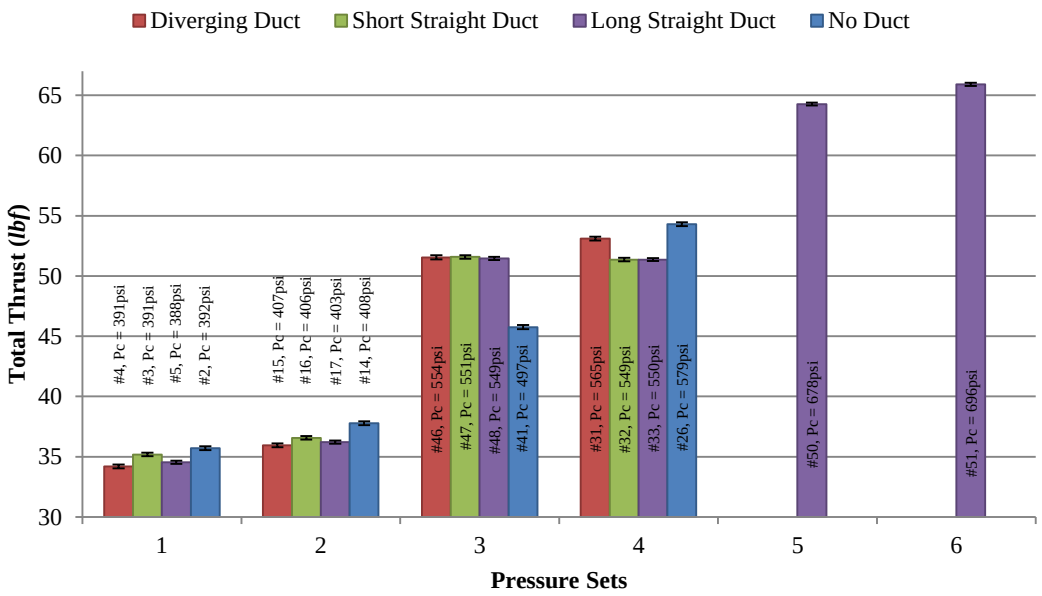

Figure 19: Solid ring, total thrust for different ducts at multiple combustion pressures.

Figure 20 shows that the no duct configuration again was best compared to all the other configurations in the figure. In pressure set 3 there is a significant difference between the no duct case and the other three cases, with the no duct case being the worst. This upset in the previous pattern is attributed to the combustion pressure differences. In pressure set 4 the combustion pressures are within a standard deviation $(\sim 6\ psi)$ and the total thrust pattern is very similar to pressure set 1 and 2.

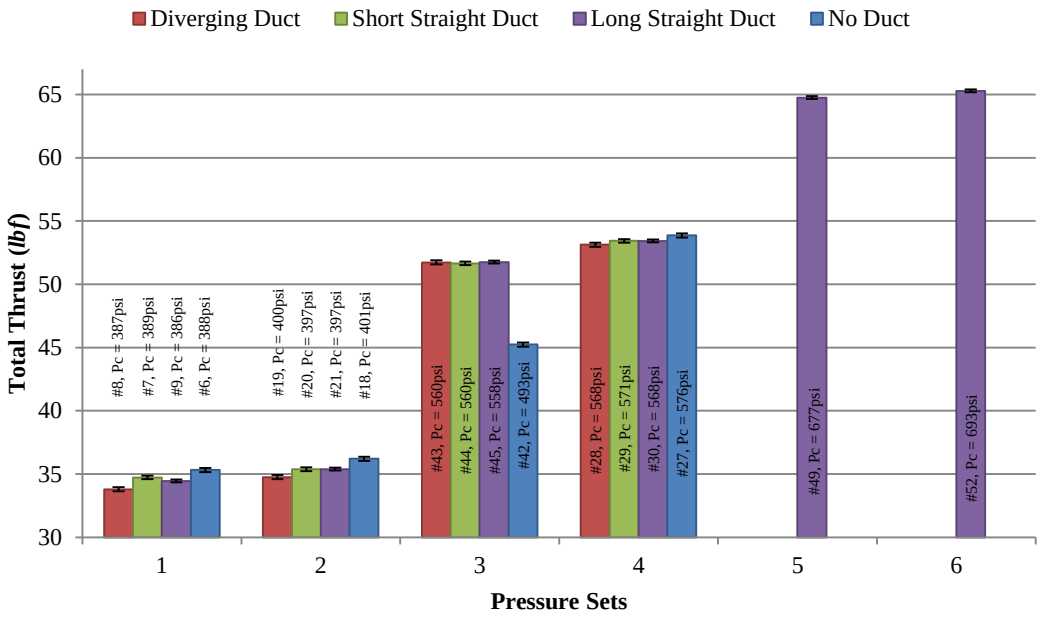

Figure 20: C-ring, total thrust for different ducts at multiple combustion pressures.

Throughout Figure 18, Figure 19, and Figure 20 the different rings at the exit of the nozzle did not cause a change to the pattern of how each duct configuration performed. Also as the combustion pressure grew the differences in thrust between the different mixing ducts decreased. As the combustion pressure increased and the nozzle became less over-expanded, the differences between the total thrust of each configuration decreased.

The pressure of the over-expanded primary flow was lower than ambient which pulled ambient air like a vacuum cleaner pulls air. As the combustion pressure increased, the exit pressure also increased and the vacuum pulling the air decreased. The reduction of secondary flow smaller thrust differences between the mixing ducts. If the primary flow was optimally expanded, the thrust differences between the mixing ducts could be insignificant. If the primary flow was under-expanded, the thrust differences would return and they might be reversed. The diverging duct would produce the most total thrust and the long duct would produce the least total thrust.

4.1.2 Total Thrust: Comparing Ring Cases

Figure 21 through Figure 24 show the total thrust of the system at six different combustion pressure sets in the same fashion as Section 4.1.1. However, each figure shows the total thrust of the system for all of the

three ring configurations while the mixing duct is held constant for each figure. The test numbers and combustion pressures are noted either above or on the respective thrust bars.

The plots show how the total thrust behaves with respect to changing ring configuration. The trends are interesting and show the total thrust is highest in the no ring condition, a little less in the solid ring, and least in the C-ring.

Figure 21 shows tests which had consistent combustion chamber pressures within each pressure group. The consistency of the chamber pressure allows for the differences in thrust to be attributed to the different rings which were tested. The no ring case performs better than the solid and C-rings, and the solid ring does better than the C-ring. The seam created by the cavity retaining nut could have also tripped the flow when testing the solid and C-rings. Note, that Figure 21 is the no duct case and this means the total thrust is equal to the engine thrust since there is no duct thrust. Whenever a no duct case is shown the total and engine thrusts are equivalent.

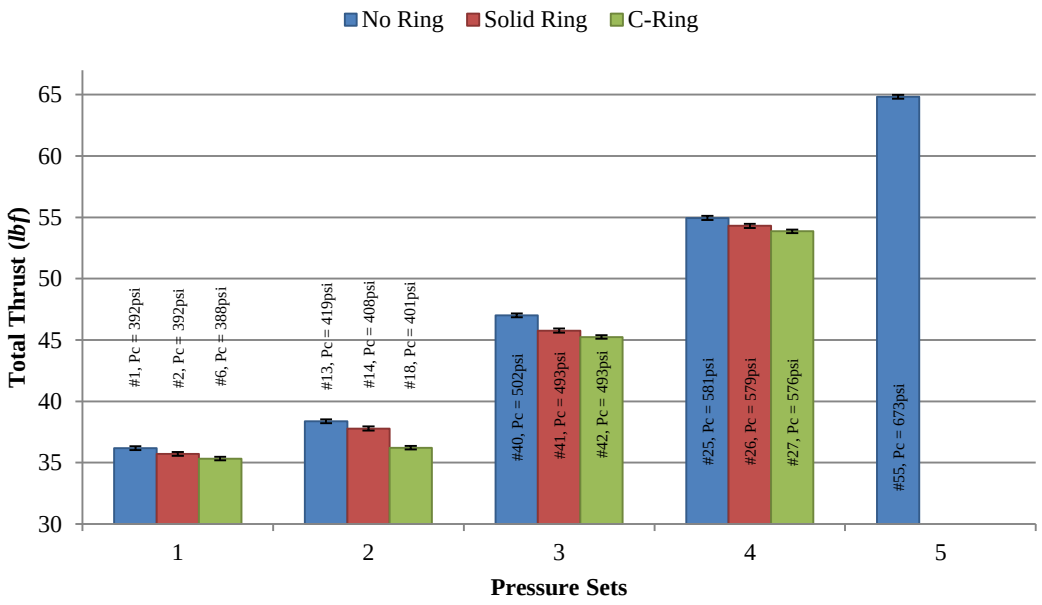

Figure 21: No duct, total thrust for different nozzle configurations at multiple combustion pressures.

Figure 22 shows that the total thrust for the diverging duct configuration and for the first pressure set has a negative slope across no ring, solid ring, and C-ring similar to Figure 21. The other pressure groups however have a different behavior with the no ring case showing that the total thrust is less than the solid

ring, C-ring, or both solid and C-ring cases. The difference in the total thrust could be caused by the significant difference in combustion pressures since the standard deviation of the combustion pressure is around 6 psi and the various cases which do not show a negative slope across no ring, solid ring, and C-ring are significantly more than 12 psi apart.

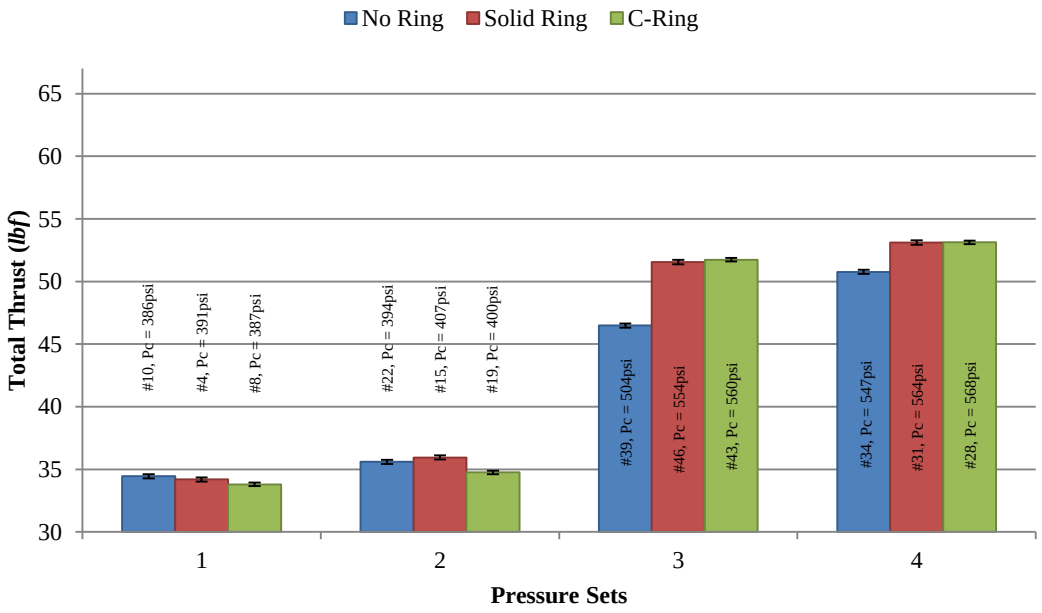

Figure 22: Diverging duct, total thrust for different nozzle configurations at multiple combustion pressures.

Figure 23 shows the short duct total thrust. The first and second pressure sets show similar trends where the solid ring produces the greatest thrust. However, for set 1 the difference between the three rings is small and within the error bars created from the standard deviation ($\sim 0.24\ lbf$). Set 3 shows the solid ring and C-ring producing the same thrust and significantly better than the no ring. Set 4 shows the C-ring produces the greatest total thrust, the solid ring less, and the no ring least. The combustion pressure is significantly different throughout sets 3 and 4, and can account for the greater thrust of the solid and C-rings.

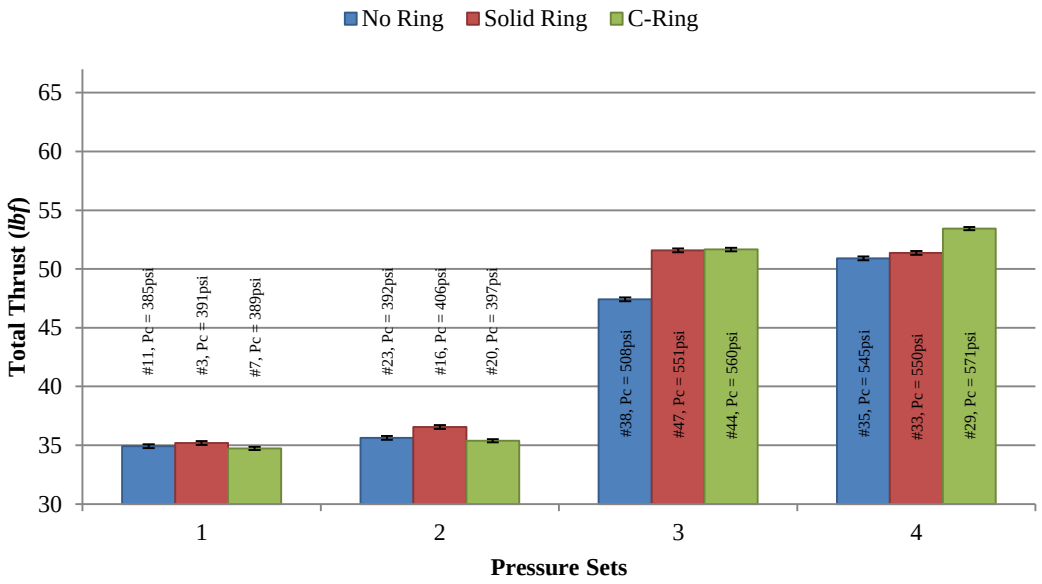

Figure 23: Short duct, total thrust for different nozzle configurations at multiple combustion pressures.

Figure 24 shows the total thrust of the long duct. This figure, relative to the previous two figures, has some of the more consistent combustion pressures within each pressure set. Sets 1 and 6 show the no ring case produces the most total thrust while sets 3 and 4 show the C-ring produces the most total thrust. In set 5 the combustion pressures are almost exactly $677\ psi$ between the three ring cases and the no ring and C-ring cases produce the same thrust, the solid ring about a pound less thrust. The solid ring produces the most total thrust in set 2, otherwise the solid ring is between the no ring and C-ring thrust outputs.

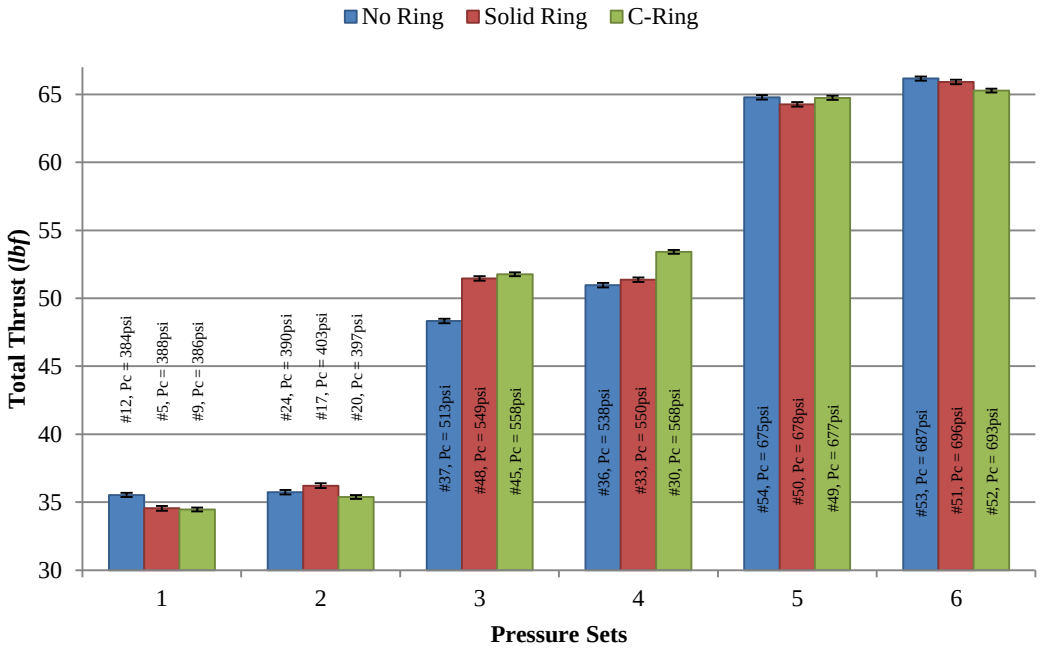

Figure 24: Long duct, total thrust for different nozzle configurations at multiple combustion pressures.

4.1.3 Total Thrust: Duct Cases Divided by Combustion Pressure and Throat Area

Figure 25 shows the total thrust divided by the combustion pressure and nozzle throat area for the no ring nozzle configuration. The result is a non-dimensional value which indicates better performance with a higher value. Dividing the total thrust by combustion pressure has helped level the figures so that differences between tests in combustion pressure are not as significant. Dividing by nozzle throat area then non-dimensionalizes the values. With no ring, the long duct case has the highest area value in four of five pressure sets. The sixth pressure set only has one bar because the longevity of the engine was at risk so only a few of the total possible configurations were tested at the maximum combustion pressure of $\sim 680\ psi$. The same explanation applies to the two bars in the fifth pressure set. The no duct case gives the second best performance after the long duct. The short and diverging duct cases follow the same trends as seen in the previous total thrust figures. At a combustion pressure $\sim 544\ psi$ (tests #34, #35, and #36) the total thrust between the diverging, short, and long duct cases respectively was about the same $\sim 50.9\ lbf$. In the same pressure set 4, the no duct case (test #25) produced a total thrust of $54.95\ lbf$, but the test's combustion pressure was $\sim 38\ psi$ greater then the other three test cases. When the total thrust of these four tests was divided by combustion pressure (as seen in Figure 25), the long duct case did best by having the

greatest thrust per pressure per area value, 1.517. The no duct case had a value of 1.514, the short duct had a value of 1.496, and the diverging duct had the lowest value of 1.486. The ~387 psi tests in pressure set 1 (tests #10, #11, #12, and #1) had the same pattern as the $\sim 544\ psi$ tests (#34, #35, #36, and #25), however the thrust per pressure per area values in the $\sim 387\ psi$ combustion pressure tests had a greater spread, a greater difference between the minimum and maximum area values. The greater difference between thrust per pressure values at $\sim 387\ psi$ was because the combustion pressure was lowest and the nozzle exit pressure was lowest (most over-expanded) so the amount of secondary flow pulled in and the drag on the engine was greatest which exaggerated the differences between the mixing duct configurations.

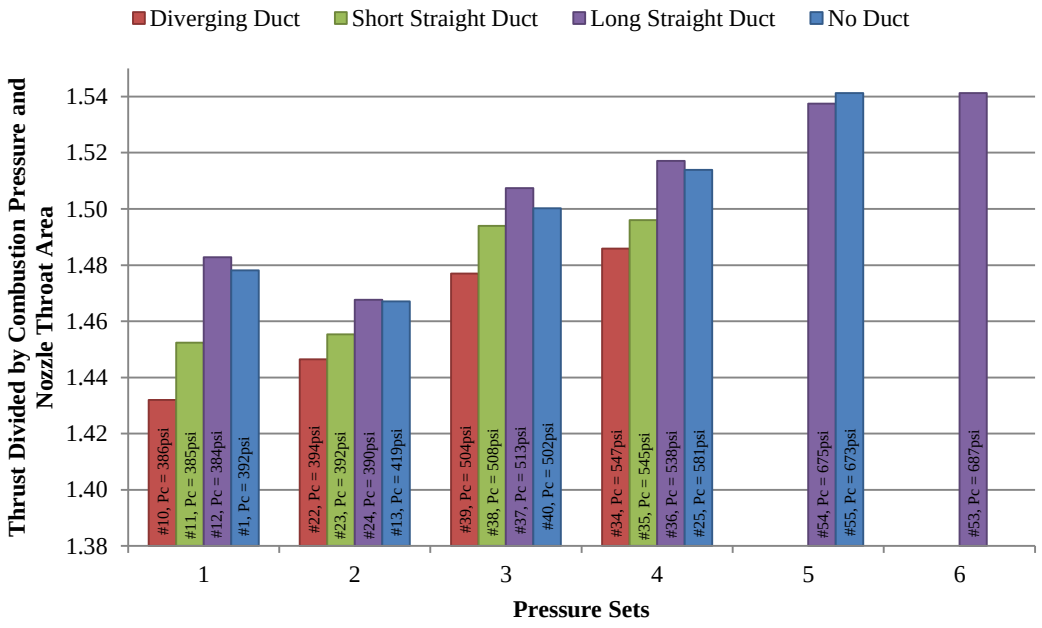

Figure 25: No ring, total thrust divided by combustion pressure and nozzle throat area for different mixing ducts at multiple combustion pressures.

Figure 26 shows the solid ring nozzle configuration and has greater variation than Figure 25. The no duct case has the highest area value in the first two sets. In set 3 the long duct has the best area value and the no duct has the worst. Set 4 is different than all the other sets presented in this section. The diverging duct has the highest area value, the no duct case is close, and the short and long ducts are less than the no duct but they are almost the same to each other. The reversal of performance of the no duct case in the first two sets in Figure 26 compared to the trend in Figure 25 could be due to the nozzle being more over-expanded in

the first two pressure sets and the solid ring causing the flow to be more turbulent which would cause the engine's thrust to be lower, entrain more secondary, reducing the secondary flow's pressure, and pulling the system downward when the ducts were attached. As the combustion pressure increased the turbulent effect of the solid ring did not have the same influence and seen in set 3 the trend in Figure 25 was reestablished.

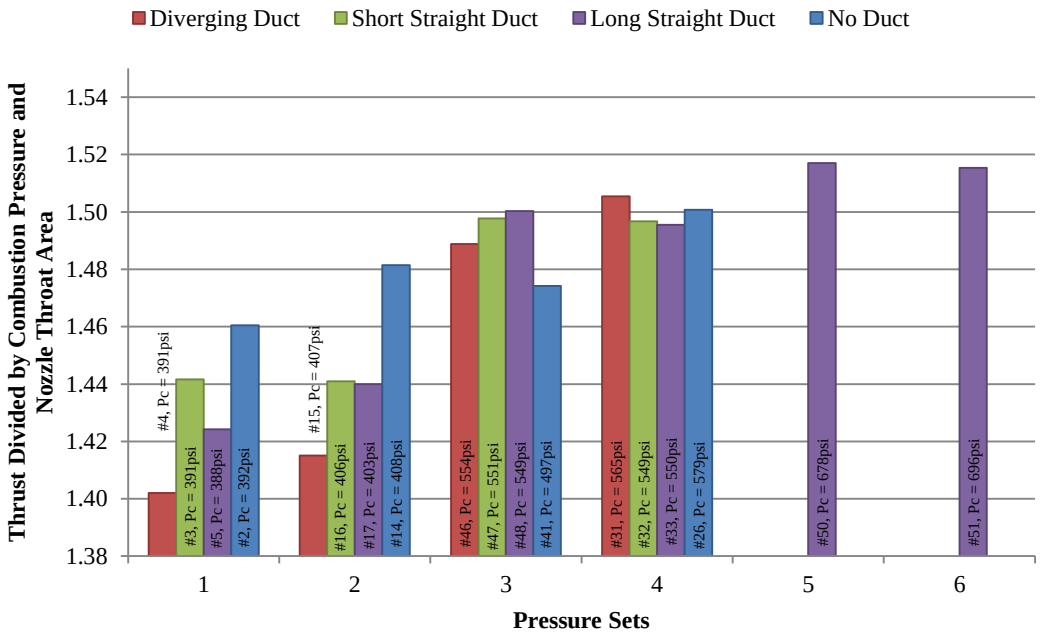

Figure 26: Solid ring, total thrust divided by combustion pressure and nozzle throat area for different mixing ducts at multiple combustion pressures.

Figure 27 shows the C-ring nozzle configuration. The pressure sets show very similar behavior to Figure 26. The no duct case has the highest area value in the first two sets, but as the combustion pressure increases then the long duct and short duct clearly overtake the no duct case. The diverging duct even performs better than the no duct case in set 3. The C-ring causes the primary flow be to much more turbulent in the first two pressure sets when the nozzle is the most over-expanded. The turbulence lowers the total thrust when a mixing duct is attached because there is greater entrain of secondary flow, higher secondary flow velocity and lower pressure which pulls the system downward. But as the combustion pressure increases the turbulent effect of the C-ring does not have the same influence, set 3 and 4 show similar trends to Figure 25. If sets 5 and 6 were tested again to include the diverging and short ducts then the trends of Figure 25 are hypothesized to occur.

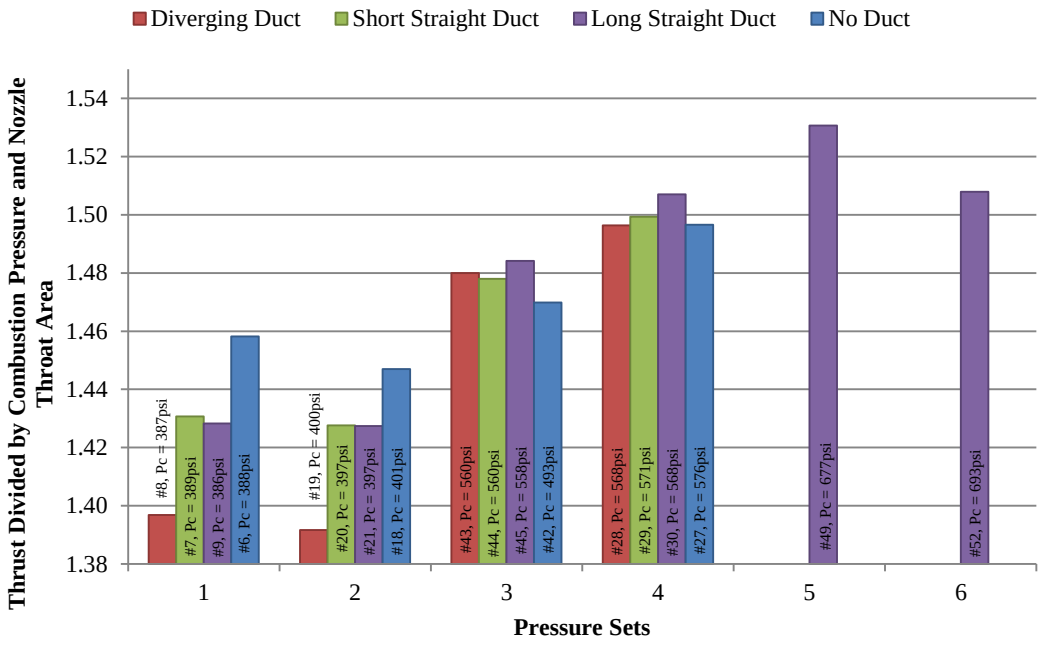

Figure 27: C- ring, total thrust divided by combustion pressure and nozzle throat area for different mixing ducts at multiple combustion pressures.

In Figure 25, Figure 26, and Figure 27 the total thrust per pressure values all increase as combustion pressure increases. As combustion pressure increases the combustion efficiency increases releasing more of the ethanol's energy and the nozzle is closer to optimal expansion, thus the total thrust per pressure values increase.

4.2 Duct Thrust Plots

The mixing duct thrust was measured directly with the 25 lbf AmCell load cell connected underneath the engine support rail (but above the engine) and to the mixing duct clamp frame. The three mixing ducts were clamped with the mixing duct clamp frame below the engine and the signal from the 25 lbf load cell was zeroed in the LabView program to account for the weight of the frame and mixing ducts. The mixing ducts are expected to produce thrust between $1 - 8\ lbf$.

4.2.1 Duct Thrust: Comparing Duct Cases

Figure 28 with no ring configuration, the diverging duct always gives a negative thrust with little change as combustion pressure increases. The short duct also changes little with combustion pressure changes, but it

does show a slight positive increase when the pressure increases. The long duct gives the greatest positive thrust and it does vary with pressure.

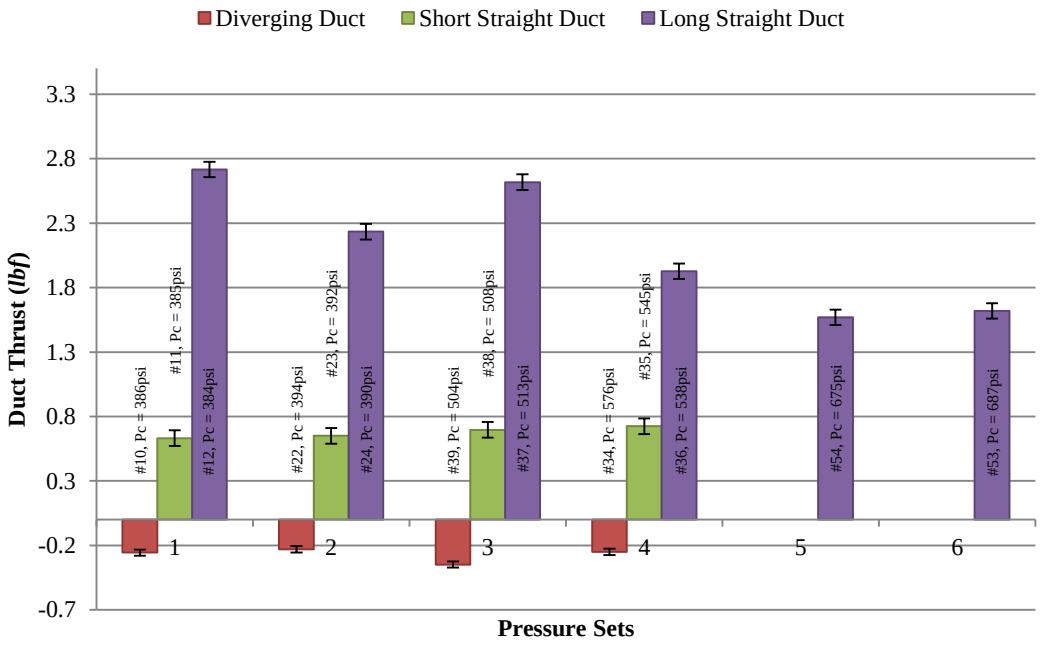

Figure 28: No ring, duct thrust at multiple combustion pressures.

Figure 29 with a solid ring, the long duct acts the same as in Figure 28. However, the diverging duct shows a different behavior; it started at about -0.7 lbf and increases positively as combustion pressure increases. The short duct does the opposite, as pressure increases the thrust decreases.

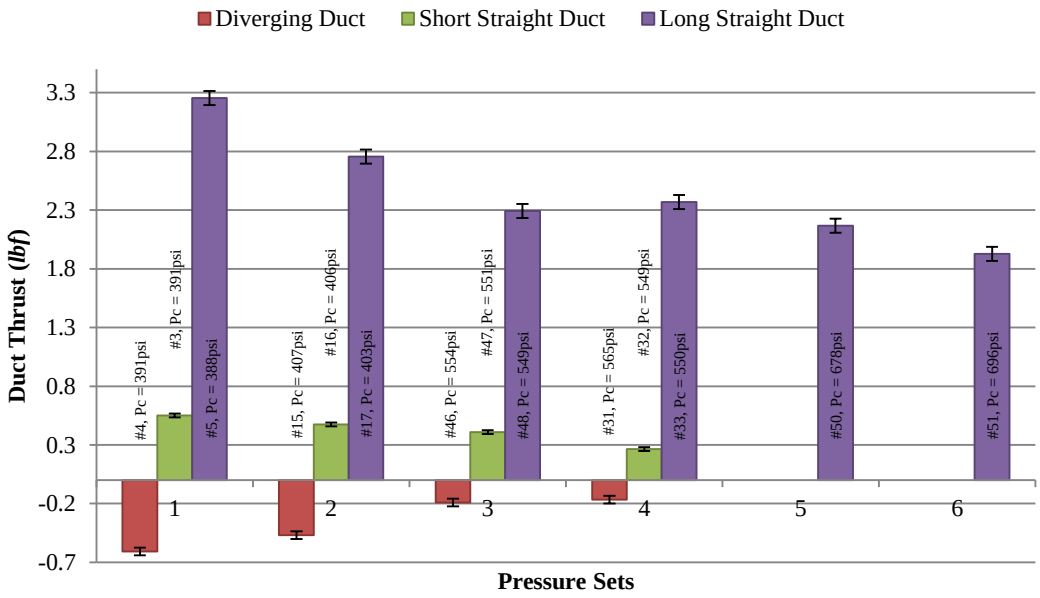

Figure 29: Solid ring, duct thrust at multiple combustion pressures.

Figure 30 is very similar to Figure 29, the long and short ducts thrusts decrease as combustion pressure increases and the diverging duct's performance improves as the pressure increases. Although it should be noted the short duct barely changes with changes in combustion pressure, the short duct's thrust remains flat. Another note to consider is that the long duct produces the most mixing duct thrust by a large margin, however, the long duct also weighs the greatest amount out of all the mixing ducts.

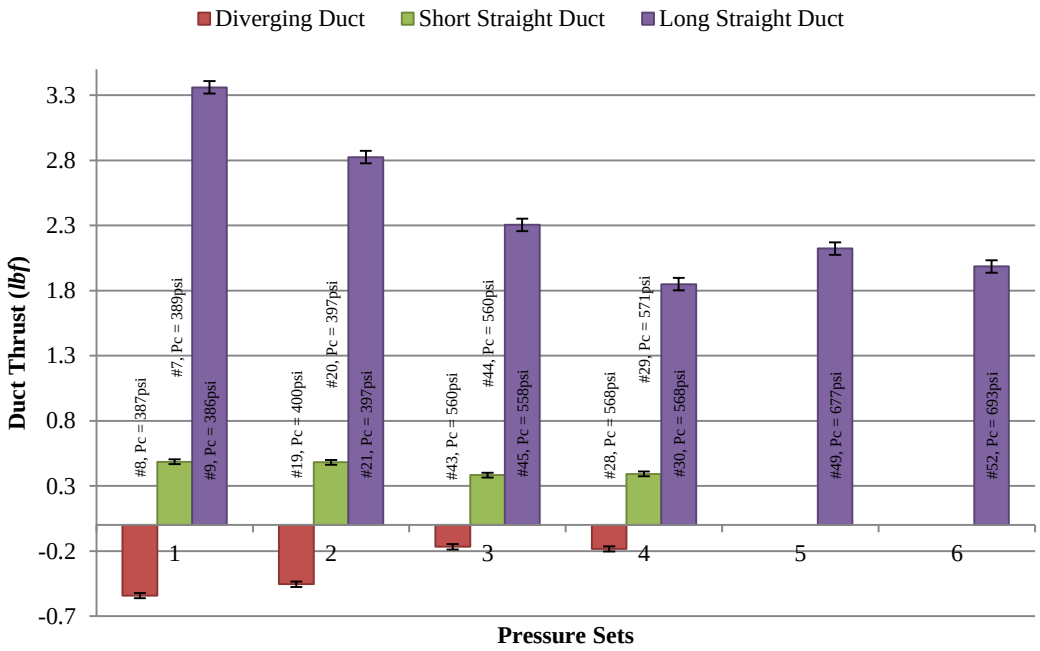

Figure 30: C-ring, duct thrust at multiple combustion pressures.

4.2.2 Duct Thrust: Comparing Ring Cases

The three ring cases are compared relative to each duct. The measured duct thrusts for each duct case, ring case and the engine's combustion chamber pressure. Figure 31 shows the diverging duct measured thrusts at the various combustion pressures and ring configurations. In the first two pressure sets the solid ring does the worst, with the C-ring almost as bad. The no ring in the first two sets does better. However, the last two pressure sets the solid and C-ring do better than the no ring.

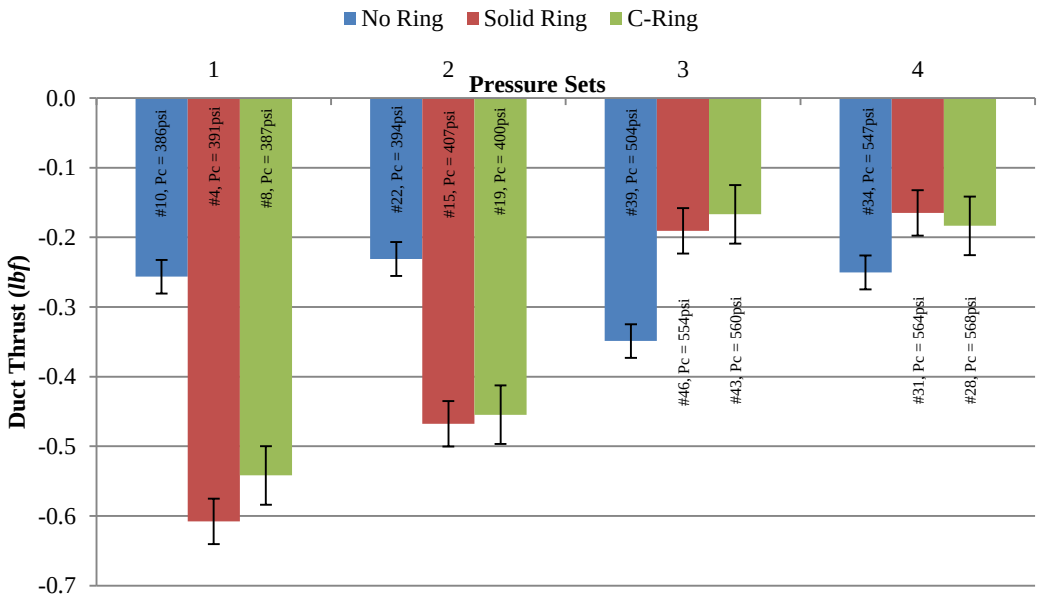

Figure 31: Diverging duct thrust for different nozzle configurations at multiple combustion pressures.

The duct thrust for the short duct is displayed in Figure 32. The three ring cases are compared and throughout the four pressure sets the no ring case does the best, the solid ring does better or the same as the C-ring in the first three sets. But in the fourth set the C-ring case registered more thrust on the mixing duct than the solid ring case. The greater thrust in the C-ring case of set 4 could be due to the higher combustion pressure.

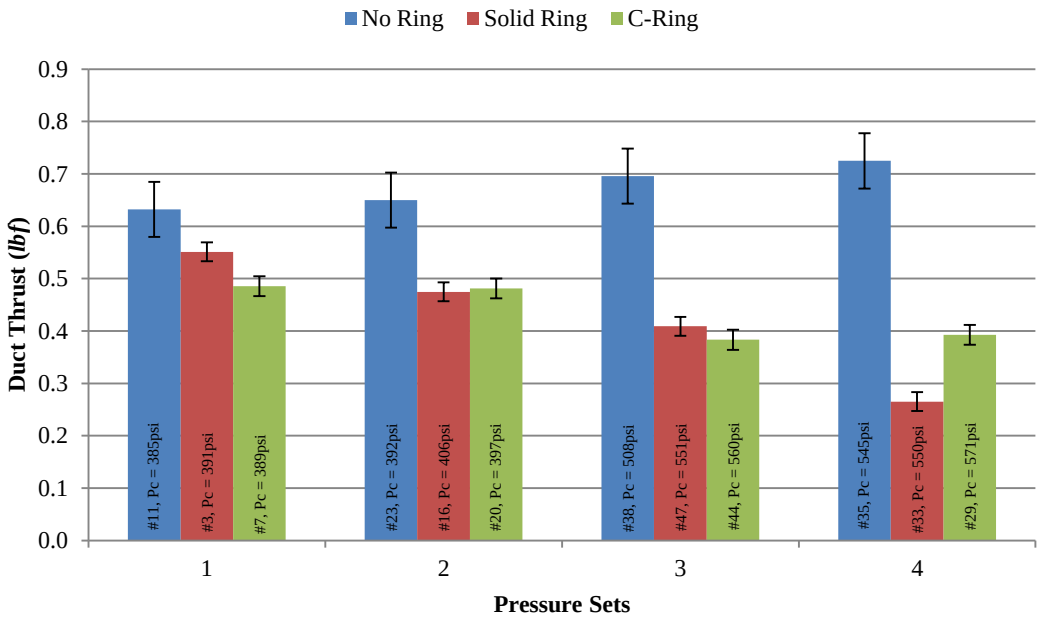

Figure 32: Short duct thrust for different nozzle configurations at multiple combustion pressures.

With the long duct attached, the measured thrusts are shown in Figure 33. Interestingly, the duct thrust is almost always greater with the solid and C-ring attached compared to no ring. The difference in behavior compared to the short duct must be because of the difference in length since all other parameters were the same. The long duct generates greater thrust with the solid and C-rings because the length allows it to extract more thrust from the higher turbulence flow created by the solid and C-rings. Another way to explain the long duct's greater thrust is to say while inside the long duct the shear layer has enough time to grow enough and generate more thrust.

The C-ring is supposed to create the most turbulence, increasing the rate of mixing between the rocket exhaust plume and the ambient, secondary air, which is at the sacrifice of a small amount of energy from the exhaust which would otherwise result in thrust. So the thrust lost with the C-ring is changed to turbulence, entraining more secondary flow, and the mixing ducts recover the energy creating more thrust. The rings operated at least qualitatively in the expected direction. Long duct case tests #12, #5, and #9 with the three ring configurations at $\sim 386\ psi$ combustion pressure, showed the C-ring produced the least total thrust (seen in Figure 24) however it produced the most mixing duct thrust for the long duct case. The total thrust for the no ring test (#12) was $35.53\ lbf$, the total thrust for the solid ring test (#5) was $34.55\ lbf$,

and the total thrust for the C-ring test (#9) was 34.46 lbf as seen in Figure 24. The no ring case produced the most total thrust and the C-ring produced the least thrust. The difference between the no ring and the other two rings was ~1 lbf, while the difference between the solid and C-ring was small, 0.09 lbf. The mixing duct thrust measured for these three tests was similar but in reverse since the generation of greater turbulence increases the mixing duct thrust. The mixing duct thrust for the no ring test (#12) was 2.72 lbf, the mixing duct thrust for the solid ring test (#5) was 3.25 lbf, and the mixing duct thrust for the C-ring test (#9) was 3.36 lbf. As the combustion pressure was increased the influence of the three rings on total thrust and mixing duct thrust was similar.

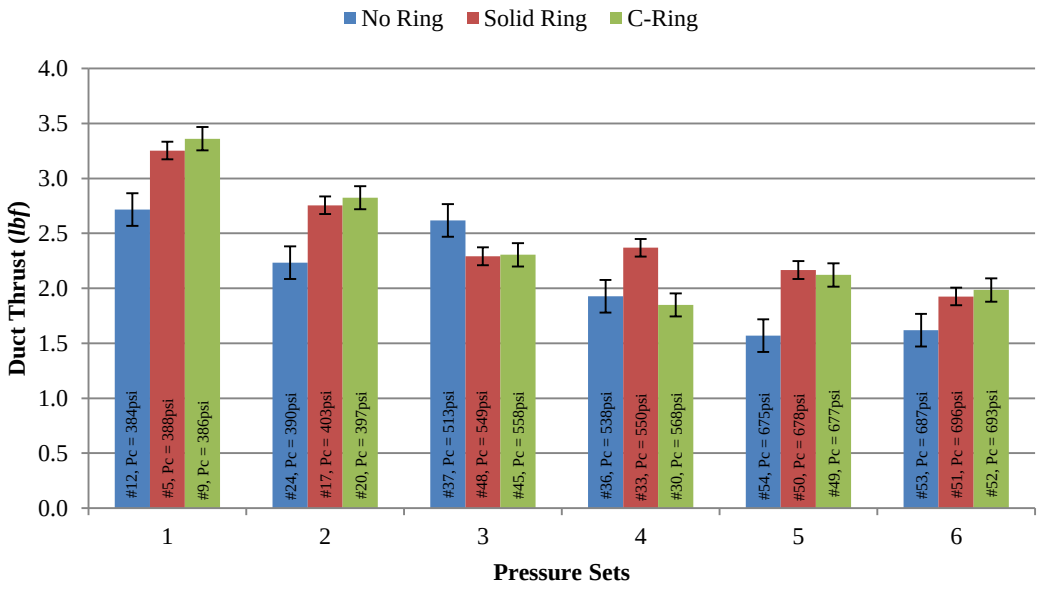

Figure 33: Long duct thrust for different nozzle configurations at multiple combustion pressures.

4.2.3 Duct Thrust: Duct Cases Divided by Combustion Pressure and Throat Area

As with the total thrust and engine thrust discussed, the duct thrusts were divided by the combustion pressure and nozzle throat area. Starting with Figure 34 the resulting values are displayed. In the no ring case, the long duct does the best and has a decreasing trend as pressure increases. The short and diverging ducts act consistent with what has been seen in previous plots and they do not seem to change a lot as pressure changes.

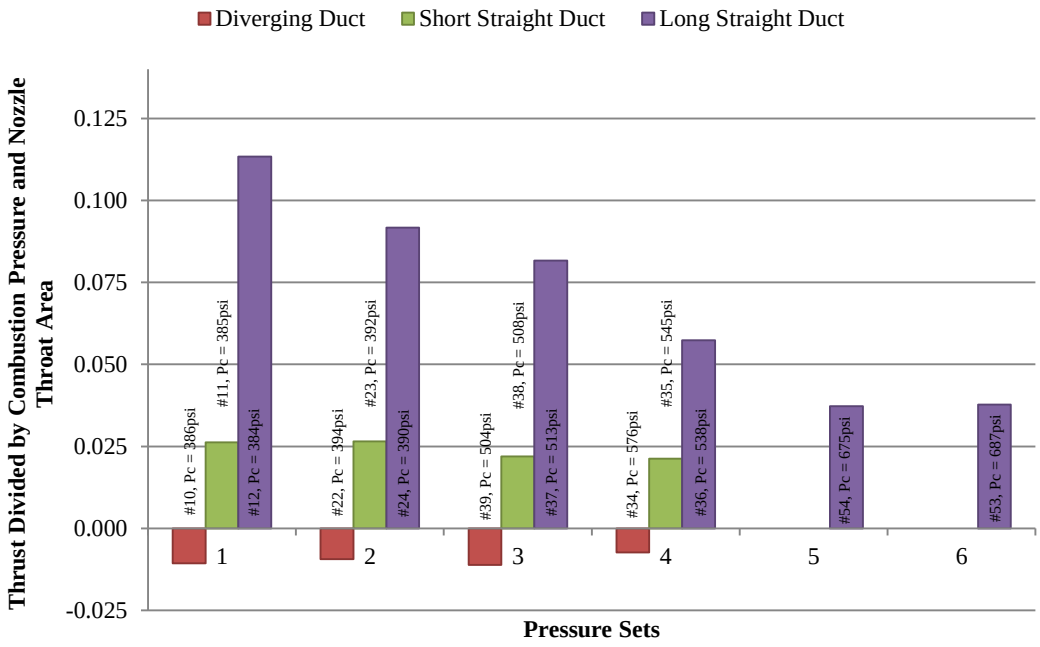

Figure 34: No ring, duct thrust divided by combustion pressure and nozzle throat area at multiple combustion pressures.

With the solid ring attached, in Figure 35 the long duct again does best and has a downward trend. However this time the short and diverging ducts also have a trend, as pressure increases they all trend towards the zero thrust line. This could indicate that as the nozzle becomes less over expanded and finally reaches optimal expansion the mixing duct thrust is zero, regardless of the mixing duct's shape. Also it should be noticed that the solid ring has greater values than the no ring cases.

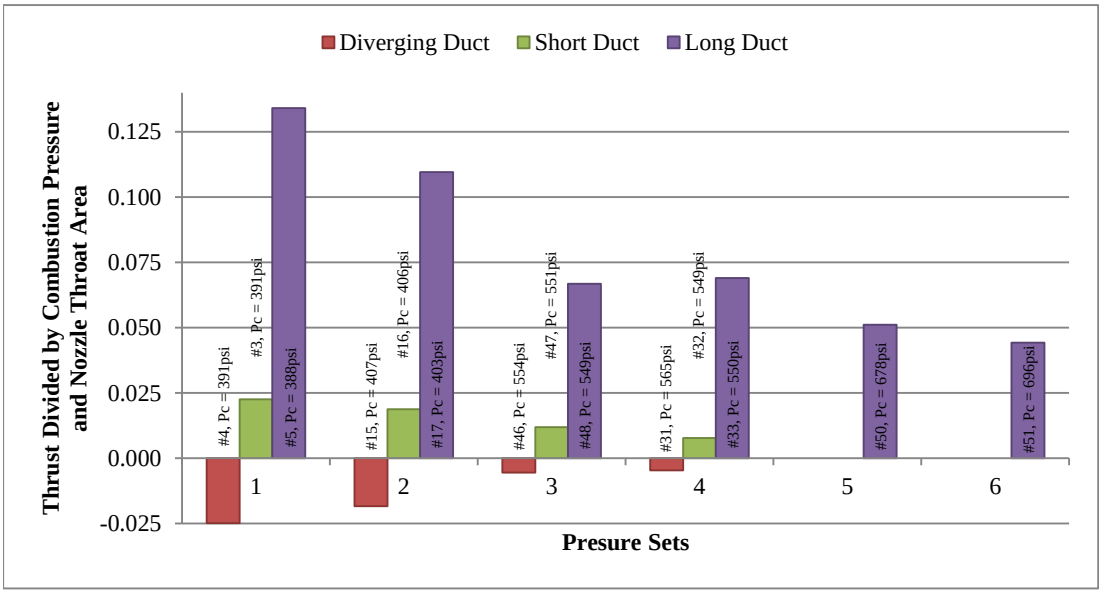

Figure 35: Solid ring, duct thrust divided by combustion pressure and nozzle throat area at multiple combustion pressures.

Finally with the C-ring attached, Figure 36 shows similar trends to Figure 35 and in some cases the values are even greater than the solid ring values. The differences are not too different but it does indicate there is some difference between the two cases, which is most likely due to the rings.

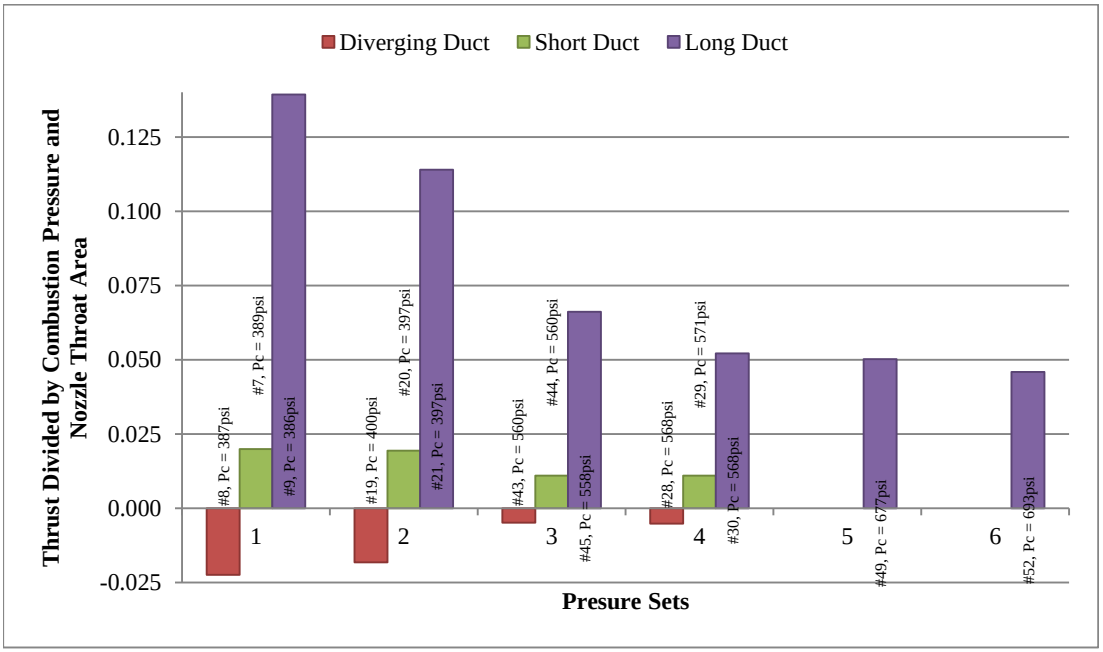

Figure 36: C-ring, duct thrust divided by combustion pressure and nozzle throat area at multiple combustion pressures.

4.2.4 Duct Thrust: Comparing Long and Short Ducts Divided by Internal Area

To understand if the length of the short and long ducts had an impact on their thrust, each test's duct thrust was divided by the internal area of the straight vertical section of the respective duct. The division resulted in a thrust per unit area which is analogous to wing loading in aircraft analysis, and for the purposes of this investigation a higher thrust per unit area value is better. Figure 37 shows the no ring tests where the long duct decreases as chamber pressure increases and the short duct increases as pressure increases. The thrust per unit area values seem to be converging and could reverse their relative positions as pressure is increased.

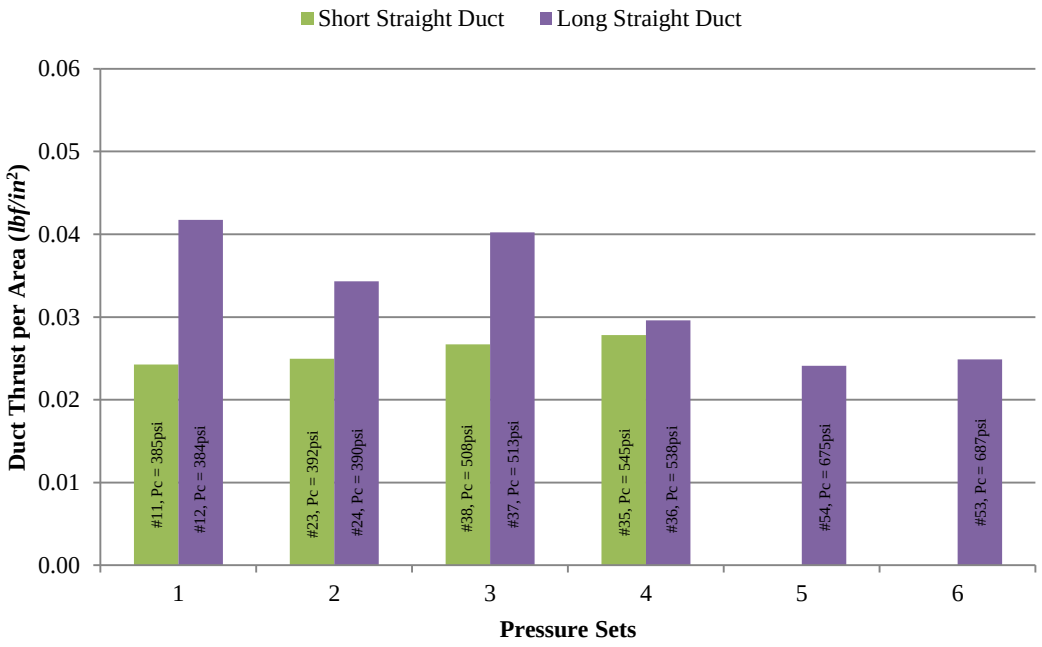

Figure 37: No ring, short and long duct thrusts divided by internal surface area at multiple combustion pressures.

The solid ring cases of the short and long duct thrusts are shown in Figure 38. The C-ring cases of the short and long duct thrusts are shown in Figure 39. The two plots show similar trends with the long and short ducts both decreasing in performance as the pressure increases. Compared to Figure 37, the differences between the two mixing ducts are much greater and the C-ring shows the best performance between the three rings, with the solid ring a close runner up, and the no ring being the least. The C-ring was designed to induce turbulence by way of the cavity and the solid ring creates some turbulence by providing a surface on which the flow's boundary layer can grow and become turbulent.

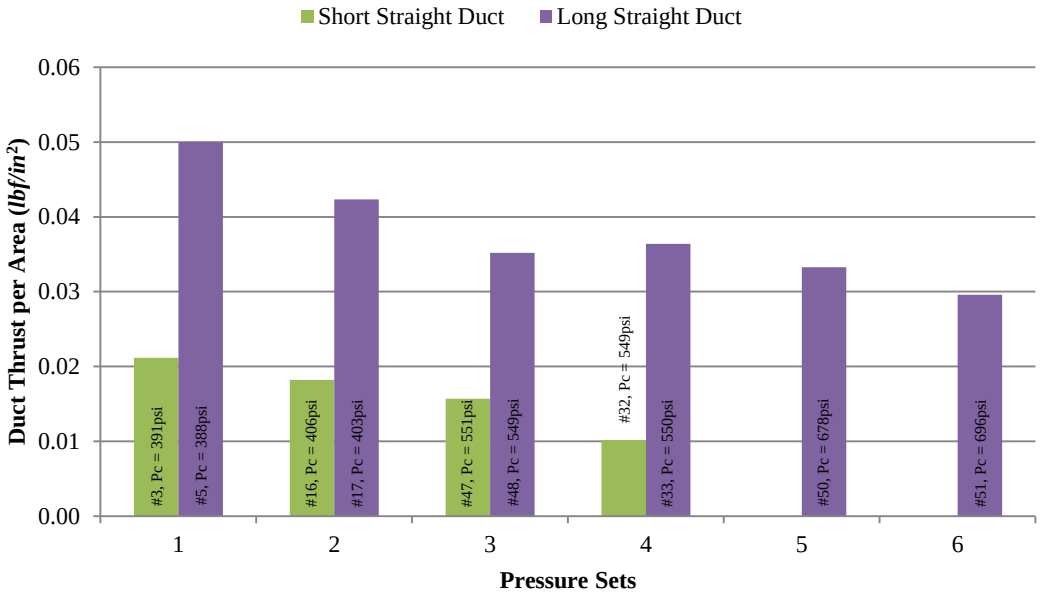

Figure 38: Solid ring, short and long duct thrusts divided by internal surface area at multiple combustion pressures.

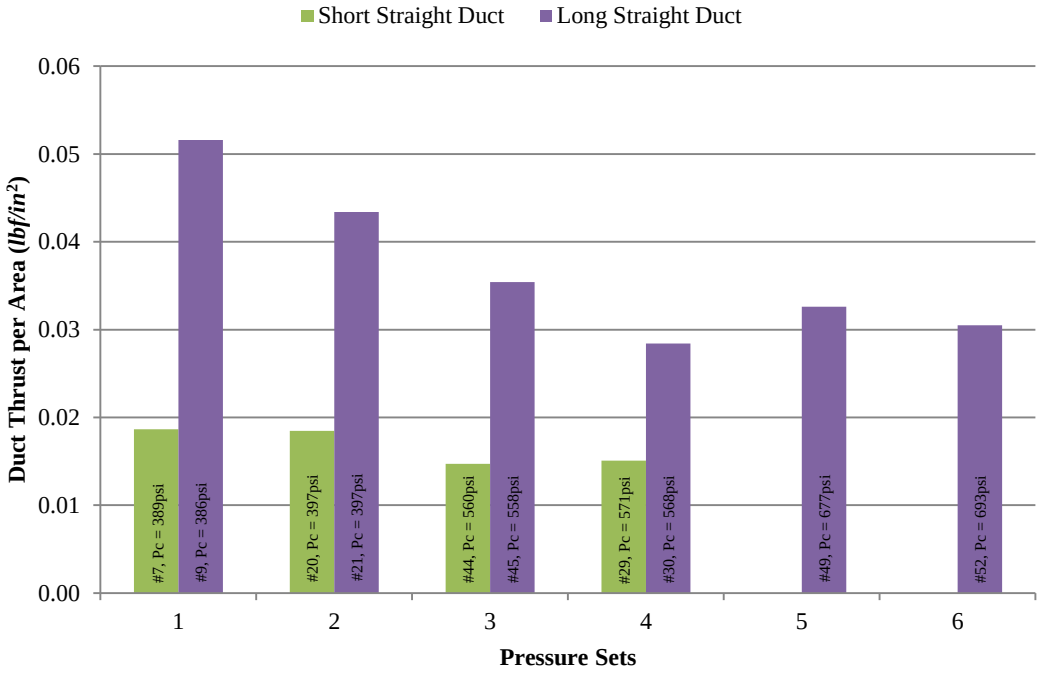

Figure 39: C-ring, short and long duct thrusts divided by internal surface area at multiple combustion pressures.

4.3 Primary Mass Flow Rate Plots

The groupings in Figure 40 highlighted the consistency of the pressure settings and mass flow rates between different tests. The combustion pressures and mass flow rates increased as the feed pressures increased. The engine was designed to use $0.0114\ slug/s$ total mass flow of ethanol and oxygen when combusting at $1{,}000\ psi$. The maximum total mass flow reached during testing was $\sim 0.01\ slug/s$. The difference between the design total mass flow rate and the measured total mass flow rate is reasonable since the maximum test combustion pressure was $\sim 680\ psi$.

The vertical groupings of the red markers in Figure 40 denote the three nominal pressure sets which have been commented on ($400\ psi$, $550\ psi$, and $680\ psi$). The long duct produced the highest thrust in all cases. In the cold flow test cases the long duct produced even more thrust than the hot fire tests because the cold flow tests had the lowest chamber pressure of all the tests and was most over-expanded. The cold flow tests had a chamber pressure of $\sim 100\ psi$ and are shown with the blue markers. The blue, cold flow, markers group together in the same fashion as the red markers.

The long duct thrust decreased as combustion pressure increased because the over-expanded exhaust from the engine, which pulls the mixing duct upward, increased in pressure and became less over-expanded as the combustion pressure increased. The diverging duct produced negative thrust because the horizontal component of surface area on the internal diverging section of the mixing duct was exposed to a lower pressure than the pressure at the surface of the entrance of the mixing duct. The short duct produced about the same amount of absolute thrust as the diverging duct; however the relative thrust was positive. The short and diverging ducts had the same inlet area and the same length for all intents and purposes; the only difference was that the internal diameter increased in the diverging duct while moving away from the inlet going toward the outlet. The length of the mixing duct was far more influential than diverging and straight walls, although a converging mixing duct might have produced more thrust than either of the short and long ducts. Lastly, since the short and diverging ducts were the same length and assuming a converging duct would be a mirror image of the diverging duct, then following the pattern created by moving from the negative to the positive thrusts it could be inferred that the converging duct would produce more thrust than the short duct if not more than the long duct.

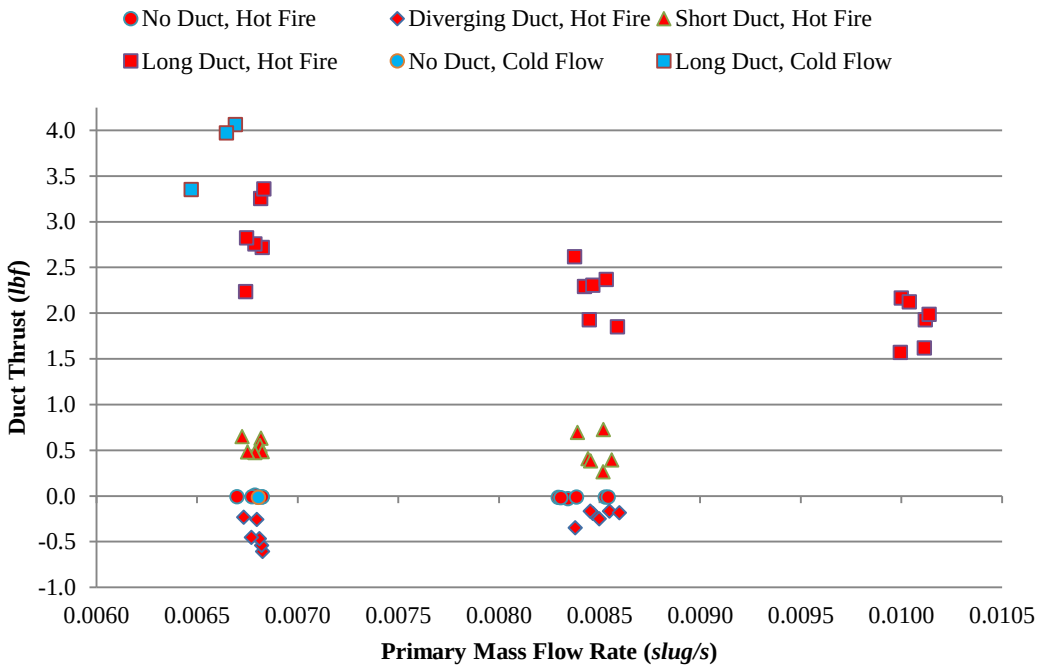

Figure 40: Duct thrust and total propellant mass flow rate for all tests.

Figure 41 showed the total thrust of the system plotted versus the total mass flow rates through the engine. Just as in Figure 40 the total thrust points again showed grouping around specific mass flow rates which were functions of the pressure settings. Pressure recovery was better for the long duct (as long as the boundary layer does not separate) since the longer the duct the slower the speed and more pressure increases were achieved as the primary and secondary flows traveled forward. The secondary flow was subsonic because the primary flow was over-expanded and it was likely that thrust would be higher if the secondary was supersonic, especially for the diverging duct cases since it would have continued to expand the flow if the secondary flow was supersonic.

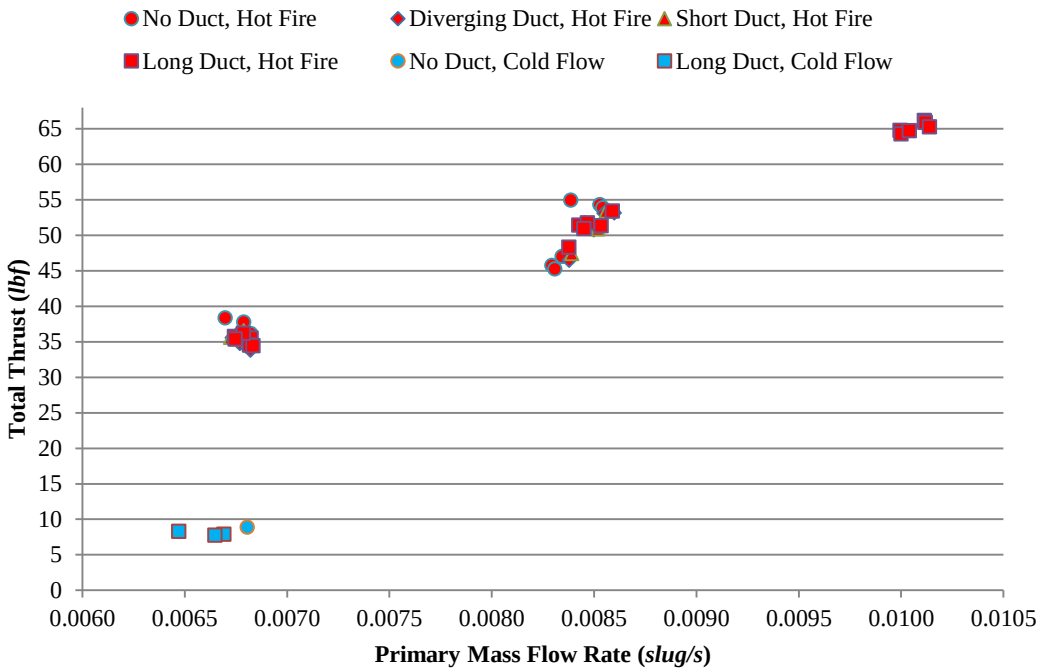

Figure 41: Total thrust and total propellant mass flow rate for all tests.

4.4 Mass Flow Rate Ratio and Pressure Ratios

The pressure ratio between combustion chamber pressure and ambient pressure along with the theoretical mass flow rate ratio were calculated since these ratios were often used to describe AAR operation.

The mixing duct inlet area to rocket engine nozzle exit area ratio is given by Equation 4-2.

$$\frac{A_3}{A_e} = \frac{40}{8.95} = 4.47 \qquad \textbf{4-2}$$

On Figure 42 the blue line is the curve created by mass flow rate ratios versus area ratios and the mass flow rate ratio corresponding to 4.47 area ratio was highlighted by the intersecting vertical and horizontal lines. The corresponding mass flow rate ratio was 1.56, which represented the theoretical mass flow rate of secondary flow being moved by the system.

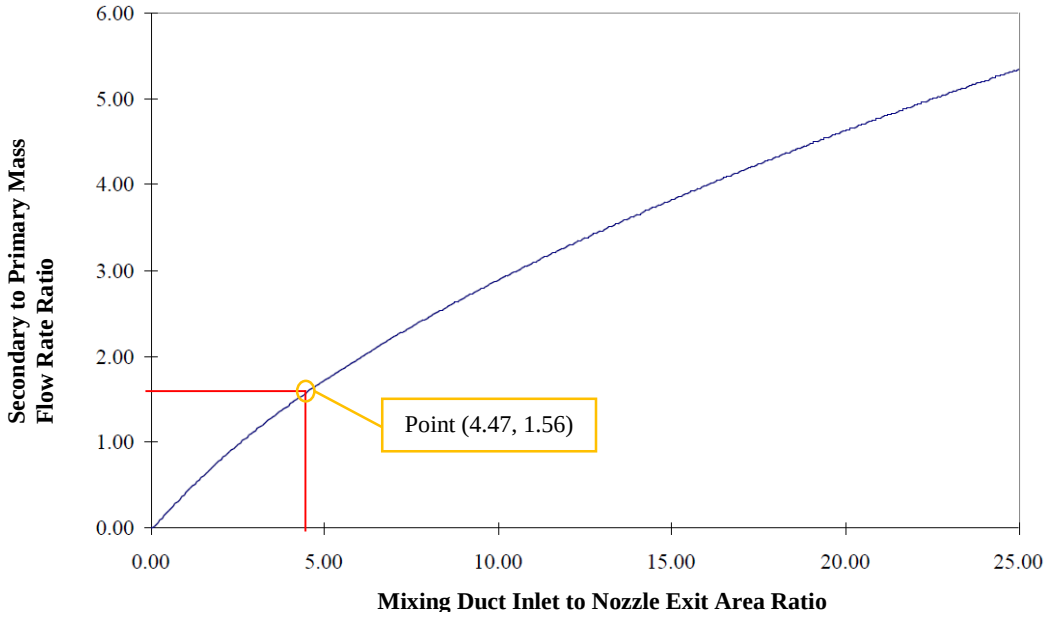

Figure 42: Ideal pumping curve showed the mass flow rate ratio versus the exit area to duct inlet area ratio (20).

Figure 43 shows the duct thrust and the total thrust plotted against the pressure ratio. The top plot on the figure shows the duct thrust and the bottom plot shows the total thrust. Both plots reference the same pressure ratios which are labeled on the bottom plot for simplicity. Also both plots reference the same legend at the top of the figure. The pressure ratios were calculated by dividing the combustion pressure for each respective test by the ambient pressure which was recorded and about 14.7 psi for all the tests.

The points plotted clearly form into groups which indicate the engine and data collection were very consistent. The impact of the mixing ducts and rings was minimal on the total thrust. The trends of the mixing duct thrusts show the long duct thrust steadily decreases, the short duct decreases as well but less steeply, and the diverging duct increases as the pressure ratio increases and becomes closer to optimal expansion of the nozzle. The minimum tested combustion pressure was $\sim 400\ psi$ and the maximum tested combustion pressure was $\sim 690\ psi$ yielding results over a nozzle pressure ratio range of $\sim 27 - 47$.

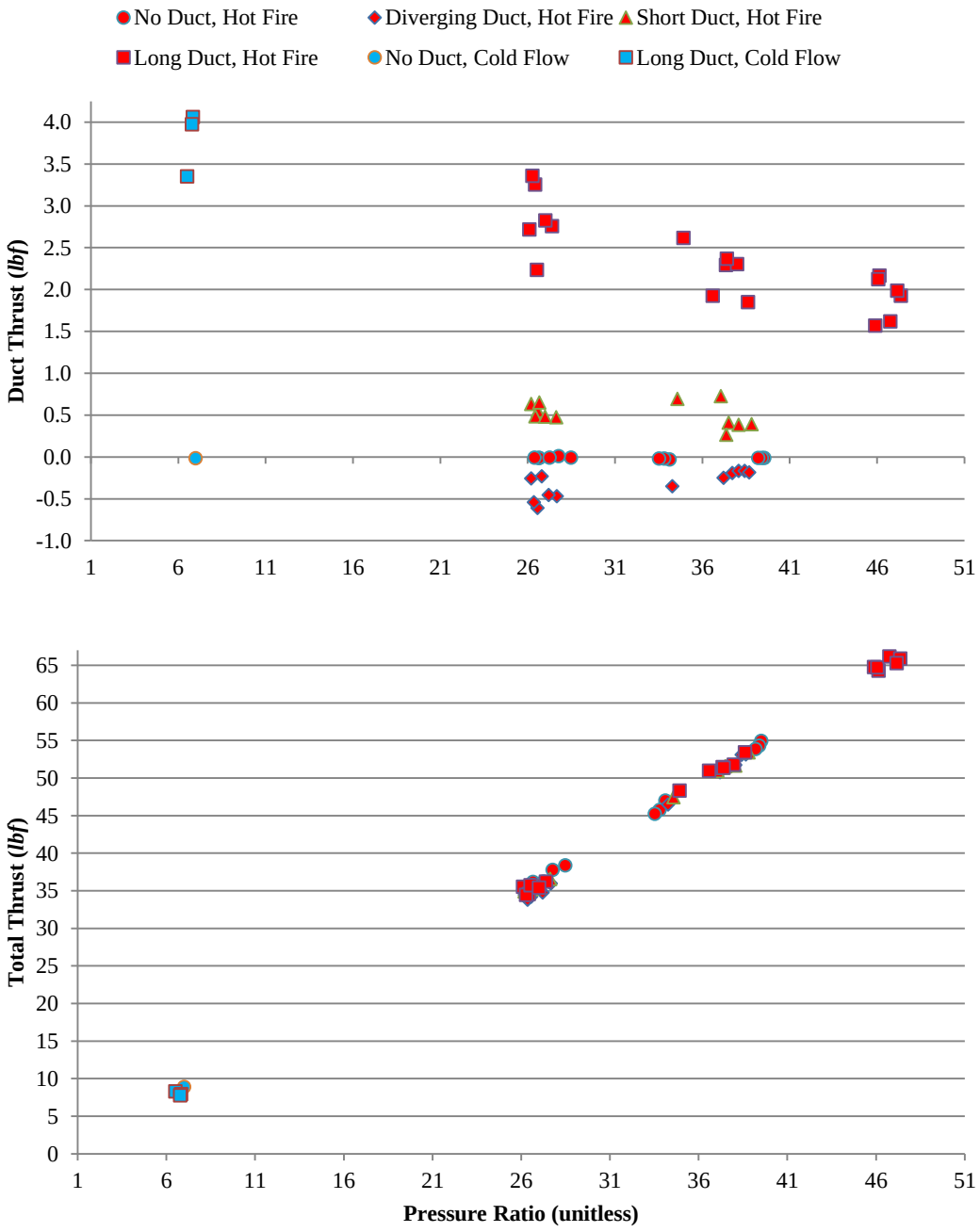

Figure 43: Duct thrust and total thrust versus pressure ratio for all tests. The top plot was duct thrust and pressure ratio for all ducts, and the bottom plot was total thrust and pressure ratio for all ducts.

4.5 Over-Expanded Nozzle Operation

The pressure losses across the injector and the entire feed system were far greater than expected. In conjunction with the maximum allowable supply pressure the attainable combustion pressure was limited to

a maximum of about $750\ psi$. The nozzle, however, was designed to expand $1{,}000\ psi$ to $14.7\ psi$ (a pressure ratio of 68) but since the real combustion pressure was limited to $750\ psi$ the nozzle was always over-expanded during all the test cases. Thankfully the engine was operable across a significant range of combustion pressures allowing for the many different cases investigated in this report. The pressures reached while testing were high enough to keep the flow attached to the nozzle because of the exit pressures calculated in Equations 4-3 and 4-4.

$$420 * \frac{14.7}{1000} = 6.17\ psi \qquad \textbf{4-3}$$

$$750 * \frac{14.7}{1000} = 11.0\ psi \qquad \textbf{4-4}$$

were higher than 40% of ambient pressure which is $5.88\ psi$ (12).

Figure 44 shows three screenshots from the footage taken during testing with Cal Poly Space System's GoPro Hero 3 camera. The three tests shown were preliminary tests done on the engine to find its maximum operating combustion pressure and are not reported in the test matrices. The figure shows frames that display how the plume looked at different levels of over-expansion. The left most image was taken when the combustion pressure was $490\ psi$, the middle image was taken at $610\ psi$, and the right most image was taken at $750\ psi$. In the $490\ psi$ case the plume was not visible until about a foot away from the engine. The $610\ psi$ and $750\ psi$ cases were much brighter than the $490\ psi$ case, and both higher pressure plumes were visible starting at the exit of the nozzle. The $610\ psi$ and $750\ psi$ tests were not too different from each other.

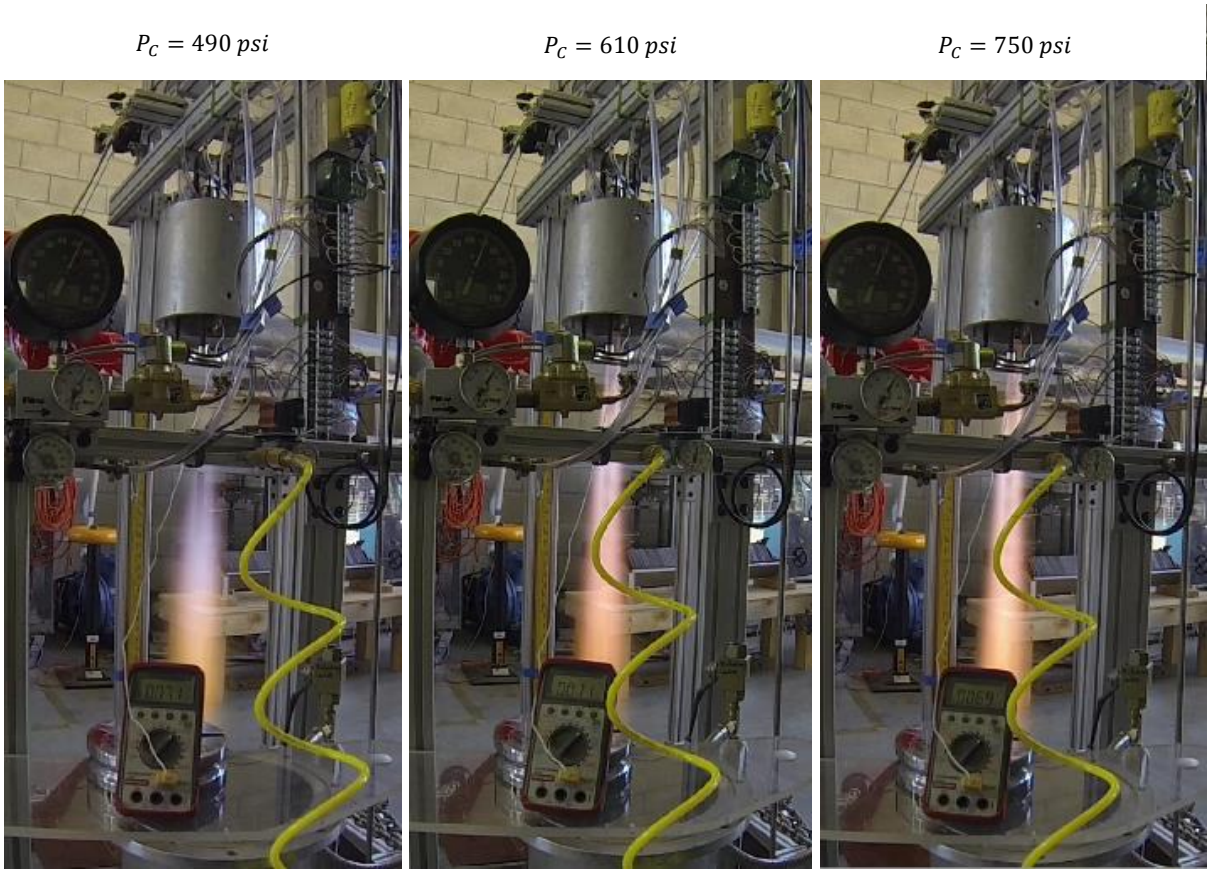

Figure 44: Screenshots of several test fires showing how the plume of the engine changes with increasing chamber pressure.

4.6 Flow Interpretation

Figure 45 through Figure 48 depict what the exhaust plume of the engine and the ambient air flow looked like.

The nozzle end of the engine is shown in Figure 45 with the three different ring configurations; the primary flow was depicted by the red arrow and the zigzag, red-to-orange gradient lines. The shear layer was represented with the burgundy swirls and as the ring configuration changed the swirls changed in size. The secondary flow was represented with the curvy, blue-to-orange gradient lines. The rendering was an artistic depiction of how the flow was believed to be behaving, which was based on the data collected, videos recorded, and the research conducted. The shear layer depicted in the figure grows as the no configuration changes from no ring, to solid ring, and to C-ring.

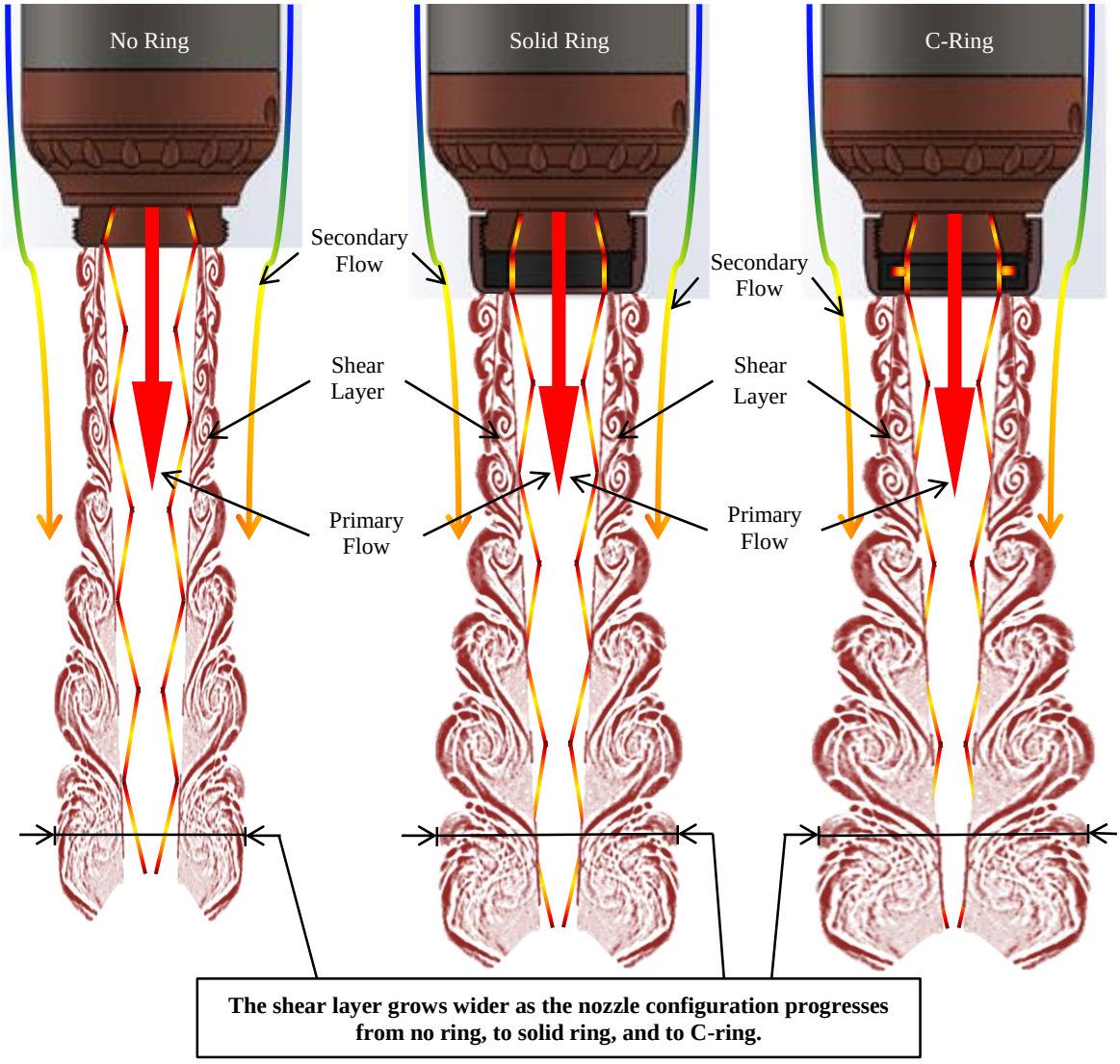

Figure 45: Depiction of how the plume and shear layer look with different rings. The nozzle and rings had been sectioned to see the details.

The videos recorded during the 550 psi nominal chamber pressure tests were very helpful and frames from six of these tests are presented in Figure 46 and Figure 47. All three ring configurations were tested without a mixing duct attached. The tests in Figure 46 were done with the oxygen and nitrogen regulators set to the same pressure (1150 psi). The tests in Figure 47 were done with the nitrogen regulator set to 50 psi higher than the oxygen regulator (1150 psi on the nitrogen regulator and 1100 psi on the oxygen regulator). So the engine was burning slightly more fuel rich in the tests shown in Figure 47. In both of the test sets the engine was combusting fuel rich, the fuel in the exhaust plume and its secondary combustion interfered with the visibility of Mach disks.

The red ellipses and circles in the two figures highlight the areas where the flow differences were the most noticeable. In both figures, the flow changes from a bright, distinct flame to a duller, fuzzy flame as the nozzle was tested with the no ring, the solid ring, and the C-ring. The difference between the no ring case and the other two cases is very prominent. The difference between the solid ring and C-ring cases is less prominent, but they coincide with what the thrust data suggested. The Mach disks are hard to discern, however the disks and the shape of the plume are more sharply defined in the solid and C-ring cases. The turbulence induced by the solid and C-rings causes the plume's outer layers to combust with the secondary flow and be clearer. In the no ring case the unburned fuel hides the plume and makes it fuzzier.

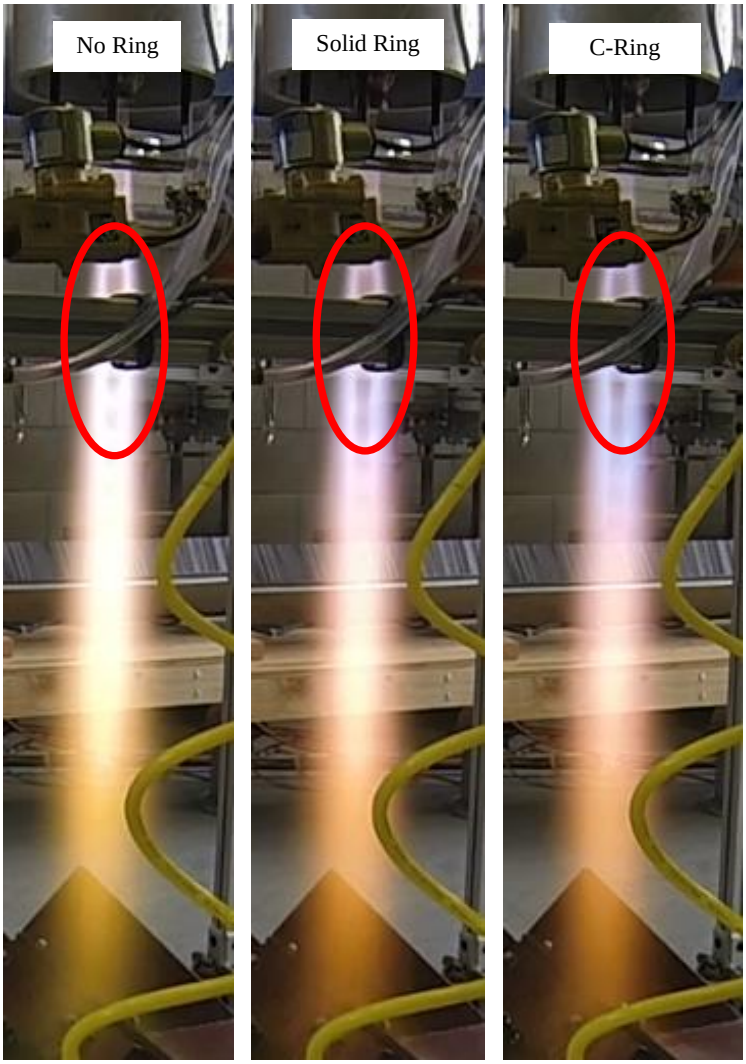

Figure 46: Screen captures of test #25, 26, 27 ($P_c = \sim 580\ psi$) in that order from left to right. The pictures show the change in the plume between the ring conditions. The red ellipses highlight where the flow differences were the most noticeable.

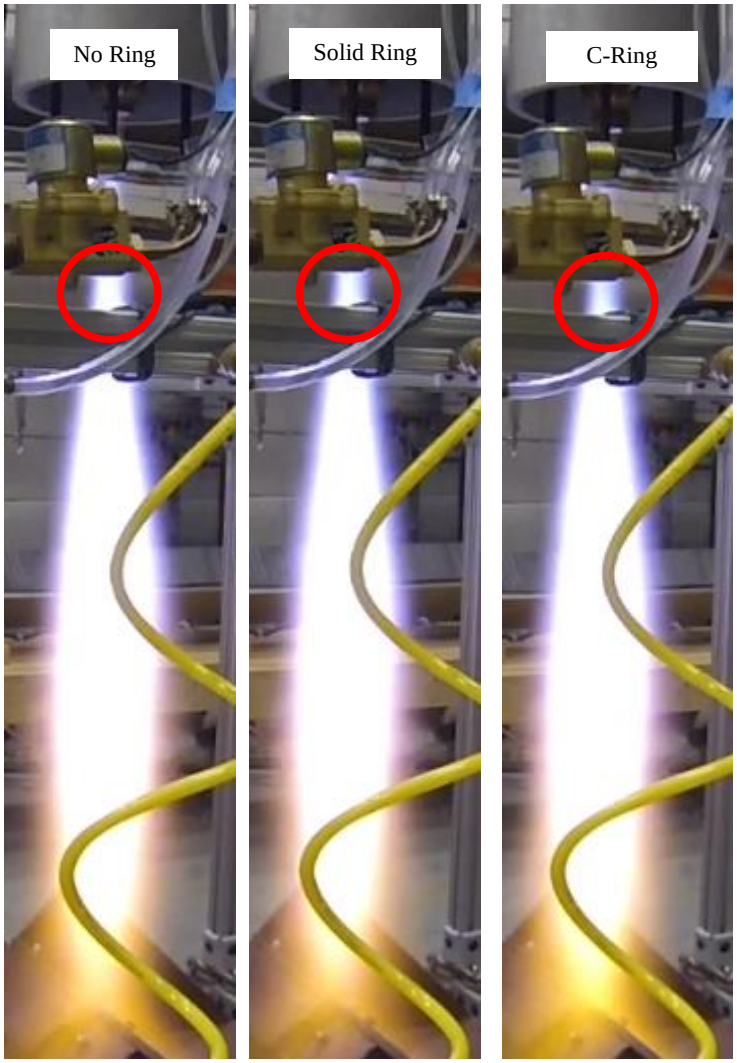

Figure 47: Screen captures of test #40, 41, 42 ($P_c = \sim 500\ psi$), in that order from left to right. The pictures show the change in the plume between the ring conditions. The red circles highlight where the flow differences were the most noticeable.

Yu and Schadow recorded their tests on a super-VHS tape. Evaluating the tape for the time-averaged visible light emission, Yu and Schadow saw greater luminosity in the exhaust plume as evidence of afterburning (10). The base idea for the C-ring was it increases afterburning and from what Yu and Schadow saw, it means the C-ring tests would produce a brighter exhaust plume. In this study the brightness based on videos of the testing was also used to indicate afterburning. But Figure 46 and Figure 47 show the opposite of what Yu and Schadow saw. AARLITE was operated with different propellants and at different conditions compared to Yu and Schadow's testing, AARLITE's nozzle was over-expanded, it had a higher exit Mach number, the mixture ratio Yu and Schadow used is unknown, and their flow expansion is unknown.

The impact the rings had on the ducts could be better understood with the artistic depiction in Figure 48. The secondary flow had increasingly greater mixing with the primary flow and greater entrainment into the ducts as the nozzle was equipped with no ring, solid ring, and C-ring. The long duct took the most advantage of the greater entrainment due to its length. The diverging duct was the most disadvantaged because it was not long enough and its internal diameter increased along its length.

The solid and C-rings act very similarly to each other and it was speculated the major mode by which they create a significantly different flow compared to the no ring case was by either having a larger recirculation zone at the exit plane of the retaining nut or by having a boundary layer trip point inside the nozzle that causes the increased shear layer growth rate. The trip point was labeled in Figure 48.

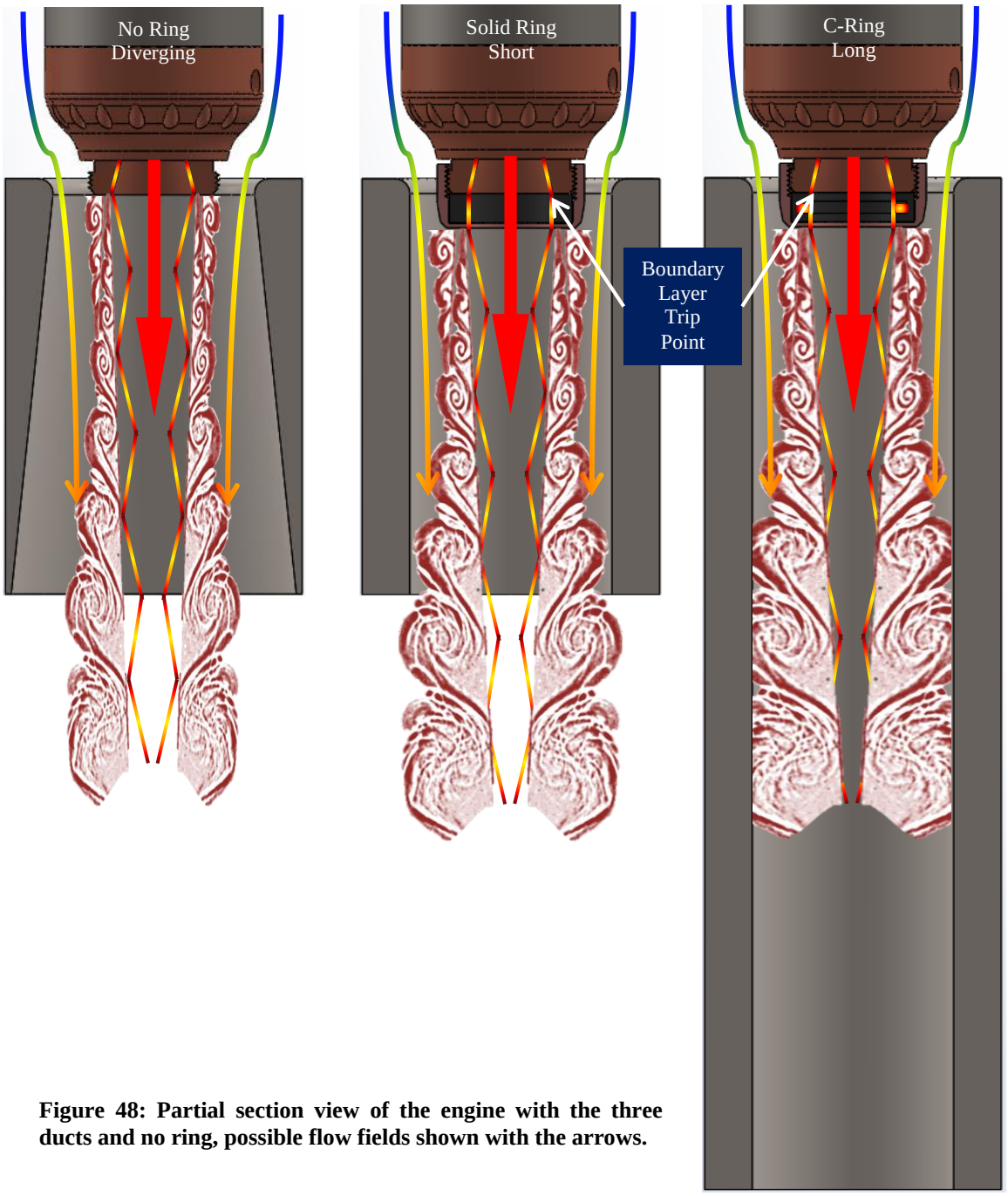

Figure 48: Partial section view of the engine with the three ducts and no ring, possible flow fields shown with the arrows.

5. Conclusion

The focus of this research was to characterize the performance of the three mixing ducts and annular cavity configurations to form a baseline set of data for future work with AAR's in the over-expanded nozzle case. Complementing the focus of the report, the major goal was to produce evidence of thrust augmentation and quantify the changes in thrust across different combustion pressures.

The rocket engine used for this research was a liquid 95% ethanol and gaseous oxygen bi-propellant engine. The mixing ducts were attached to the test stand's 25 lbf load cell in a ducted rocket configuration. A graphite annular cavity facing parallel to the direction of the primary flow at the end of the nozzle was tested alongside the mixing ducts. The nozzle was also tested with no ring and a solid ring (no groove). The pressure loss across the injector was about five times higher than the design pressure loss and did not allow for the $1{,}000\ psi$ design combustion pressure to be reached. The engine was always operated in the over-expanded condition. The three nominal combustion pressure sets tested were $\sim 400\ psi$, $\sim 550\ psi$, and $\sim 680\ psi$, yielding a pressure ratio range of $\sim 27 - 47$ relative to $14.7\ psi$ ambient pressure.

The rings and mixing ducts created significant changes to the total thrust of the system when they were attached. The no duct case generally produced the most total thrust, especially in the lower combustion pressure, pressure sets. Of the three mixing ducts the long duct created the greatest increase in total thrust relative to the other two mixing ducts. The diverging duct produced the least total thrust of the three mixing ducts, and the short duct performed in the middle of the long duct and diverging duct.

Tests at ~387 psi with no ring showed the long duct produces the greatest total thrust and mixing duct thrust augmentation. The solid and C-rings produced the same pattern as the no ring, however, the total thrusts for the cases was shifted down by 0.65 to $1.07\ lbf$. When the rings were cycled through and tested with each of the mixing duct configurations, the no duct case produced the most total thrust and of the mixing ducts, the long duct again performed best and the diverging duct was the worst.

Even though the mixing ducts created positive thrust, except in the case of the diverging duct, all the mixing ducts created a drag force on the system which was the same or greater than the mixing duct thrust.

Meaning the total thrust was the same or reduced when the mixing ducts were attached, so total performance was not increased. The drag force was high because the nozzle was always operated in the over-expanded condition. In the over-expanded condition the exhaust plume is a lower pressure than ambient air so the ambient air gets pulled toward the exhaust plume because of a pressure differential, not by being entrained in the shear layer. Imagine a vacuum being placed at the nozzle end of the engine. The vacuum pulls upward on the mixing ducts, creating thrust, and pulls downward on the engine, creating drag. The pulling of the engine downward was significant when the mixing duct was attached because the mixing ducts cause the low pressure flow to concentrate around the base area of the engine's nozzle. As the combustion pressure increased, the thrust from the mixing ducts and the drag on the engine decreased.

If the engine is operated with optimal expansion, the mixing ducts would either have no impact or they will create augmented thrust without pulling the engine downward. Furthermore if the engine is under-expanded, the plume would most likely impart even more energy to the mixing ducts and have significantly greater performance with the mixing duct compared to the conventional, ductless configuration. In the optimally expanded and under-expanded cases, the diverging duct is predicted to create the same or more thrust than the short and long ducts.

The long duct produced the most thrust, the diverging duct produced the least thrust, and the short duct produced a middle range thrust. In the tests in pressure set 1 the diverging duct thrust was $-0.257\ lbf$, the short duct thrust was $0.632\ lbf$, and the long duct thrust was $2.717\ lbf$. The thrust of the long duct was about four times greater than the short duct while its mass was only about 2.4 times greater. The behavior repeated when the solid and C-rings were attached. With the rings attached the differences between the mixing duct thrusts was again more exaggerated in the same pattern as the total thrust. As combustion pressure increased the mixing ducts' thrusts also followed a converging trend like the total thrust.

The solid and C-rings extend the nozzle without changing the exit area. Both rings reduced the total thrust a small amount and as expected the C-ring reduced the thrust the most. Tests with no duct, the diverging duct, and the short duct also show the same trend as the long duct thrust trend. One clarification: since the diverging duct produced negative mixing duct thrust the solid and C-ring increased the absolute mixing duct thrust while the actual thrust was decreased further.

In conclusion, testing showed the mixing ducts to produce more drag than thrust and the rings reduced the total thrust of the system at over-expanded nozzle operation. However, the short and long ducts did produce positive thrust and the attachment of the solid and C-rings increased the absolute thrust produced by all the mixing ducts. The long duct produced the most mixing duct thrust showing it augmented thrust the most in the over-expanded nozzle condition. The nozzle exit pressure (the over-expanded flow) had a major impact on the total thrust and mixing duct thrust because as the combustion pressure increased the total thrusts tended to become closer to each other and the mixing duct thrusts tended to converge. Testing the system at optimal and under-expansion of the nozzle should produce useful results to better characterize the operation of the rings and mixing ducts.

6. Future Work and Suggestions

Throughout the work done for the current report there were many ideas that came up for how to improve and build on the work done. Table 9 listed the ideas which had come up throughout the process. The table was divided into two levels of complexity. Level I ideas were considered work an undergraduate engineering student could completer and Level II were considered work a graduate engineering student could complete.

Table 9: Ideas for improvement and future research were categorized by two levels of complexity.

Level I	Level II
Add a thermo couple (tap) to the nozzle right at the water inlet distribution channel to monitor the temperature near the throat. Test Materials for heat resistance using the ring retention nut to hold them onto the end of the nozzle.	Test the level of augmentation by varying the distance between the nozzle exit plane and the duct inlet plane. The ducts were engraved with scale marks to make this option easy.
Improve the injector/manifold gasket sealing capability.	Flip the short and long ducts to see if the radiused inlets make a difference.
Make a new nozzle for the chamber pressures attainable. Make multiple nozzles or nozzle inserts with different area ratios to test the engine at multiple pressure ratios.	Add pressure ports along the side of the ducts and instrument the ducts with differential pressure transducers. At the very least add two ports one at the entrance and one at the exit of each duct.
Move the fuel and oxygen actuators/valves, check valves, and Venturi flow measurement tubes as close to the engine as possible.	Test the same cases multiple times to get a more accurate understanding of the repeatability between individual tests.
Create Matlab code to run through all of the Excel data from LabView more efficiently than hand calculating all the averages.	Test with greater than ~50psi pressure difference between the O2 and N2 regulators to have a greater range of mixture ratios. Vary the regulator pressure differences by at least 150psi. This will allow for better conclusions to be drawn about how fuel rich combustion affects thrust augmentation, especially if using a cavity to induce turbulence, mixing, and after burning.
Manifold at least three oxygen and nitrogen cylinders in order to get more tests and more consistent results. Possibly get higher pressure ($6{,}000\ psi$) oxygen cylinders, nitrogen cylinders, and regulators.	Attach a large diameter and long length pipe section closer to the engine. This large volume will act as a plenum and allow for easy measurement of the stagnation pressure of the feed line before going into the manifold. Attach pressure transducers on the plenum.
Get true differential pressure transducers for the Venturi tubes.	Make and test a thin(er) walled mixing duct to see how the area at entrance and exit end of the duct affects the thrust from the duct.
Attach the engine to its own dedicated load cell which directly measures the engine's thrust. Allows for calculation of the mixing duct drag term in Equation 4-1.	Equip the ducts with fuel injection nozzles to experiment with secondary fuel injection. By injecting fuel directly into the secondary flow the nature of AAR function is more thoroughly explored.
Test with more fuel in the fuel tank so the engine does not run out of fuel when the feed system time delay relays turn off.	Flip the diverging duct around to see what happens when the area is "reversed". Flipping the diverging duct will make it a converging duct.
Investigate how feed pressures are connected to combustion pressure. Come up with some relation, for example: if the ethanol and oxygen feed pressures are the same and divided by a constant. Creating an estimate of the combustion pressure to within 10psi.	Experiment with and investigate different cavity dimensions and designs with the engine. For example test round bottom cavities or dove tail cavities. Continue and extend the work of Yu and Schadow.
	Test multiple annular cavities in series. For example two of the same C-rings stacked back to back and held on by the cavity retaining nut.

BIBLIOGRAPHY

1. Gist, R. *Examination of Flow Field Characteristics and Fabri-Choking of a 2-D Air Augmented Rocket.* San Luis Obispo : California Polytechnic State University, 2007. Thesis.

2. Foster, R. W., Escher, W. J. D. and Robinson, J. W. *Air Augmented Rocket Propulsion Concepts.* Madison, WI : Astronautics Corporations of America Technology Center, 1988. F04622-86-C-0094.

3. DeTurris, D., Gist, R. and Foster, T. *Examination of Fabri-Choking in a Simulated Air Augmented Rocket.* San Luis Obispo : California Polytechnic State University.

4. Smith, T. D., Steffen, C. J. and Yungster, S. *Performance of an Axisymmetric Rocket Based Combined Cycle Engine During Rocket Only Operation Using Linear Regression Analysis.* s.l. : NASA, 1998. Technical Paper. NASA/TM-1998-206632.

5. Johnson, K. *Axisymmetric Air Augmented Methanol/GOX Rocket Mixing Duct Experimental Thrust Study.* San Luis Obispo : California Polytechnic State University, 2013. Thesis.

6. Papamoschou, D. *Structure of the Compressible Turbulent Shear Layer.* Pasadena : California Institute of Technology, 1991.

7. Papamoschou, D. and Roshko, A. *The Compressible Turbulent Shear Layer: an Experimental Study.* Pasadena : California Institute of Technology, 1988.

8. Smits, A. J. and Dussauge, J. P. *Turbulent Shear Layer in Supersonic Flow.* New York : Springer, 2006.

9. Rossiter, J. E. *Wind-Tunnel Experiments on the Flow Over Rectangular Cavities at Subsonic and Transonic Speeds.* London, England : Her Majesty's Stationery Office, 1966.

10. Yu, K. H. and Schadow, K. C. *Role of Large Coherent Structures in Turbulent Compressible Mixing.* Research and Technology Division, Naval Air Warfare Center, China Lake, California. New York : Elsevier Science Inc.

11. Huzel, D. and Huang, D. *Design of Liquid-Propellant Rocket Engines.* 2nd. s.l. : AIAA, 1992.

12. Sutton, G. P. and Biblarz, O. *Rocket Propulsion Elements.* New York : John Wiley & Sons, INC, 2001. 0-471-32642-9.

13. Young, W. and Budynas, R. *Roark's Formulas for Stress and Strain.* 7th. s.l. : McGraw Hill, 2002.

14. John, J. and Keith, T. *Gas Dynamics.* 3rd. s.l. : Prentice Hall, 2006.

15. Muss, J. *Cal Poly Thesis Project CEA Assistance.* [Email] 2014.

16. Johnson, K. *AAR Duct design/sizing.* [Email] November 15, 2014.

17. Hirahara, H., Kawahashi, M. and Kahn, M. U. *Experimental Investigation of Fluid Dynamic Instability in a Transonic Cavity Flow.* s.l. : Elsevier, 2007.

18. American Society of Mechanical Engineers. *ASME PTC 19.5-2004: Flow Measurement.* 2004.

19. International Organization of Standards. *ISO 5167-4: Measurement of Fluid Flow by Means of Pressure Differential Devices Inserted in Circular Cross-Section Conduits Running Full.* 2003.

20. Presz, W. Jr. and Werle, M. *Multi-Stage Mixer/Ejector Systems.* s.l. : AIAA, 2002.

APPENDICES

Appendix A: Testing Procedure

AARLITE FIRING PROCEDURES

Bipropellant Rocket Engine Firing Procedure

Last Modified: 12/1/2015 10:31:00 PM

Last Printed: 12/1/2015 10:31 PM

PROCEDURE HAZARDS, REQUIRED PERSONAL PROTECTIVE EQUIPMENT (PPE), AND SAFETY GUIDELINES:

- Test firing the engine involves the use of liquid ethanol for fuel:
    - Ethanol (CAS 64-17-5):
        - Flammable: keep away from open flames, high heat sources, sparks, or other sources of ignition

- Safety glasses ("ANSI Z87+" or better) must be worn at all times in the test cell along with closed toe shoes, long pants, and sleeved shirt.
- The bi-prop rocket engine is extremely loud so ear protection is required in the control room at all times while the engine is running.
- No personnel are allowed to be in the test cell, in direct line of sight of the engine when there is only one switch flip (or other actuation mechanism) keeping the three components of the fire triangle separate (in this case gaseous oxygen, ethanol, and electric spark).
- Safety is number one! When in doubt (with respect to safety):
    - Secure the area, do not allow anyone to enter the "danger zone"
    - In case of large "danger zone" or earthquake, evacuate to parking lot immediately south of the lab
    - Call lab and/or project advisor
    - Call Cody Thompson (Aerospace Dept. Safety Coordinator: 805-756-1309)
    - Call Environmental Health and Safety (for immediate assistance: 805-756-6661)
    - Call 911

PROCEDURE DETAILS:

- This procedure is formatted as a checklist; please print out a hardcopy and use it as such. During the lab activity, please make hand-written notes of any deviations from nominal behavior, if any errors are found, or if any additions or changes must be made to the procedure to allow for better subsequent operations. All corrections, additions, or changes must be recorded as soon as possible and all old versions collected and disposed of properly to prevent use of out of date documentation.

PROCEDURE CONVENTIONS:

- General heading titles are UNDERLINED AND ALL UPPERCASE LETTERS, e.g. PROCEDURE CONVENTIONS.
- Important notes and heading titles are **UNDERLINED, BOLD, AND ALL UPPERCASE LETTERS**, e.g. **TEST CELL PREPARATION**.
- Buttons, switches, and other controls manipulated by an operator are highlighted in **bold** font, e.g. **Fuel Enable**
- Readouts or other information displays are highlighted in *italicized* font, e.g. *Elapsed Run Time*

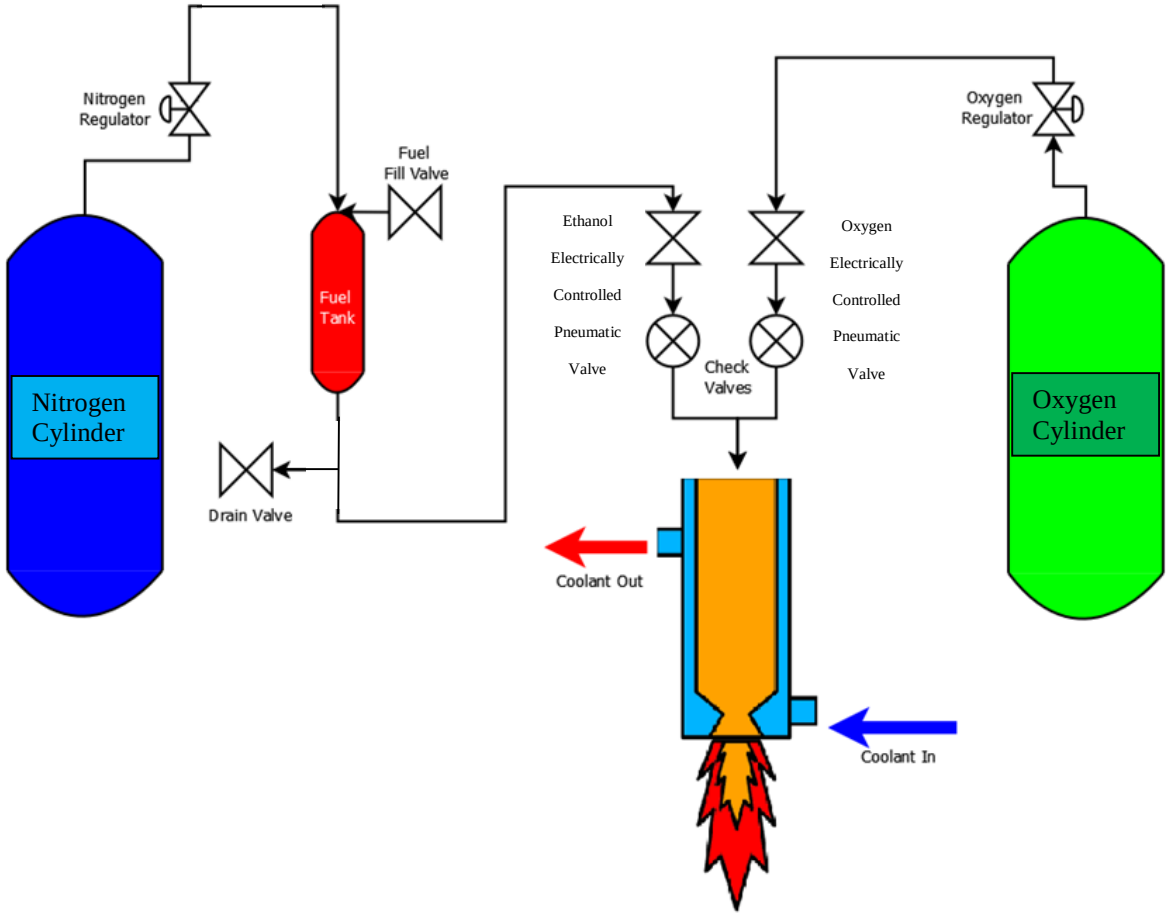

A. TEST CELL PREPARATION

☐	A.1. Post signs outside around the perimeter of the Propulsion Laboratory to warn passersby of the loud noises from the tests to be performed
☐	A.2. Warn people in the surrounding laboratories of the loud noise from the tests to be performed
☐	A.3. Fully open both test cell "roll-up" doors and lock the doors' chain in place
☐	A.4. Clear test cell area of any loose objects near the rocket test stand (anything that may be kicked up by the rocket)
☐	A.5. Clear test cell area of any flammable materials (put away in flammables cabinet or put outside the building)
☐	A.6. Check the test cell area for fuel spills or leaks; clean up any spills or leaks

B. PERSONNEL PREPARATION

Note: while you can hear people yelling during a firing, you will likely only know that you are being yelled at if you're looking at the person who is yelling. So coordinate how you plan to communicate while the engine is running. (Make use of hand signal…)

☐	B.1. Familiarize all personnel with features of the rocket apparatus, including fuel and oxidizer flows, load cell(s), and ignition system
☐	B.2. Review all safety information for the facility and lab. Refer to the front cover page for emergency contact numbers and evacuation exits/location
☐	B.3. Point out where the fire extinguishers are located
☐	B.4. Familiarize all personnel with the lab procedure (go over the section headings) and control room set up (data collection computer and control box)
☐	B.5. Clearly determine which personnel will execute the various duties of the lab activity
☐	B.6. Dry-run Sections C through H (as appropriate) of this procedure with the personnel who will execute those activities prior to running the procedure "for real"

C. ROCKET PREPARATION

☐	C.1. All personnel in test area don ear and eye protection
☐	C.2. Attach/place **water source** and **water return hoses** at the sink and test stand. Make sure the hoses are secure and will not flail about when pressurized, especially the water return hose during the water exhaust process
☐	C.3. Open the **spigot valve** at the sink and confirm the water hose is connected to pressurized water supply by looking at the water pressure gauge on the test stand. It must indicate a minimum of 60 psi with the flow control solenoid off (it should normally be 90 psi)
☐	C.4. Turn on **water flow control solenoid**
☐	C.5. Watch for water flow through the clear vinyl feed and return hoses going to the engine, and listen for water flow in the sink in order to confirm the coolant system is primed for action
☐	C.6. With the water flowing fill a gallon (preferably larger) bucket and time how long it takes to fill the bucket
☐	C.7. Confirm the water fills 1 gal every 15 seconds, 2 gal every 30 seconds, 3 gal every 45 seconds, 4 gal every minutes, etc.
☐	C.8. Turn off **water flow control solenoid** and test conductor carries the keys to the key switch
☐	C.9. Unscrew **nitrogen regulator adjustment screw** setting the regulated pressure to zero (do not unscrew all the way, just until no resistance is felt)
☐	C.10. Place glass fuel beaker below **fuel drain valve**
☐	C.11. Confirm no residual fuel in system by opening the **fuel drain** and then the **fuel fill valves**
☐	C.12. Close **fuel drain** and **fuel fill valves**
☐	C.13. Turn on the **sensor power** on the test stand
☐	C.14. Power on the DAQ computer and open LabView VI

☐	C.15. Test operation of VI and sensors: a. Click the **Run** button (white arrow, top of the VI window under the menu bar) b. Enter a **test data file name** and **file location** in the prompt (a default file name will appear which can be used or changed) c. Verify that the VI is operating (the readouts for *thrust* and *pressure* should start updating) d. **Tare/zero** all readouts in the VI when all the load cells and pressure transducers are at zero. Before zeroing all the sensor readouts should be within +/- 5lbf on the load cell and +/-10psi on the pressure transducer readouts. If they're not, that means something is wrong
☐	C.16. Once the load cell readings have been zeroed, the load cells may be loaded with the engine support rail and the duct attachment harness. The engine support rails bolts must be tightened starting with bolt labeled 1 and then bolt 2 using a ½" combo wrench. The duct harness bolt must be tightened by using 7/16" combo wrench on the bolt and a ½" (support) open-end wrench on the live end of the load cell. **Never torque the load cell without a support wrench.** The engine load cell output should be ~36lbf and the duct load cell output should be ~2lbf. Tare the readings of the load cells as required

D. <u>COLD GAS THRUSTER PROCEDURE (no fuel)</u>

If cold gas thruster demonstration is not required skip to Fuel Filling Procedure, section E.

<u>Only the minimum number of personnel are to take part in any steps which require entering the test cell.</u>

☐	D.1. Make sure the **power cord** to the control box is unplugged, the test conductor has the **firing keys**, and the **air supply hose** to the pneumatically actuated valves is unplugged
☐	D.2. Slowly open the **nitrogen cylinder valve** until the cylinder pressure gauge stops moving, then fully open the valve
☐	D.3. Set **nitrogen pressure regulator** to desired test pressure (maximum 1,500 psi), confirm using LabView VI
☐	D.4. Unscrew the **oxygen pressure regulator** until no resistance is felt in the adjustment screw
☐	D.5. Slowly open the **oxygen cylinder valve** until the cylinder pressure gauge stops moving, then fully open the valve
☐	D.6. Set **oxygen pressure regulator** to desired test pressure (maximum 1,500 psi) , confirm using LabView VI
☐	D.7. Plug in **air supply hose** to the pneumatic valves
☐	D.8. All personnel enter the control room and close doors
☐	D.9. Plug in the **power cord** to the control box and turn on the **main 6A breaker**
☐	D.10. Click the **Record button** in the LabView program to begin recording data
☐	D.11. On Control Box ___a. Turn on the **Key Power Switch** ___b. Turn on **Fuel Enable** and trigger the fuel control valve for 2 seconds ___c. Turn off **Fuel** ___d. Turn on **Oxygen Enable** and trigger the oxygen control valve for 2 seconds ___e. Turn off **Oxygen** ___f. Turn on the **Fuel**/**Oxygen Enable** and trigger for 2 seconds ___g. Turn off **all switches**, the **Key Power Switch** goes back in the hands of the test conductor, turn off the **main 6A breaker**, and unplug the **power cord**
☐	D.12. Click the **Record** button to stop LabView recording data

☐	D.13. Before entering the test area confirm proper safety equipment is worn a. Ear Protection b. Eye Protection
☐	D.14. Close **oxygen cylinder valve** and **nitrogen cylinder valve**
☐	D.15. All personnel return to control room and close doors
☐	D.16. Plug in the control box **power cord**
☐	D.17. Turn on the **main 6A breaker** and turn on the **Key Power Switch**
☐	D.18. Enable and trigger the **Oxygen Control Valve** until no sound is heard, the oxygen regulator pressure gauges read zero, and the LabView displays less than 1 psi in the oxygen system
☐	D.19. Turn off the **Oxygen Control Valve**
☐	D.20. Enable and trigger the **Fuel Control Valve** until no sound is heard, the nitrogen regulator pressure gauges read zero, and the LabView displays less than 1 psi in the fuel system
☐	D.21. Turn off **Fuel Control Valve**
☐	D.22. LabView program may now be stopped by pressing any of the **stop buttons** (however it is not necessary to stop the program since it can be used to monitor the sensors)
☐	D.23. Turn off and remove the **Key Power Switch** (test conductor keeps possession of the key), **all other control box switches**, and unplug the **power cord**
☐	D.24. Unplug the a**ir supply hose** on the test stand
☐	D.25. The oxygen and nitrogen **regulator screws** are released (turning them off), unless subsequent tests require the regulators to be set at the current pressure output

E. FUEL FILLING PROCEDURE

- **SAFETY NOTE**: Fuel filling is a potentially dangerous procedure, ethanol is flammable. Review the MSDS and use proper procedures and safety equipment when handling. Be sure to ground any containers or people handling ethanol to reduce the chance of static electricity. The fuel handler must wear gloves and grounding wrist strap.

  Again, no personnel are allowed to be in the test cell, in direct line of sight of the engine. In other words, no personnel are allowed in the test cell when there is only one switch flip (or other actuation mechanism) keeping the three components of the fire triangle separate (in this case gaseous oxygen, ethanol, and electric spark). Recheck all personnel are wearing the proper personal protective equipment.

  Only the minimum number of personnel is to take part in any steps which require entering the test cell.

  If Cold Gas Thruster (section D) procedure has already been followed, skip to check point E.6.
  If Rocket Firing (section F) procedure has already been followed, skip to check point E.5.

☐	E.1. Make sure the **power cord** to the control box is unplugged and once inside the test cell unplug the **air supply** to the pneumatic valves
☐	E.2. Slowly open **nitrogen cylinder**
☐	E.3. Set **nitrogen regulator** to 100psi
☐	E.4. Close **oxygen cylinder**

☐	E.5. Close **nitrogen cylinder**
☐	E.6. **WARNING LOUD** – Depressurize fuel line by slowly opening the **fuel drain (needle) valve**, close the valve when no more noise is heard
☐	E.7. Pull out the cap on the **Fuel Drum** to deploy the spout and remove cap
☐	E.8. Use syringe to pull out the desired amount of fuel (300mL max)
☐	E.9. Open **fuel fill valve**
☐	E.10. Make sure the nitrogen line that feeds into the fuel tank is above the fuel tank to prevent ethanol from flowing backwards to the nitrogen regulator and cylinder
☐	E.11. The fuel handler must ground himself/herself
☐	E.12. Inject the ethanol into the fuel tank, make sure fuel does not back up and overflow
☐	E.13. If one syringe full of fuel is not enough return to E.8 and repeat up to 300mL total fuel in the fuel tank
☐	E.14. Close **fuel fill valve**
☐	E.15. Remove grounding method
☐	E.16. Unless previous tests set the regulators to the required pressure output and it would be difficult to set them to the same value, make sure the nitrogen and oxygen pressure regulators are unscrewed (set to zero)
☐	E.17. Slowly crack open the **nitrogen cylinder**, once the regulator high pressure gauge stops moving fully open the cylinder valve
☐	E.18. Unless previously set, now set the **nitrogen pressure regulator** to desired testing pressure (maximum 1,500 psi)
☐	E.19. Slowly crack open the **oxygen cylinder**, once the regulator high pressure gauge stops moving fully open the cylinder valve
☐	E.20. Unless previously set, now set the **oxygen pressure regulator** to desired testing pressure (maximum 1,500 psi)
☐	E.21. Plug in the **air supply** to the pneumatic valves and **all personnel** return to the control room and close the doors to the test cell

F. ROCKET FIRING

Before firing the rocket with fuel it is important to make sure all personnel return to the control room, the control room doors are secured/closed, and that these procedures are strictly followed.

Only the minimum number of personnel are to take part in any steps which require entering the test cell.

☐	F.1. All personnel return to the control room from the test cell
☐	F.2. Post range safety officers outside around the perimeter of the Propulsion Laboratory to warn passersby of the loud noises from the tests to be performed
☐	F.3. Confirm all switches on the control box are in the OFF position
☐	F.4. Plug in the **control box**
☐	F.5. Confirm the **sensor power switch** is turned ON and the sensors are active

☐	F.6. On the LabVIEW GUI: a. Click the **Run** button to begin LabVIEW GUI b. Enter in file name when prompted c. Click the **Record** button on the front panel of the VI
☐	F.7. Power ON the control box (plug in, turn on power breaker, plug in and turn on the key switch)
☐	F.8. **CRITICAL** – Turn ON **Coolant Timed Relay Override Switch** and confirm coolant flow, observing a strong steady stream of water coming out of coolant exit and the water pressure gauge reading about 50psi
☐	F.9. Press and hold the **Spark** switch ON
☐	F.10. Switch the **Fuel Enable** and **Oxygen Enable Switches** to ON a. Trigger the actuators b. If the rocket ignites with combustion in the chamber release the **Spark** switch c. If the rocket does not ignite or ignites outside the combustion chamber, turn all control box switches to OFF and skip to misfire procedures section G
☐	F.11. At the end of the run, switch **Fuel Enable** and **Oxygen Enable Switches** to OFF
☐	F.12. On the LabVIEW GUI a. Click the **Record** button to stop LabVIEW data recording b. You may click the **Stop** button to stop running the LabVIEW GUI, but it is not necessary if further monitoring of the sensors is required
☐	F.13. Allow coolant to circulate through the engine for at least 10 extra seconds after the firing
☐	F.14. Turn all control box switches to OFF
☐	F.15. If multiple runs are required continue to section G, if not skip to section H: Rocket Safing and Closeout

G. ROCKET MISFIRE AND/OR MULTIPLE RUNS

Only the minimum number of personnel are to take part in any steps which require entering the test cell.

☐	G.1. Confirm all switches on **Main Control Box** are in the OFF position and the box is unplugged
☐	G.2. Confirm no residual ignition source is in test area by checking for flames, heat waves, or other signs of fire
☐	G.3. Enter the test cell and check or troubleshoot the system while taking no action a. If the system is in correct working order go back to section F or E (as appropriate) and repeat if multiple runs are desired. If multiple runs are not desired proceed to section H b. If the system is not in correct working order, close **cylinder valves**, reenter control room, and vent all remaining pressure in the **oxygen** and then the **fuel lines** as done in H6 and H7 sections. After depressurizing the system enter test cell and disconnect oxygen and nitrogen cylinders. Proceed with system investigation and troubleshooting. If at any point in doubt, secure the area and contact advisor, department safety coordinator, EHS, and/or campus police as described under the first section "PROCEDURE HAZARDS…"

H. ROCKET SAFING AND CLOSEOUT

☐	H.1. Before entering test area confirm there is no ongoing combustion or fire by checking for flames, heat waves, or other signs of fire. Unplug the **power cord** to the control box and the test conductor has possession of the **control key**
☐	H.2. Close **oxygen cylinder**
☐	H.3. Close **nitrogen cylinder**
☐	H.4. Return to control room, plug in the **power cord** to the control box
☐	H.5. Depressurize oxygen line by turning ON the **Power Breaker Switch**, the **Key Switch**, the **Oxygen Enable Switch**, and the **Fire Trigger** until no sound is heard, the regulated pressure gauge reads zero, and the LabView output on the Oxygen Venturi Pressures is zero. Turn OFF the **Oxygen Enable Switch**
☐	H.6. Depressurize nitrogen line by turning ON the **Power Breaker Switch**, the **Key Switch**, the **Fuel Enable Switch**, and the **Fire Trigger** until no sound is heard, the regulated pressure gauge reads zero, and the LabView output on the Ethanol Venturi Pressures is zero. Turn OFF the **Fuel Enable Switch**
☐	H.7. Turn OFF the **Power Breaker Switch** and unplug the **power cord** to the control box
☐	H.8. The test conductor has possession of the Key to the Key Switch and now enter test cell
☐	H.9. In case there is any fuel left in the fuel tank, place glass fuel beaker below **fuel drain (needle) valve** and drain the residual fuel by opening the **fuel drain (needle) valve** and **fuel fill valve**
☐	H.10. Close **fuel drain (needle) valve** and **fuel fill valve**
☐	H.11. Residual fuel in beaker can be disposed of in the hazardous waste container supplied by EHS. Continue to follow the same static electricity precautions and wearing gloves as when disposing. If the container cannot be found or it is full contact EHS for a replacement
☐	H.12. Unscrew **nitrogen regulator** (turn it OFF)
☐	H.13. Slowly open **nitrogen cylinder**
☐	H.14. Set **nitrogen regulator** to 100psi
☐	H.15. Reenter control room and plug in the **power cord** to the control box
☐	H.16. Double check that the fuel line is clear by turning the **Power Breaker Switch**, the **Key Switch**, and the **Fuel Enable Switch** to ON
☐	H.17. Pulse the **Fire Trigger** until no liquid is seen exiting the rocket nozzle
☐	H.18. Turn OFF the **Fuel Enable**, the **Key Switch**, and the **Power Breaker Switch**, test conductor has possession of the key, enter the test cell, and close the **nitrogen cylinder**
☐	H.19. **WARNING LOUD** – Depressurize fuel line by slowly opening the **fuel drain (needle) valve**
☐	H.20. Unplug **air supply hose**
☐	H.21. Close **coolant water supply valve**
☐	H.22. Turn ON the control box and flip the C**oolant Override Switch** so the coolant solenoid valve is kept open. The pressure on the water pressure gauge should go to zero
☐	H.23. Attach the air supply hose to the water spigot fork and slowly open the valve on the fork, allowing the shop air to pressurize the water and start the drying process
☐	H.24. Warning: When only a few feet of the water are left in the return hose, the end of the return hose will want to flail around throwing water everywhere! So keep the end secured and covered
☐	H.25. Run air through the coolant system for about 3 minutes, and then turn OFF the air supply at the large wall supply valve. Open the water supply hose at the end connected to the test stand and spray a little bit of Sili Kroil (or similar Kroil lubricant/water displacer) into the water inlet then reconnect the water supply hose and turn the air back ON. The Sili Kroil helps prevent oxidation of the components of the engine and help reduce hard water deposits

☐	H.26. After 5-6 minutes of running shop air through the coolant system, there should be no more liquid seen in the clear vinyl tubing supplying the engine. Once that is checked, turn OFF the wall air supply valve and close all valves on the coolant supply fork
☐	H.27. Turn OFF coolant override switch, turn OFF control box, and remove the key. The test conductor has possession of the key
☐	H.28. Put away the air supply hose and control box key
☐	H.29. Close LabView

I. LAB CLOSE-OUT

☐	I.1. Close roll up doors
☐	I.2. Clean up any remaining tools, equipment, etc. and lock up equipment cabinet
☐	I.3. Replace ear and eye protection in the cabinet
☐	I.4. Test conductor collects all hard copies of the procedures and makes sure none are left floating around. This is to make sure only the most up-to-date version is used
☐	I.5. Close lab

Appendix B: Cold Flow Test Plan

AARLITE Cold Flow Test Plan

- Background/Intro

Cold flow testing using GOX and GN2 must be done in order to check the engine and feed system for leaks, structural capability, overall system functionality, and instrumentation functionality. Only GOX and GN2 are used without ethanol to simulate the setup of the experiment without having the added complication of combustion.

While hot-firing the AARLITE system is expected to generate combustion pressures of about 1000 psig, cold flow testing is expected to operate at much lower pressures because the nozzle will not be choked.

- Test Objectives
    - Demonstrate and improve testing procedures
    - Determine if there are any feed system leaks at feed pressure
    - Measure cold flow chamber pressure
    - Determine if the engine seals function properly at cold flow chamber pressure
    - Demonstrate sufficient engine strength at the cold flow combustion pressures
    - Demonstrate the feed system can supply the engine with propellant
    - Use the data acquisition system to collect data as a measure of system capability
    - Demonstrate the Venturi flow measurement nozzles give reasonable values
    - Determine if the chamber pressure measurement tap reads the chamber pressure
    - Demonstrate the coolant system is leak free
    - Calibrate or quantify bias of pressure transducers and load cells

- Firsts
    - Use of UCAR 323 and 0.010” thick Grafoil gasket for manifold/injector and combustion chamber sealing

- Use of the multiple part engine design
- Use of the data processing, acquisition, and measurement system
- Use of the engine control system

- Test matrix

Test number	Gaseous Nitrogen Feed Pressure (PSIG)	Measured Nitrogen Feed Pressure (PSIG)	Gaseous Oxygen Feed Pressure (PSIG)	Measured Oxygen Feed Pressure (PSIG)	Planned Run Time (sec)	Actual Run Time (sec)	Comments	Notes
1	100		100		5 to 10		Required test	
2	200		200		5 to 10		Required test	
3	300		300		5 to 10		Required test	
4	400		400		5 to 10		Not required, may be skipped but not by more than 400PSIG	
5	500		500		5 to 10		Not required, may be skipped but not by more than 400PSIG	
6	600		600		5 to 10		Not required, may be skipped but not by more than 400PSIG	
7	700		700		5 to 10		Not required, may be skipped but not by more than 400PSIG	
8	800		800		5 to 10		Not required, may be skipped but not by more than 400PSIG	
9	900		900		5 to 10		Not required, may be skipped but not by more than 400PSIG	
10	1000		1000		5 to 10		Not required, may be skipped but not by more than 400PSIG	
11	1100		1100		5 to 10		Not required, may be skipped but not by more than 400PSIG	
12	1200		1200		5 to 10		Not required, may be skipped but not by more than 400PSIG	
13	1300		1300		5 to 10		Not required, may be skipped but not by more than 400PSIG	
14	1400		1400		5 to 10		Not required, may be skipped but not by more than 400PSIG	
15	1500		1500		5 to 10		Not required, may be skipped but not by more than 400PSIG	

- Measurements (instrumentation)

Engine thrust using 200lbf AmCell load cell. Duct thrust using 25lbf AmCell load cell. Both load cell signals are conditioned and amplified by two Tacuna Systems signal conditioners and amplifiers.

Five 3,000 psi amplified pressure transducers are used to measure the combustion chamber pressure at the face of the injector and the differential pressures across the ethanol and oxygen Venturi flow measurement nozzles.

The data signals are sent to a USB NI DAQ and recorded using a LabView program.

- Risks

The engine's structural capability has not yet been proven. Testing from low pressure (100 psi) and incrementally increasing the pressure is conducted to mitigate the chances of the engine structure not behaving as expected.

Components which carry oxygen may have contaminants which can combust unexpectedly. Testing from low pressure (100 psi) and incrementally increasing the pressure is conducted to mitigate the chances of unexpected combustion. Stringent cleaning practices based on industry standards and approved by Cal Poly EH&S is employed to mitigate the chances of combustible contaminants being in parts which carry oxygen.

Appendix C: Hot Fire Test Readiness Review (TRR) for More than 420psi Chamber Pressure

AARLITE Hot Fire Test Readiness Review (TRR) V4/4

- Process
  - Hot fire testing using GOX and ethanol must be done in order to check the engine and feed system for leaks, structural capability, overall system functionality, and

instrumentation functionality. GOX and ethanol pressurized with GN2 are used. Also refer to the AARLITE Hot Fire Test Plan for more information.

- Unit Under Test
    - Predicted structural margin
        - Assuming a 1,500psi chamber pressure, a 2.6 Factor of Safety (FoS) exists on the 16 #2-56 bolts which hold the nozzle on the engine. This FoS is the lowest throughout the engine and means the 16 bolts will break in tension before any other component will fail.
    - Predicted thermal margin
        - Assuming the heat transfer rate at the throat of the nozzle applied to the entire inner area of the engine, a mass flow rate of ~1 lbm/s of water is required to keep the engine cool. This estimate is extremely conservative and it must be noted the steel shell which is the main structural component of the engine is shielded from combustion temperatures and kept below 200degF.
    - Ballistic and performance predictions
        - 1,000psi nominal combustion pressure and 100lbf nominal thrust
    - Validation data or risk mitigation approaches for all of the above
        - The engine will be injected with ethanol and oxygen starting at 100psi and incrementally working up to higher pressures in 100psi increments (100, 200, 300, 400…900, 1000psi). The chamber pressure and thrust will be monitored to make sure the chamber pressure does not spike to dangerous levels. If a trend of high pressure (over 1,500psi) becomes apparent when testing at lower injection pressures, then increasing the feed pressures will not proceed any further. Additionally the nozzle will be inspected for erosion with each firing.
        - ½" thick, 9" long, 8" diameter aluminum pipe surrounds engine during first few firings
    - Expected failure modes in event of overpressure
        - The 16 bolts holding the nozzle onto the engine will break and release the nozzle from the rest of the engine. The nozzle will fall downward opening the combustion chamber and releasing all combustion pressure.

- Test Setup
    - See Cold Flow TRR notes and the Cold Flow Test Plan

- Procedures
    - Refer to the Cold Flow Test Plan, the Hot Fire Test Plan, and the AARLITE Firing Procedures
    - The engine will be injected with ethanol and oxygen starting at 100psi and incrementally working up to higher pressures in 100psi increments (100, 200, 300, 400…900, 1000psi chamber pressure). The chamber pressure and thrust will be monitored to make sure the chamber pressure does not spike to dangerous levels. If a trend of high pressure (over 1,500psi) becomes apparent when testing at lower injection pressures, then increasing the feed pressures will not proceed any further. Additionally the nozzle will be inspected for erosion with each firing.
    - ½" thick, 9" long, 8" diameter aluminum pipe surrounds engine during first few firings

Appendix D: Hot Fire Test Plan for More than 420psi Chamber Pressure

AARLITE Hot Fire Test Plan V5/5

- Background/Intro

Hot fire testing using GOX and ethanol must be done in order to check the engine and feed system for leaks, structural capability, overall system functionality, and instrumentation functionality. GOX and ethanol pressurized with GN2 are used.

- Test Objectives
    - Measure hot fire duct thrusts
    - Test above 420 psi chamber pressure

- Firsts
    - Test above 420 psi chamber pressure

- Test matrix

Test number	Nitrogen Regulator Pressure (PSIG)	Measured Nitrogen Feed Pressure (PSIG)	Oxygen Regulator Pressure (PSIG)	Measured Oxygen Feed Pressure (PSIG)	Planned Run Time (sec)	Actual Run Time (sec)	Comments	Notes
1	100		100		1 to 5	1 to 2	Required test	Done in previous tests
2	200		200		1 to 5	1 to 2	Required test	Done in previous tests
3	300		300		1 to 5	1 to 2	Required test	Done in previous tests
4	400		400		1 to 5	1 to 2	Not required, may be skipped but not by more than 400PSIG	Done in previous tests
5	500		500		1 to 5	1 to 2	Not required, may be skipped but not by more than 400PSIG	Done in previous tests
6	600		600		1 to 5	1 to 2	Not required, may be skipped but not by more than 400PSIG	Done in previous tests
7	700		700		1 to 5	1 to 2	Not required, may be skipped but not by more than 400PSIG	Done in previous tests
8	800		800		1 to 5	1 to 2	Not required, may be skipped but not by more than 400PSIG	Done in previous tests
9	900		900		1 to 5		Not required, may be skipped but not by more than 400PSIG	
10	1000		1000		1 to 5		Not required, may be skipped but not by more than 400PSIG	
11	1100		1100		1 to 5		Not required, may be skipped but not by more than 400PSIG	
12	1200		1200		1 to 5		Not required, may be skipped but not by more than 400PSIG	
13	1300		1300		1 to 5		Not required, may be skipped but not by more than 400PSIG	
14	1400		1400		1 to 5		Not required, may be skipped but not by more than 400PSIG	
15	1500		1500		1 to 5		Not required, may be skipped but not by more than 400PSIG	

- Measurements

Pre-test fire	During test fire	Post-test fire
Feeler gauges are used to check the gap between the nozzle and steel outer shell	Engine thrust using 200lbf AmCell load cell. Duct thrust using 25lbf AmCell load cell. Both load cell signals are conditioned and amplified by two Tacuna Systems signal conditioners and amplifiers	Feeler gauges are used to check the gap between the nozzle and steel outer shell
Visual inspection of the chamber either by completely taking apart the engine or simply looking into the nozzle with a flashlight	Five 3,000 psi amplified pressure transducers are used to measure the combustion chamber pressure at the face of the injector, the differential pressure across the ethanol and oxygen Venturi flow tube meters	Visual inspection of the chamber either by completely taking apart the engine or simply looking into the nozzle with a flashlight
Water temperature is monitored	The data signals are sent to a	

and recorded before hot firing	6210 USB NI DAQ and recorded using a LabView program	
	Water temperature and pressure gauges are monitored for any off nominal behavior: temperature spikes and pressure changes not normally seen during cold flow testing	

- Risks

Higher chamber pressure and temperature will be experienced relative to cold flow testing. This could create unexpected leaks. This risk is mitigated by doing low pressure testing and limiting operating time.

External combustion risk is mitigated by limited fuel quantities, no personnel, in the test cell, no fuel neat the test stand, and having fire extinguishers handy. See the Rocket Engine Firing Procedures for further detailed explanation – This did **not** occur with 420 psi chamber pressure testing.

Maximum regulated feed pressure is 3,000 psi, maximum plumbing pressure downstream of the check valves is 2,200 psi, and the mitigation of this risk is handled by the Firing Procedure.

The engine's structure may not be capable of handling ignition of ethanol/GOX and 1,000psi nominal operating combustion pressure. Testing from low pressure (100 psi) and incrementally increasing the pressure is conducted to mitigate the chances of the engine structure not behaving as expected. Additionally an 8" diameter, 3/8" thick, 8" long aluminum pipe is placed around the engine to protect against the possibility of explosion.

The engine creates a loud noise when firing with combustion pressures about a few hundred pounds per square inch. A guard is posted outside the door of the propulsion laboratory to warn people going by that there will be a loud noise and to keep track of how loud it is outside.

There are many events taking place in the span of one test firing which is a few seconds of time. For example what the water outlet temperature gauge is doing, what the plume of the engine looks like, what the plume is doing (burning stuff it shouldn't be burning), etc. To capture all events for further analysis a camera(s) is used to film all test fires.

Appendix E: Oxygen Cleaning Procedure

AARLITE Project Gaseous Oxygen Service Cleaning Procedure

Preparation of Components for Gaseous Oxygen (GOX) Service

Purpose:
Parts used for the transfer of oxidizing liquids or gasses can fail with catastrophic results if a reducing agent (hydrocarbons, alcohol, etc.) is present where the oxidizing matter is present. This cleaning procedure will ensure that residual reducing agent(s) are cleaned to an acceptable level where the oxidizer will be present.

References:

ASTM G0093-03R11
CGA G-4.1
MIL-STD-1330D

Overview:
Five step cleaning process:

1. Pre-cleaning
2. Deep cleaning
3. De-ionized/distilled water rinse
4. Inspection
5. Purging with nitrogen

Chemicals to be used:

- Methylene Chloride: toxic, irritant, and registered carcinogen
- De-ionized/Distilled water
- Nitrogen gas

Follow Standard Operating Procedure for further information regarding handling and required precautions.

Step 1: Pre-cleaning
Ensure cleaning area is clean and free of possible sources of contamination. Remove all dust, or other lose contaminates with a brush, paper towel, or other suitable method from the part. Once loose contaminants are removed the part is rinsed with clean water.

Step 2: Deep cleaning
An oxygen service safe cleaning agent is used to thoroughly clean the part by hand. Dynaflux Safety Solvent (methylene chloride) is chosen for use in this procedure. A fume hood, nitrile gloves doubled with neoprene gloves, and splash protective goggles must be used to minimize exposure (for additional information see the project SOP and the University of Michigan's SOP on Methylene Chloride).

Dynaflux Safety Solvent is used to clean all remaining contaminants. Lint free Kimtech Kimwipes and powderless nitrile gloves are used where wiping is required and possible. The solvent is sprayed on the part until the part is thoroughly covered in solvent. Where possible the Kimwipes are used to wipe away the solvent and the dissolved contaminants until all areas are dry. For areas that are not accessible with Kimwipes, solvent is sprayed on until it starts to drip off, the part is then left to sit allowing the solvent to drain and dry off (normally takes about 10 minutes). For all areas the spraying and wiping/draining/drying process is repeated 3 times.

When handling part with gloved hands, ensure gloves only contact required items (i.e. never contaminate gloves and part by touching oily rags, dirty clothing, etc.).

Step 3: De-ionized/distilled water rinse
Part is soaked and then rinsed 3 times with de-ionized/distilled water as an extra measure to remove any residual methylene chloride, which has not evaporated. Lint free Kimwipes and powderless nitrile gloves are used where wiping is required and possible.

Step 4: Inspection
A three part inspection process on all parts is used:

- Visual
- Wipe
- UV Light

Visually inspect the part looking for obvious loose contaminates, grease, etc. If the part passes the initial visual inspection, accessible areas are wiped with a white lint free cloth (Kimwipe). The cloth must emerge clean to pass and move on to UV inspection. Finally, a UV light is used to check for any contaminants which could have been missed by the other inspection methods. The UV light will cause contaminants to fluoresce, if there is no fluorescence the part passes the UV light test.

If any part of the inspection process reveals contamination, the part is cleaned again and re-inspected.

Step 5: Purging with nitrogen
Part is purged (and therefore dried) using clean compressed nitrogen. The part may be assembled into the full assembly or purged individually. The main purpose is to ensure any remaining water is exhausted from the system and will not interfere with nominal operation. Otherwise de-ionized water will not combust with oxidizer or otherwise sustain/aid combustion.

Use of part(s) after cleaning, inspection, and purging:
The part is immediately installed or cleanly bagged/capped, and tagged for later use. Before a bagged or capped part is installed into a system, the inspection process is repeated to verify that the part was not contaminated while stored.

Appendix F: Project Safety Operation Plan (SOP)

Air Augmented Rocket with Large Induced Turbulence Engine (AARLITE) Standard Operating Procedure (SOP)

This is a Standard Operating Procedure (SOP) for the Air Augmented Rocket with Large Induced Turbulence Engine (AARLITE). It is a written set of instructions that document safety involving AARLITE's hazardous operations. The SOP was written for procedures that pose an identified potential risk to the health and safety of laboratory personnel. A print out of the completed form is kept readily accessible in the lab (also an electronic copy is always available through the Dropbox folder).

Process:

There are two processes required for the AARLITE project that could be hazardous: oxygen service cleaning and static test firing. The static test firing of the engine will use gaseous oxygen (GOX) as the oxidizer and 190 proof denatured ethanol as the fuel. Methylene chloride is used for chemical cleaning of oxygen service components.

Purpose:

Static test firing: Combustion of the fuel and oxidizer is the primary focus of this study. During a static test fire the combustion chamber will be strapped down to an instrumented test stand which will record the needed data. With an ignition spark the fuel and oxidizer are injected into the combustion chamber, combust, and exit through the nozzle of the engine. Ethanol is used as the fuel in the rocket engine and GOX is used as the oxidizer. A spark plug is used for ignition.

Oxygen service cleaning: components that contain and are in contact with GOX must be clean of all combustible substances to prevent unexpected combustion. Methylene chloride is used for chemical cleaning of oxygen service components.

Potential Hazards/Toxicity:

Potential Acute Health Effects:
Ethanol is flammable and toxic. Ethanol can cause skin and/or eye irritation in case of contact; otherwise it is non-corrosive to skin, to eyes, and lungs. Gaseous oxygen (GOX) is a strong oxidizer and is kept under pressure. Methylene chloride is toxic and a registered carcinogen.

Engineering Controls:

Provide exhaust ventilation or other engineering controls to keep the airborne concentrations of vapors below their respective threshold limit value. The roll up doors to the laboratory must always be fully open when using ethanol and/or GOX.

Methylene chloride must be used in a fume hood.

Ensure that eyewash stations and safety showers are proximal to the work-station location.

Personal Protective Equipment (PPE)-

Hand Protection:
Nitrile gloves must be worn whenever handling chemicals. Nitrile gloves must be doubled with neoprene gloves for handling methylene chloride.

Eye Protection:
All personnel must have and wear safety glasses (Z87+ or better). Splash protective goggles must be worn when working with methylene chloride.

Skin and Body Protection:
Personnel working with the ethanol and methylene chloride need to wear full-length clothing or its equivalent, closed-toe footwear with no exposed skin.

Hygiene Measures:
Wash hands after working with the hazardous substances and when leaving the lab/shop.

First Aid Procedures for Chemical Exposures

In all cases, notify supervisor as soon as possible.
If inhaled:
If inhaled, remove to fresh air. If not breathing call 911 and give artificial respiration. If breathing is difficult, call 911.
Serious Inhalation:
Evacuate the victim to a safe area as soon as possible. Loosen tight clothing such as a collar, tie, belt or waistband. If breathing is difficult, administer oxygen. If the victim is not breathing, perform mouth-to-mouth resuscitation. Seek medical attention. Call 911
In case of skin contact:
In case of contact, immediately flush skin with plenty of water for 15 minutes. Remove contaminated clothing and shoes. Wash clothing before reuse. Thoroughly clean shoes before reuse. Get medical attention as necessary.
In case of eye contact:
Immediately flush eyes with running water for at least 15 minutes, keeping eyelids open. Check for and remove any contact lenses. Get medical attention.
If swallowed:

Do NOT induce vomiting unless directed to do so by medical personnel. Never give anything by mouth to an unconscious person. Loosen tight clothing such as a collar, tie, belt or waistband. Call 911 as appropriate.

Special Handling and Storage Requirements for Hazadrous Materials
Precautions:
Keep locked up. Keep away from heat. Keep away from sources of ignition. Ground all equipment containing material. Do not ingest. Do not breathe gas/fumes/ vapor/spray. Wear suitable protective clothing. In case of insufficient ventilation, wear suitable respiratory equipment. If ingested, seek medical advice immediately and show the container or the label. Avoid contact with skin and eyes. Keep away from incompatibles such as oxidizing agents, acids, alkalis, moisture.

Storage:

Store in a segregated and approved area. Keep container in a cool, well-ventilated area. Keep container tightly closed and sealed until ready for use. Avoid all possible sources of ignition (spark or flame). Do not store above 23°C (73.4°F).

Spill and Accident Procedure

Chemical Spill Dial 911 and (805) 756-6661

Spill – Assess the extent of danger, the number one concern is personal safety and the safety of those around you. Evacuate the spill area. Help contaminated or injured persons. Avoid breathing vapors. If safe, confine the spill to a small area using a spill kit or absorbent material. Keep others from entering contaminated area (e.g., use caution tape, barriers, etc.).

- **If Small Spill (less than 1gal)** – Dilute with water and mop up, or absorb with an inert dry material and place in an appropriate waste disposal container.
- **If Large Spill (more than 1gal)** – Evacuate spill area, the number one concern is personal safety and the safety of those around you. Evacuate the spill area. Help contaminated or injured persons. Avoid breathing vapors. Flammable liquid. If safe, keep away from heat or other sources of ignition. Stop leak if without risk. If safe, absorb with DRY earth, sand or other non-combustible material. Do not touch spilled material. If safe, prevent entry into sewers, basements or confined areas; dike if needed. Dial **911** and EH&S at (805) 756-6661 for assistance. Remain available in a safe, nearby location for emergency personnel.

- **Medical Emergency Dial 911 or (805) 756-6661**

Life Threatening Emergency, After Hours, Weekends And Holidays – Dial 911
Note: All serious injuries must be reported to Supervisor/PI within 8 hours. Note: Any and all loss of consciousness requires a 911 call

Non-Life Threatening Emergency –

- Students: Seek medical attention at the campus Health Center M, T, Thu, Fr 8:00 am – 4:30 pm and W 9:00 am – 4:30 pm
- Emergency Medical services in the community are available at any time at hospital emergency rooms and some emergency care facilities.

For STUDENTS: All injuries must be reported to PI/Supervisor immediately and follow campus injury reporting. Follow procedures for reporting of student, visitor injury on the EH&S website at: http://afd.calpoly.edu/riskmgmt/incidentreporting.asp

- Paid staff, students, faculty: seek initial medical attention for all non-life threatening injuries at:

  - MED STOP, 283 Madonna Road, Suite B (next to See's Candy in Madonna Plaza) (805) 549-8880 Hours: M-F 8a - 8p; Sat/Sun 8a - 4p
  - **After MED Stop Hours:** Sierra Vista Hospital Emergency Room 1010 Murray Avenue (805) 546-7651, Open 24 hours

For EMPLOYEES: All injuries must be reported to PI/Supervisor immediately and follow campus injury reporting for employee injuries (Workmen's Comp.). Follow procedures on the EH&S website at: http://afd.calpoly.edu/riskmgmt/incidentreporting.asp

Decontamination/Waste Disposal Procedure

General hazardous waste disposal guidelines:

Label Waste

- Affix a hazardous waste tag on all waste containers as soon as the first drop of waste is added to the container. Generic waste labels can be found here: http://afd.calpoly.edu/ehs/docs/hazwaste_label_template.pdf

Store Waste

- Store hazardous waste in closed containers, in secondary containment and in a designated location
- Double-bag dry waste
- Waste must be under the control of the person generating & disposing of it

Dispose of Waste

- Dispose of regularly generated chemical waste as per guidelines on EH&S website at: http://afd.calpoly.edu/ehs/docs/csb_no6.pdf
- Prepare for transport for pick-up. Use secondary containment.

Call EH&S at (805) 756-6661 for questions.

Empty Containers-

- Dispose as hazardous waste if container once held extremely hazardous waste (irrespective of the container size) A list can be found at: http://afd.calpoly.edu/ehs/docs/extremely_hazardous_wastes.pdf
- All other containers are legally empty once a concerted effort is made to remove, pour out, scrape out, or otherwise completely empty the vessel. These may be disposed of as recycling or common trash as appropriate.

Safety Data Sheet (SDS) Location

Online SDS can be accessed at: http://siri.org/msds/index.php

or MSDSOnline at: http://hq.msdsonline.com/csuedusl/Search/Default.aspx

or see the attached GOX and ethanol MSDS

Protocol/Procedure (Add lab specific Protocol/Procedure here)

Please see attached AARLITE FIRING PROCEDURES and OXYGEN SERVICE CLEANING PROCEDURE

NOTE: Any deviation from this SOP requires approval from PI.

Date: **P.I. or Supervisor: Dr. Dianne DeTurris**

Signature of P.I. or Supervisor:

Documentation of Training (signature of all users is required)

- The Principal Investigator must ensure that his/her laboratory personnel have attended appropriate laboratory safety training or refresher training within the last one year.
- Training must be administered by PI or Lab Manager to all personnel in lab prior to start of work with particularly hazardous substance or newly synthetic chemical listed in the SOP.

- Refresher training will need to be provided when there is a change to the work procedure, an accident occurs, or repeat non-compliance.

I have read and understand the content, requirements, and responsibilities of this SOP:

Name	Signature	Date

Appendix G: Microsoft Visual Basic Program Written by Ross Gregoriev

The following code was written by Ross Gregoriev to help filter and compact the data which was obtained using LabView. The code calculated the moving average on the data from LabView which filtered a large amount of noise and sharp spikes, and reduced the data from 10,000-30,000 rows to a few hundred rows. The filtered and compacted data was more manageable, manipulatable, and more easily understood than the data that came out of LabView.

The code:

```
Attribute VB_Name = "Module1"
'Allen Editable
Const DividerVal As Double = 100

Sub DoRunningAverage()
'selected range should be somewhere inside the data.
'It assumes contiguous data for everything to work properly
Call RunningAverage(ActiveSheet.Range("A16"), DividerVal)
End Sub

Sub RunningAverage(DataLoc As Range, DividerIn As Double)

Dim tmpArr() As Variant
Dim StartRow As Long
Dim pasteArr() As Variant
Dim pasteArrIndx As Long
Dim DstCol As Integer

tmpArr = DataLoc.CurrentRegion
```

```
For y = LBound(tmpArr, 1) To UBound(tmpArr, 1)
   If IsNumeric(tmpArr(y, 1)) And tmpArr(y, 1) = 0 Then
      StartRow = y
      Exit For
   End If
Next

Dim ArrSum As Double
Dim SrcRange As Range
Set SrcRange = DataLoc.CurrentRegion

For x = LBound(tmpArr, 2) To UBound(tmpArr, 2)
pasteArrIndx = 1
ArrSum = 0
   For y = StartRow To UBound(tmpArr, 1)
      If y Mod DividerIn Then 'IsNumeric(tmpArr(y, x)) And
      ArrSum = ArrSum + tmpArr(y, x)
      Else
      ArrSum = ArrSum + tmpArr(y, x)
      ReDim Preserve pasteArr(pasteArrIndx)
      pasteArr(pasteArrIndx) = ArrSum / DividerIn
      pasteArrIndx = pasteArrIndx + 1
      ArrSum = 0
      End If
   Next

   Dim OutArr As Variant
   ReDim OutArr(1 To UBound(pasteArr) + 1, 1 To 1)
   For i = 1 To UBound(pasteArr)
   OutArr(i, 1) = pasteArr(i)
   Next

   DstCol = SrcRange.Column + SrcRange.Columns.Count + x
   With Sheets(DataLoc.Parent.Index)

   .Columns(DstCol).Clear

   .Range(.Cells(StartRow + SrcRange.Row - 1, DstCol), .Cells(StartRow + UBound(OutArr, 1) +
SrcRange.Row - 3, DstCol)) = OutArr
   End With
Next
End Sub
```

Appendix H: Example Input File to Chemical Equilibrium Application (CEA)

The following is the input file written and given to the CEA program. Access to the program was granted by Jeff Muss of Sierra Engineering Inc.

```
reac
     oxid O2  wtfrac= 1   t(k)= 293
     fuel C2H5OH(L)   wtfrac= 1   t(k)= 293

prob   case = EthGOX_RO_FAC
```

ro, fac ac/at=5,

p(psi)=559.65, o/f = .9586

!o/f = 0.7,1.5,1.8,2.1,2.4,2.7 !longer set of ox/fuel ratios
!note: stoichiometric mix = 2.1

output siunits trace=1.e-15

end

Appendix I: Full Engine Performance and Design Calculations

Calculate the exit velocity:

- Calculate throat and exit conditions (assuming choked CD nozzle)
- Calculate throat and exit conditions (assuming supersonic CD nozzle)
- The nozzle of the engine is calculated to be optimally expanded at sea level
- Exit velocity (12):
  - $V_e = \sqrt{\frac{2\gamma}{\gamma-1} * R * T_c * \left(1 - \left(\frac{P_{amb}}{P_c}\right)^{\frac{\gamma-1}{\gamma}}\right)} = \sqrt{\frac{2*1.1922}{1.1922-1} * 334.9 * 3489.7 * \left(1 - \left(\frac{101325}{6894757.29}\right)^{\frac{1.1922-1}{1.1922}}\right)} = \mathbf{2,675\frac{m}{s}}$
- Exit Mach number (14):
  - $Me = \sqrt{\frac{2}{\gamma-1}\left(\left(\frac{P_c}{P_{amb}}\right)^{\frac{\gamma-1}{\gamma}} - 1\right)} = \sqrt{\frac{2}{1.1922-1} * \left(\left(\frac{6894757.29}{101325}\right)^{\frac{1.1922-1}{1.1922}} - 1\right)} = \mathbf{3.18\ Mach}$

Thrust Coefficient (12):

- $C_f = \sqrt{\frac{2\gamma^2}{\gamma-1}\left(\frac{2}{\gamma+1}\right)^{\frac{\gamma+1}{\gamma-1}}\left(1 - \left(\frac{P_{amb}}{P_c}\right)^{\frac{\gamma-1}{\gamma}}\right)} = \sqrt{\frac{2*1.1922^2}{1.1922-1} * \left(\frac{2}{1.1922+1}\right)^{\frac{1.1922+1}{1.1922-1}} * \left(1 - \left(\frac{101325}{6894757.29}\right)^{\frac{1.1922-1}{1.1922}}\right)} = \mathbf{1.60}$

Nozzle Throat and Exit:

- Throat area (12):
- $A_t = \frac{F}{C_f * P_c} = \frac{444.822}{1.60*6894757.29} = \mathbf{4.03 \times 10^{-5}\ m^2 = 0.0625\ in^2}$
- Throat radius:
- $R_t = \sqrt{\frac{A_t}{\pi}} = \sqrt{\frac{4.03\times10^{-5}}{\pi}} = \mathbf{0.00358\ m = 0.141\ in}$
- Nozzle expansion ratio (14):
- $\varepsilon = \frac{1}{M_e}\left(\frac{2}{\gamma+1}\left(1 + \frac{\gamma-1}{2}M_e^2\right)\right)^{\frac{\gamma+1}{2(\gamma-1)}} = \frac{1}{3.18} * \left(\frac{2}{1.1922+1} * \left(1 + \frac{1.1922-1}{2} * 3.18^2\right)\right)^{\frac{1.1922+1}{2*(1.1922-1)}} = \mathbf{8.95}$
- Exit radius:
- $R_e = R_t\sqrt{\varepsilon} = 0.00358\sqrt{8.95} = \mathbf{0.0107\ m = 0.422\ in}$

Thrust Chamber:

- The contraction ratio is the chamber area to throat area ratio: $\varepsilon_c = \frac{A_c}{A_t}$

- The contraction ration should be at least 4 to assure the isentropic flow assumptions are valid for the design of the engine
- Assume chamber is 5 times the size of R_t
- Chamber radius:
  - $R_{c,max} = 5R_t = 5 * 0.00358 = \mathbf{0.0179\ m = 0.705\ in}$
- **Note, min chamber radius:**
  - $R_{c,min} = 4R_t = 4 * 0.00358 = \mathbf{0.01432\ m = 0.564\ in}$
- Chamber area:
- $A_{c,max} = \pi R_c^2 = \pi * 0.0179^2 = \mathbf{0.00101\ m^2 = 1.57\ in^2}$
- **Note, min chamber area:**
  - $A_{c,min} = \pi R_{c,min}^2 = \pi * 0.01432^2 = \mathbf{0.0006442\ m^2 = 0.9985\ in^2}$

- Characteristic chamber length from Johnson (5). He used methanol/GOX, but assume ethanol/GOX will be close enough:
  - $L^\star = 80in$
  - Convert to metric [m]: $L^\star = L^\star * \frac{2.54}{100} = 2.032\ m$
- Chamber volume:
- $V_c = L^\star * A_t = 2.032 * 4.03 \times 10^{-5} = 8.19 \times 10^{-5} m^3$
- Chamber length:
- $L_c = \frac{V_c}{A_{c,max}} = \frac{8.19 \times 10^{-5}}{0.00101} = \mathbf{0.0811\ m = 3.19\ in}$

Mass flow rates:

- Total propellant mass flow rate:
- $\dot{m} = \frac{F}{V_e} = \frac{444.822}{2675} = \mathbf{0.166\ \frac{kg}{s} = 0.366\ \frac{lbm}{s} = 0.0114\ \frac{slug}{s}}$
- Mixture ratio: $mixRatio_{stoichometric} = 2.1$
- Oxygen mass flow rate:
- $\dot{m}_{Ox} = \frac{\dot{m}}{1 + mixRatio} * mixRatio = \frac{0.166}{1+2.1} * 2.1 = \mathbf{0.112\ \frac{kg}{s} = 0.247\ \frac{lbm}{s} = 0.00767\ \frac{slug}{s}}$
- Fuel mass flow rate:
- $\dot{m}_{Fuel} = \frac{\dot{m}}{1 + mixRatio} = \frac{0.166}{1+2.1} = \mathbf{0.0535\ \frac{kg}{s} = 0.118\ \frac{lbm}{s} = 0.00366\ \frac{slug}{s}}$
  - Side note the SCFH are:
    - $SCFH_{Ox} = \frac{R_{Ox} * T_{room}}{P} * \dot{m}_{Ox} = \frac{48*530}{1500*144} * .3 * 3600 = \mathbf{104.7\ \frac{ft^3}{hr}}$
- Total mass of fuel and oxygen used if $\boldsymbol{t_{burn} = 5\ sec}$:
  - $m_{Ox} = \dot{m}_{Ox} * t_{burn} = 0.112 * 5 = \mathbf{0.560\ kg = 1.232\ lbm}$
  - $m_{Fuel} = \dot{m}_{Fuel} * t_{burn} = 0.0535 * 5 = \mathbf{0.2675\ kg = 0.5885\ lbm}$
  - If ethanol's density is $\rho_{Fuel} = 0.789 \frac{g}{cm^3}$ then the volume of ethanol needed per burn is:
    - $v_{Fuel} = \frac{m_{Fuel}}{\rho_{Fuel}} = \frac{0.2675*1000}{0.789} = \mathbf{339\ cm^3 = 0.339\ L}$

Specific Impulse (12):

- Total propellant mass flow rate:
- $I_{sp} = \frac{F}{\dot{m} * g_0} = \frac{F}{\dot{w}} = \frac{444.822}{0.166*9.81} = \mathbf{273.2\ s}$

Appendix J: Pressure Transducers, Load Cells, and Load Cell Conditioners

The five pressure transducers used throughout the test stand are made by Wika, are rated to $3{,}000\ psi$, and were ordered from McMaster. The transducers' data sheets are in the following picture and what each transducer measures is hand written on the data sheets.

The 200 lbf and 25 lbf load cells were made by AmCell and purchased from Tacuna Systems.

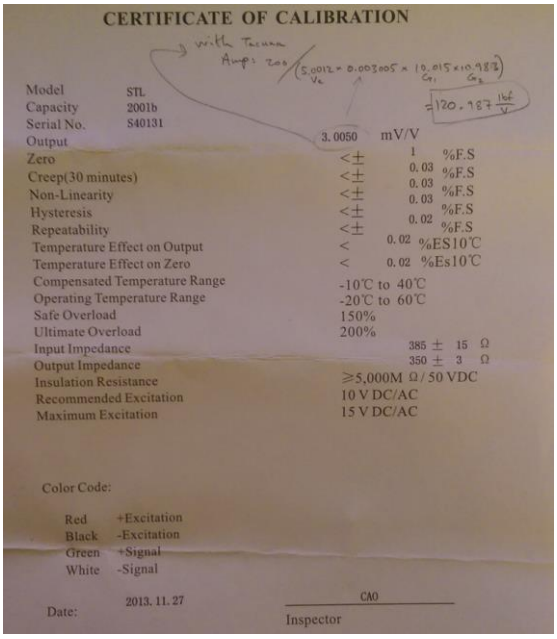

CERTIFICATE OF CALIBRATION

with Tacuna Amp: 200

$\frac{5.0012}{V_E} = 0.003005 \times \frac{10.015}{G_1} \times \frac{10.983}{G_2}$

$= 120.787 \frac{lbf}{V}$

Model	STL		
Capacity	200lb		
Serial No.	S40131		
Output		3.0050	mV/V
Zero		<± 1	%F.S
Creep(30 minutes)		<± 0.03	%F.S
Non-Linearity		<± 0.03	%F.S
Hysteresis		<± 0.03	%F.S
Repeatability		<± 0.02	%F.S
Temperature Effect on Output		< 0.02	%ES10℃
Temperature Effect on Zero		< 0.02	%Es10℃
Compensated Temperature Range		-10℃ to 40℃	
Operating Temperature Range		-20℃ to 60℃	
Safe Overload		150%	
Ultimate Overload		200%	
Input Impedance		385 ± 15	Ω
Output Impedance		350 ± 3	Ω
Insulation Resistance		≥5,000M Ω / 50 VDC	
Recommended Excitation		10 V DC/AC	
Maximum Excitation		15 V DC/AC	

Color Code:

Red	+Excitation
Black	-Excitation
Green	+Signal
White	-Signal

Date: 2013. 11. 27

CAO

Inspector

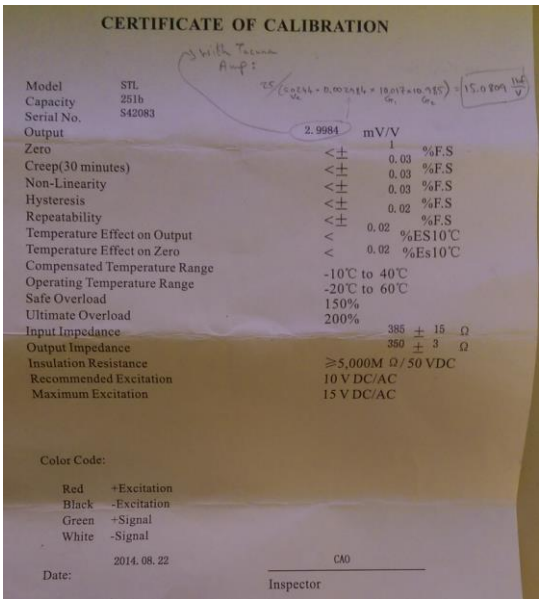

CERTIFICATE OF CALIBRATION

with Tacuna Amp:

Model	STL	
Capacity	25lb	
Serial No.	S42083	
Output	2.9984	mV/V
Zero	<± 1	%F.S
Creep(30 minutes)	<± 0.03	%F.S
Non-Linearity	<± 0.03	%F.S
Hysteresis	<± 0.03	%F.S
Repeatability	<± 0.02	%F.S
Temperature Effect on Output	< 0.02	%ES10℃
Temperature Effect on Zero	< 0.02	%Es10℃
Compensated Temperature Range	-10℃ to 40℃	
Operating Temperature Range	-20℃ to 60℃	
Safe Overload	150%	
Ultimate Overload	200%	
Input Impedance	385 ± 15	Ω
Output Impedance	350 ± 3	Ω
Insulation Resistance	≥5,000M Ω / 50 VDC	
Recommended Excitation	10 V DC/AC	
Maximum Excitation	15 V DC/AC	

Color Code:

Red	+Excitation
Black	-Excitation
Green	+Signal
White	-Signal

Date: 2014. 08. 22

CAO

Inspector

The signal conditioners used to power, amplify, and filter the load cells were purchased from Tacuna Systems. The conditioners' data was written on labels on the back of the conditioners.

Appendix K: CPConnect Funding Proposal

The following are the correspondences with the CPConnect committee at Cal Poly.

Proposal

CPConnect was created to help fund interdisciplinary student projects and the CPConnect group sends a request for proposals yearly. A proposal was written in 2014 to help several undergraduates from various departments learn about air augmented rocket research, design, and testing. This funding was crucial to the successful testing of the many different configurations used in this thesis project. The proposal follows.

CPConnect

Enabling Interdisciplinary Project-based Learning

Request for Funding of Project Proposal

Application Form

Title of Project:

AIR AUGMENTED ROCKET ENGINE TESTING

Proposal Authors: Allen Capatina and Dr. Dianne DeTurris

Faculty Advisor: Dr. Dianne DeTurris **Department:** Aerospace Engineering

Faculty Advisor email: ddeturri@calpoly.edu **Telephone:** (805) 756-1515

Anticipated Start Date: 1-1-14

Anticipated End Date: 12-15-14

Student Team Members & Departments:

Allen Capatina (AERO), Daniel Johnson (AERO), AdamWhitmarsh (AERO), Samantha Rawlins (AERO), Steven Rieber (ME), Ross Gregoriev (MatE), Kyle Rosenow (MatE)

Total Funds Requested ($): 4,700.00

Previous CPConnect Funding: NO

Signature of Faculty Advisor: _____ **Date:** _____

0

Summary

The bi-propellant (bi-prop) liquid rocket engine to be manufactured for this project will be an improvement on previous senior and Master's thesis projects. The current engine and test stand, which were made for a senior project and a Master's thesis, are insufficient for the intended tests and so a new engine and engine test stand must be made. The research team is led by Allen Capatina and made of students from different majors with a passion for propulsion and rocket systems. The team has a diverse background, with many applicable skills and experiences to guarantee successful testing. Some of the data collected will go toward Allen's Master's thesis and several of the underclassmen on the team intend to carry on the work for their upcoming senior projects. In addition, upgrading the engine and engine test stand will directly benefit the aerospace engineering senior level propulsion course because it will allow for combustion pressure measurement and consistent ignition, which are currently impossible with the present engine and equipment. Furthermore, Cal Poly Space Systems (CPSS), a rocket system engineering student club, is working toward high altitude (100,000 feet or higher) rockets for testing CubeSats and other small satellite systems. The rocket engine and parameters being test have applications in CPSS rockets for attitude control thrusters or as the primary flight engine.

This project is part of the Aerospace Engineering Hypersonic Systems Program. The program plans to test the bi-prop engine, with the exhaust plume inserted in a mixer duct and induce large coherent structures to alter or augment the thrust to increase efficiency. This mode of operation is known as an air augmented rocket (AAR). The engine will achieve a pressure ratio on the order of $P_{combustion}/P_{ambient} = 70$, which is important for reaching the aerodynamic choking condition in the mixer. The key parameters to be tested with the engine are the mixer duct geometry and induction of large coherent structures via annular cavity.

The project will consist of fabricating a new rocket engine, the support equipment, test stand, and testing in an AAR configuration. The team will write and publish an AIAA report that will be submitted to the Joint Propulsion Conference (JPC) in the summer of 2015. Additionally, future students will able to use the new engine, which will allow for chamber pressure measurement and consistent ignition.

Background

Currently, a single stage to orbit (SSTO) rocket is impractical because of the large amount of propellant needed to carry itself and the corresponding structural mass. Launch vehicles right now are multi-staged and they are expensive because complexity (therefore cost) increases with the number of stages. With only one stage launch vehicle costs are much lower, thus SSTO can improve affordable access to space. To become reality, engines must use air breathing technology. An Air Augmented Rocket (AAR) is an operating mode of the rocket based combined cycle (RBCC) that promises higher efficiency with low added complexity and mass. An AAR is a rocket engine that exhausts (the primary flow) into a larger diameter duct entraining a secondary flow (from the ambient atmosphere), increasing total mass flow, mixing ambient oxygen with fuel rich

exhaust allowing for secondary combustion and increased thrust. The engine's efficiency or specific impulse is thus increased. Figure 1 on the following page shows the higher specific impulse possible with AAR's versus other systems, with respect to flight velocity[1]. The green arrow highlights the higher efficiency air augmented rockets can achieve while the near horizontal black line shows the much lower efficiency of simple rocket engines.

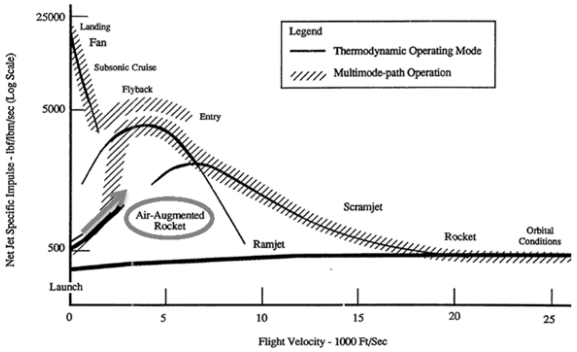

Figure 1: Efficiency versus velocity[1].

Several senior and thesis projects have led up to the construction and testing of the current engine as a static fire gaseous oxygen and liquid methanol in the axisymmetric AAR configuration[2]. The engine was tested to a maximum nominal 300 psi combustion pressure and 20 lbf thrust, with two duct geometries. The duct saw positive thrust, however, the system had a net decrease in thrust. The end area of the engine was large and the low pressure secondary flow, shown in blue in Figure 2, pulled the engine down decreasing total thrust as explained by Kyle Johnson in his thesis[2]. To investigate performance enhancements for this AAR technology further, the test stand, engine, and support equipment must be upgraded to get a net thrust increase and measure combustion pressure. The improvements will also benefit the aerospace engineering senior level propulsion course because combustion pressure will be measureable and the ignition system will be upgraded to include a spark plug for improved consistency and safety, compared to the current setup which cannot measure combustion pressure or ignite consistently and safely.

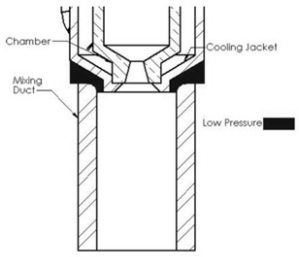

Figure 2: Previously tested bi-prop engine in the AAR configuration[2].

Proposed Project

The existing AAR test equipment and procedures for the axisymmetric methanol oxygen rocket will be used as a base. Any equipment on the current engine and test stand will be used if possible. In addition all the testing will take place in the same location, the propulsion lab in building 41. Previous testing did not yield a net increase in thrust, this project will attempt to increase the net thrust by increasing combustion pressure, engine mass flow rate, and decreasing the end area of the engine. Mixture ratio, duct profile, and large induced coherent structures will be studied as shown in the test matrix, Table 1. Additionally, the new engine will use ethanol due to safety concerns with use of methanol.

Table 1: Test matrix. Each test will last 5 seconds and combustion pressure will be 1,000 psi. The stoichiometric oxygen to fuel (O/F) ratio is 2.1. The duct shapes to test are Converging = C, Diverging = D, Converging-Diverging = CD, Straight = S.

Test Number	Engine Thrust (lbf)	Duct Thrust (lbf)	O/F Ratio	Large Induced Coherent Structures	Duct shape	Duct area ratio	Duct inlet to nozzle ratio
0a	100	No duct	2.1	N	No duct	No duct	No duct
0b	99	No duct	2.1	Y	No duct	No duct	No duct
1	98	4	2.7	N	C	10	4
2	100	6	2.1	N	C	10	4
3	102	8	1.5	N	C	10	4
4	97	7	2.7	Y	C	10	4
5	99	9	2.1	Y	C	10	4
6	101	11	1.5	Y	C	10	4
7	98	4	2.7	N	D	10	4
8	100	6	2.1	N	D	10	4
9	102	8	1.5	N	D	10	4
10-48	97-102	4-13	1.5-2.7	Y/N	C, D, CD, S	10 or 20	4 or 8

The engine will have a smaller end area near the nozzle exit plane, higher thrust (100 lbf) to increase measured thrust, and higher combustion pressure ($P_{combustion}$ = 1,000 psi) to increase exit velocity and achieve a pressure ratio on the order of 70 ($P_{combustion}/P_{ambient}$ = 1,000/14.7 = 68) to reach aerodynamic choking in the mixer[3]. The injector manifold, injector, combustion chamber, and nozzle will be made of copper and bolted to an outer structural steel shell. The complete engine will measure 6" long with a 2.3" OD and 1" ID. Coolant holes will be drilled axially into the copper combustion chamber and water will be pumped to keep the chamber cool.

Figure 3 shows a SolidWorks model of the engine with the cross sectional view to highlight the stated features and the paths of the primary and secondary flows. The fuel and oxidizer feed system will supply 1,200 psi of propellant while allowing for different mixture ratios to be tested. Pressure transducers in the system will provide input data and allow calculation of mass flow rates. Allen Capatina will research the design and manufacture of the new engine and propellant feed system.

Steve Rieber will be in charge of maintaining the project's budget, included as Appendix 2, because of his experience as CPSS's president. The budget includes the cost of purchasing 1" square aluminum T-slot to rebuild the test stand because the test stand must be stronger to handle the increase in thrust from 20 lbs to 100 lbs. A 250 lbs capable load cell is also included in the budget to account for the increased thrust and possible upgrades. Daniel Johnson will upgrade the test stand to meet the capabilities required by the new engine. He will strengthen the load carrying supports and improve the routing of feed lines to the engine. His work will be the base on which all the testing relies.

Kyle Rosenow works as a student lab technician for the Aerospace Engineering Department and will be the safety coordinator for the all fabrication and testing. Ross Gregoriev will handle the instrumentation of the stand with pressure transducers, load cells, and control relays. Ross will integrate them into LabView for data collection and control of the firing sequence.

There will be four mixing duct geometries consisting of converging (C), diverging (D), converging-diverging (CD), and straight (S) cylinders. The C, D, and CD cylinders will be tested at inlet to outlet area ratios between high (20) and low (10). The S cylinder will be tested at duct inlet to nozzle area ratios corresponding to the high and low ratios of the other cylinders. Adam Whitmarsh and Samantha Rawlins will undertake the geometric design and fabrication of these mixer ducts. The new configurations will be based on nondimensionalizing Kyle Johnson's duct geometry[2] by dividing with the old nozzle exit diameter and a NASA report on CFD analysis of a RBCC operating in rocket only mode[4]. The duct will be 5" long with 4" max. OD and 3" min. ID and placed at the exit plane of the nozzle. Adam will be responsible for creating the method of aligning and maintaining correct alignment of the ducts during use. The ducts will be made of aluminum on a CNC machine.

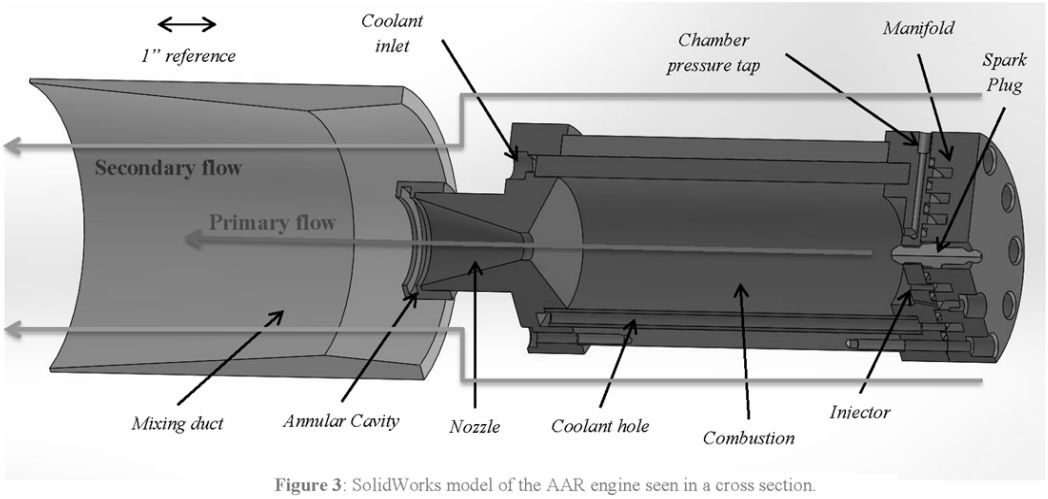

Figure 3: SolidWorks model of the AAR engine seen in a cross section.

Large coherent structures will be induced into the flow by having an annular cavity added to the nozzle exit plane as can be seen in blue in Figure 3. Induced large coherent structures will increase mixing of secondary air with the primary rocket engine exhaust, increasing the total mass flow rate

and the mixing of secondary oxygen with fuel rich exhaust leading to secondary combustion of unused fuel[5]. Samantha has experience with pressure oscillations in solid rocket motors and will handle analyzing the frequency response of the annular cavity.

The duct geometries and annular cavity will be tested with lean (2.7), stoichiometric (2.1), and rich (1.5) mixture ratios. The ultimate goal of the project is to understand how the thrust is augmented and find an optimum configuration. All team members will be involved with the testing process. Allen will use part of the collected data for his Master's thesis. The project is scheduled to take about a year and a timeline is included in Appendix 1. In addition to handling the budget, Steve will keep track of the schedule. The final report will be written at the conclusion of the project next Fall quarter. The report will be submitted as a paper for the 2015 AIAA Joint Propulsion Conference (JPC). The JPC is not shown in the schedule.

Team Members

Allen Capatina is an Aerospace Engineering Master's Student, 5th year. Allen is overall project leader. He will design the engine and propellant feed system. Parts of the results of these experiments will be used in an analysis of large coherent structures that will make up Allen's Master's thesis. His experiences include being Chief Operations Officer of CPSS and being a Machine Shop Student Technician at the Hangar and Mustang '60 for the last 4 years.

Daniel Johnson is an Aerospace Engineering Major, 2nd year. Daniel will upgrade the test stand to handle the thrust load and improve how the engine is fed. He will handle the upgrades that must be made to the stand. His experience includes: design and fabrication of a vacuum chamber for the production of hybrid rocket fuel and filament winder home switch redesign and manufacture.

Samantha Rawlins is an Aerospace Engineering Major, transfer student. Samantha will undertake the frequency analysis of the annular cavity along with mixer duct geometry. She was part of a project where they related vortex shedding to pressure oscillations in a solid rocket motor[6]. Her experience with LabView and motor analysis will help Ross with test stand instrumentation.

Adam Whitmarsh is an Aerospace Engineering Major, 2nd year. Adam will assure the proper integration of the mixing duct with the engine by designing an alignment method. His experience includes: working on gas and electric model RC planes, and rebuilding two 1,000lbf linear actuators for the CPSS launch trailer.

Steven Rieber is a Mechanical Engineering Major, 4th year. Steve will help review everyone's designs, keep track of the budget, and make sure the project stays on schedule. He is currently President of CPSS (for 2013-2014), project manager of the CPSS 60,000ft altitude rocket project, and tested a co-axial grain hybrid rocket motor for his senior project (2012-2013).

Ross Gregoriev is a Materials Engineering Master's Student, 5th year. Ross will instrument the test stand and tie it to LabView to be able to control the firing sequence and collect accurate data. His experience includes being in charge of the electronics used on the CPSS 60,000ft altitude rocket's control system and the instrumentation of CPSS's hybrid rocket static fire test stand[7].

Kyle Rosenow is a Materials Engineering Major, 2nd year. Kyle will insure everyone safe stays safe at all staged of the project. In addition, he can assist Steve with keeping an accurate budget. His experience includes being Treasurer of CPSS for 2013-2014 (in charge of a budget on the order of $25,000) and works for Cody Thompson, Aerospace Department Lab Technician.

The team members have many reasons for involvement, including but not limited to:

- "This is outside of my major, but I feel like I can be a helpful hand with the project. I want to be part of the project because it will be a good way to see if I like propulsion. Right now, I am interested in the subject, and if I like it I can think of a way of studying it more in depth. But if I don't like the subject, the project is another talking point I can put on my resume or mention it to a potential employer."
- "I'd like to be a part of this project so I can gain experience with bi-prop rocket engines. I want to go into propulsions so this is an excellent opportunity for me to learn and possibly get some class credit. My involvement with this project might very well turn into my senior project. I would love for that to happen."
- "The reason why I want to help with your project is, when the idea was explained to me, I understood no-one has ever made it work. I would love to be part of the group that adds a little bit to the world's knowledge about rocket science. On a slightly lesser note, I would also like to learn more about bi-prop engines."
- "I want to gain more experience setting up LabView files for data collection and system control, running engine tests, analyzing data, and troubleshooting complex systems. Plus I like liquid rocket engines like the F1 on the Saturn V and I want to learn more about them. I really appreciate the chance to be part of a project that will get submitted to a professional conference."

Appendix 1: Schedule

Year:	2014											
Month:	Jan.	Feb.	Mar.	Apr.	May	June	July	Aug.	Sep.	Oct.	Nov.	Dec.
Design and support												
Project goals												
Funding proposal												
Research and understand system												
Calculate engine parameters												
Engine and test stand design												
Finalize bill of materials												
Purchase materials												
Fabrication												
Machine all components												
Integrate engine												
Route plumbing and instrument engine												
Motor Testing												
Pressure test engine, plumbing, and sensors												
Cold flow test engine												
Double check all subsystems												
Static testing edsf												
Analysis test results												
Final Report and Defense												
Write report												
Review eport												
Present report												

Appendix 2: Proposed Project Budget

Materials	Supplier	Quantity	Cost per unit	Total cost
Multipurpose Copper (Alloy 110), 2-1/2" Diameter, 1' Length	McMaster	1	177.9	177.9
High Strength 1144 Medium Carbon Steel Rod Extra-Strength, 2" Diameter	McMaster	1	47.88	47.88
Permatex 85420 Permashield Fuel Resistant Gasket Dressing & Sealant, 2 oz Tube	Amazon	1	8.99	8.99
MIL-Spec. Fluorosilicone O-Rings, 5 different sizes	McMaster	5	7.5	37.5
Black-Oxide Alloy Steel Socket Head Cap Screw, 4-40 Thread, 1" Length	McMaster	1	5.31	5.31
Rimfire Z1 Spark Plug	Morrison and Marvin	1	23	23
Cleaned and Capped Copper Tubing 1/8" Tube Size, 1/4" OD,.19" ID, .030" Wall, 50' Coil	McMaster	1	37.76	37.76

Victor Model SR 4J-540 Heavy-Duty High Pressure Oxygen Regulator, CGA-540	Weld Fabulous	1	556.03	556.03
High-Pressure Gas Regulator 200-3000 PSI Pressure	McMaster	1	361.36	361.36
Oxygen tank refill	Airgas	4	58	232
Nitrogen tank refill	Airgas	4	10	40
Lab Grade Denatured Ethanol Fuel	Duda Diesel	4	8.5	34
Aluminum Inch T-Slotted Framing System Four-Slot Single, 1" Solid Extrusion 10ft	McMaster	6	31.59	189.54
Linear Bearing for T-Slotted Framing for 1" Width Rail, Side-Mount, 4" Length	McMaster	2	55.86	111.72
Aluminum Inch T-Slotted Framing System 90 Degree Bracket, Single, 4-Hole, for 1"	McMaster	10	4.56	45.6
Aluminum Inch T-Slotted Framing System Corner Connector, 3-Way, for 1" Extrusion	McMaster	8	9.86	78.88
Std Zinc-Plated STL End-Feed Fastener, for 1" Aluminum Inch T-Slotted Framing System	McMaster	20	2.3	46
Aluminum Inch T-Slotted Framing System Twist-in Cable Tie Holder for 1" Extrusion	McMaster	20	0.72	14.4
3000 psi gage pressure range, cable connection PX309-3KGV	Omega	5	175	875
Pulsation-Damping Snubber with Filtering Disc Type 303 SS, 1/4 NPT Connections, 15000 PSI, 0.5 micron	McMaster	1	14.71	14.71
Custom PCB manufacture	Imagineering Inc.	1	25	25
Load cell amplifier IC	Mouser	2	10	20
Hansen Series 600 Oxygen Service Female NPT End Connection Sockets	Amron International	2	15.4	30.8
Hansen Series 600 Oxygen Service Male NPT End Connection Plugs	Amron International	2	4.53	9.06
Steel ISO-B Hose Coupling Plug, 1/4 Coupling, 1/4" NPTF Female	McMaster	2	7.65	15.3
Steel ISO-B Hose Coupling Sleeve-Lock Socket, 1/4 Cplg, 1/4" NPTF Female	McMaster	2	18.7	37.4
250 lb Capacity Cantilever Beam Load Cell	Omega	1	360	360
Safety Solvent - 15.1oz Aerosol Spray Can	Regulator and Torch Exchange, Inc.	3	8.75	26.25

Multipurpose Aluminum (Alloy 6061) Tube 4" OD, 3" ID, .500" Wall Thickness, 3' Length	McMaster	2	167.09	334.18
Drill bits, endmills, boring bars, key seat cutters, taps, carbide inserts	Various	--	75	75
Brass and aluminum bar stock, pipe fittings, nuts and bolts, tubing, wiring, zip ties, PTFE tape	Various	--	200	200
	Total Material Cost =		4070.57	
	Shipping (8%) =		325.65	
	Tax (7.75%) =		315.47	
	Total =		**4711.68**	

Appendix 3: References

1. R. W. Foster, Escher, W. J. D. and J. W. Robinson. *Air Augmented Rocket Propulsion Concepts.* Madison, WI: Astronautics Corporations of America Technology Center, 1988. F04622-86-C-0094.
2. Kyle Johnson. *Axisymmetric Air Augmented Methanol/GOX Rocket Mixing Duct Experimental Thrust Study.* Thesis project, Aerospace Engineering Department, California Polytechnic State University, CA, March 2013.
3. Trevor Foster. *Rectangular Ducted Methane/GOX Thruster.* Aerspace Engineering, California Polytechnic University. San Luis Obispo: s.n., 2008. Master's Thesis.
4. Timothy D. Smith, Christopher J. Steffen Jr., Shaye Yungster, Dennis J. Keller, *Performance of an Axisymmetric Rocket Based Combined Cycle Engine During Rocket Only Operation Using Linear Regression Analysis.* National Aeronautics and Space Administration Lewis Research Center. 1998. NASA Technical Paper. NASA/TM-1998-206632.
5. K. H. Yu, and K. C. Schadow. *Role of Coherent Structures in Turbulent Compressible Mixing.* Research and Technology Division, China Lake, California. Elsevier Science, New York, Inc. 1997. 0894-1777.
6. J. Palmore Jr., S. Rawlins, E. Stevens, and N. Zarbo. *Relating Pressure Oscillations and Vortex Shedding in Solid Rocket Motors.* NASA Propulsion Academy at Marshall Space Flight Center. 2011.
7. Adam Casuga, Katherine Conway, Corina Harvey, and Steven Rieber. *Design and Implementation of a Coaxial Fuel Grain Hybrid Rocket Motor.* Senior Project Report, Aerospace Engineering Dept., Cal Poly, San Luis Obispo, CA 2013.

Proposal Award Letter

After the proposal for funding was submitted CPConnect made their decisions and awarded funds to the project. The award letter follows. The scoring section of the letter was omitted.

CP CONNECT Cal Poly State University

CP Connect Project Proposal Awards Winter 2014

Date: February 25, 2014

To: Professor DeTurris

From: CPConnect Committee, Lily Laiho

Subject: Congratulations On Your Proposal – Air Augmented Rocket Engine Testing

The CPConnect committee has reviewed your proposal and recommended that it be funded with **$4,700**. The funds are immediately available and all funds must be utilized for the project detailed in your proposal. Please note any funds that are not spent by **March 2015** will remain in the CPConnect pool of funds and will not be available for your project. You should submit all expense reports, check requests, or purchase requisitions to the CENG Dean's office (Room 192-301, 756-2131). Make sure to include the project advisor's name, project title on all documents and correspondence you submit along with appropriate receipts. Note: If you are placing a charge with a State Procard, you will need to send a copy of the receipt showing the credit card number and total charge amount to Cassi Goldsmith in the Dean's office. In addition, the person placing the order for you on their Procard will need a copy of the receipt in order to submit it to Cal Poly Foundation when charging back the expense to the Foundation orgkey on their Procard statement. If there are any questions regarding the credit card charge back, please contact Wynette Winkler in the Dean's office.

Part of our mandate is to ensure that the donors see the impact that their funds have made toward supporting interdisciplinary projects and enhancing the learning experience of students at Cal Poly. Accordingly, a comprehensive project report along with an executive summary is due to the CPConnect committee by **March 2015.** Please make sure your report is submitted to the Director of Interdisciplinary Projects (Dr. Lily Laiho, llaiho@calpoly.edu). Please include any photos that show students working on the project and be sure to indicate if the results from the project will be presented at any conferences or national competitions.

Please note that the faculty advisor will be responsible for tracking all materials purchased with CPConnect funding. All equipment/parts ordered using these funds should be delivered to the faculty advisor's department address. All equipment must be identified and tracked as per University Property Accounting practices.

For future reference your scoring results from the CPConnect Committee are included here. Refer to the RFPP Scoring Rubric for details on each criterion. We hope this will help guide you through making improvements on your next project proposal.

Proposal Summary and Thank You Report

A report was written In March 2015 to thank CPConnect for the funding and update them on how the funds were used. The report follows.

AIR AUGMENTED ROCKET ENGINE TESTING

Final Report for CPConnect

April 2015

Author: Allen Capatina

Faculty Advisor: Dr. Dianne DeTurris

CPConnect awarded $4,700 to the Air Augmented Rocket Engine Testing project approximately one year ago. Thanks to the funding received from CPConnect the project has been highly successful. Testing is underway and design improvements are continuing that will give many opportunities for future student projects.

The bi-propellant (bi-prop) liquid rocket engine that was manufactured for this project is an improvement on previous senior and Master's thesis projects. The engine is being used in a ducted rocket configuration to ascertain whether thrust augmentation can occur with various ducting configurations. Figure 1 shows several students machining parts for the engine.

Figure 1: Parts being machined for the rocket engine.

From top left to right then down there is George Georgiou using a Haas TM1 CNC mill to machine the injector of the engine, Kyle Rosenow using the same machine as George to machine the copper combustion chamber liner, and Joe Vanherweg using a Haas TL1 CNC lathe to machine the engine's copper nozzle.

The engine turned out exquisitely and has thus far been used in several tests going toward Allen Capatina's Master's thesis which focuses on a high speed rocket based combined cycle application. The experiments are used to show if there are performance improvements to be gained by the air augmented (ducted) configuration of the engine. Testing of an annular cavity at the exit plane of the engine's nozzle is also investigated in conjunction with air augmentation.

Figure 2 shows the SolidWorks engine and duct models from the March 2014 proposal and Figure 3 shows the final design after further aerodynamic refining of the SolidWorks model, final machining, and assembly. The mixing duct is not shown in Figure 3, only the rocket engine's annular cavity, nozzle, combustion chamber, injector, manifold, adapter plate, and feed tubes are visible.

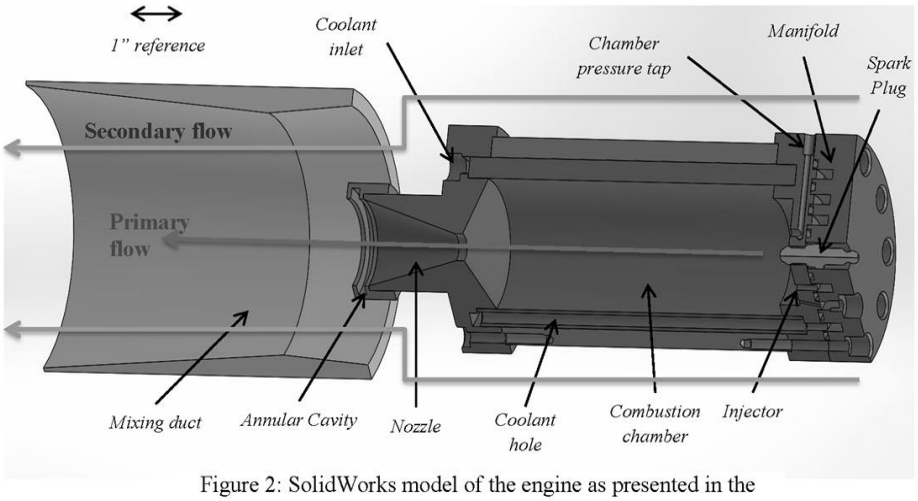

Figure 2: SolidWorks model of the engine as presented in the original proposal in March 2014.

Figure 3: Rocket engine assembly.

The engine is mounted and integrated onto a specially constructed test stand. The final picture in Figure 4 on the next page shows the test stand fully integrated and prepared for testing.

All of the instrumentation, hoses and cables, raw metal stock, tooling, and other miscellaneous parts were possible to purchase and use because of the funding granted by CPConnect. Many students were involved in designing, building, and testing of this rocket. In addition, the students also participated in systems integration and troubleshooting throughout the assembly and operation process. Furthermore the product which remains can be used by many more for future projects. In particular the engine will be an upgrade to the current bi-propellant engine used by the Aerospace Engineering Department for the required senior level Aero 401: Propulsion class. The upgrades allow students to understand much more about rocket propulsion than they were previously able to experience; enhancing the learn-by-doing philosophy of the university.

The group would like to extend our thanks to CPConnect for granting us the funding to make this all reality. Thank you!

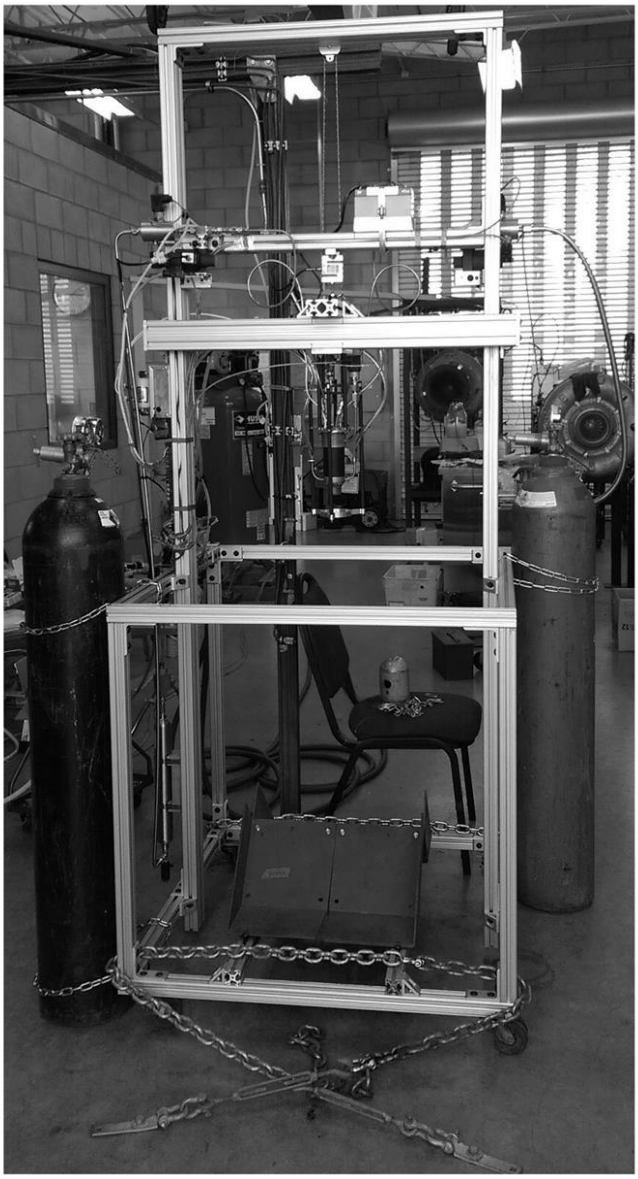

Figure 4: Rocket mounted on the test stand.

Appendix L: LabView Front Panel and Block Diagram

The following two images are for reference, to understand what the data collection program looked like. The first image is the front panel and the second image is the block diagram of the program.

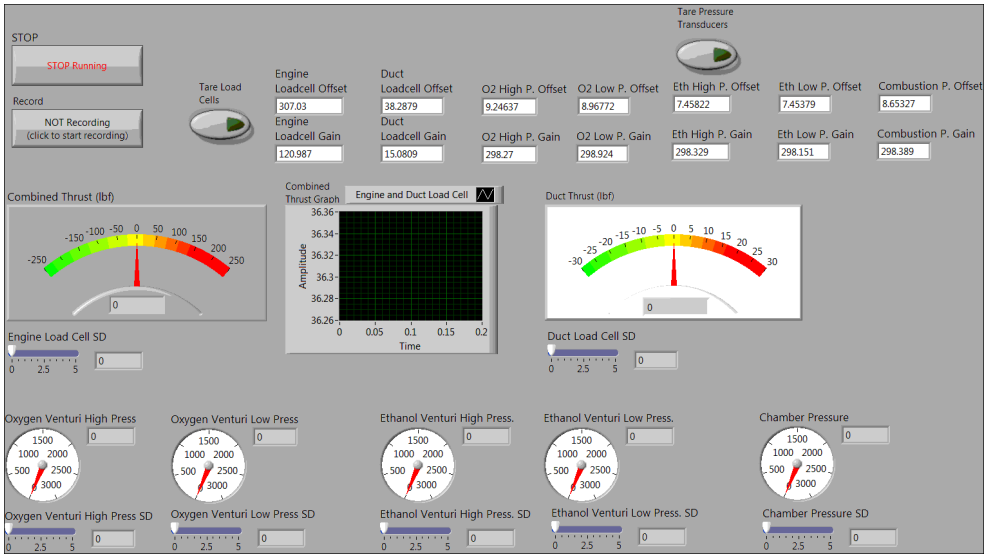

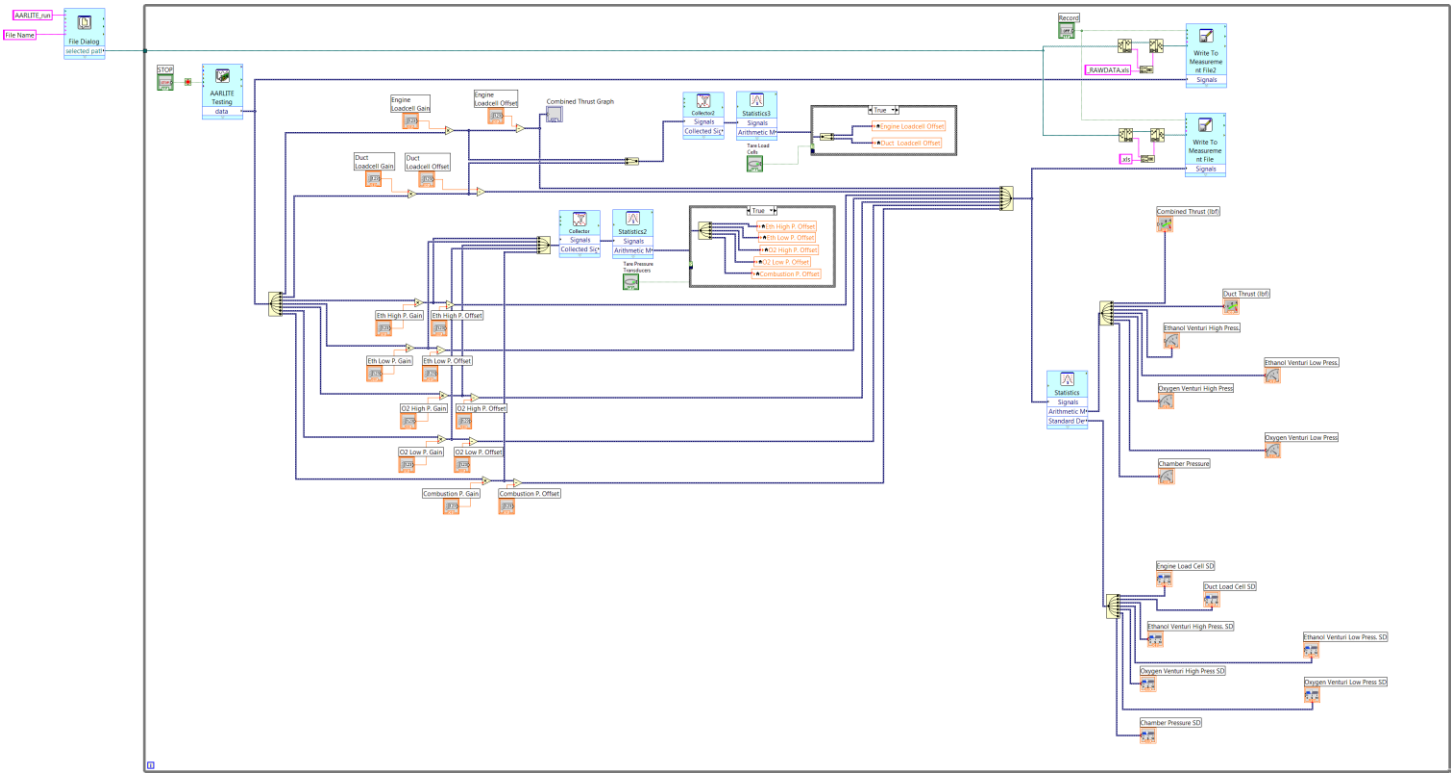

Appendix M: Major Purchases

Order from McMaster, May 29th, 2014. Page 1 of 2

McMASTER-CARR

Order Confirmation

562-692-5911
562-695-2323 (fax)
la.sales@mcmaster.com

Ship to

California Polytechnic State University
1 Grand Ave
San Luis Obispo CA 93407-9000

Attention Cody
Aerospace Engineering

Order Date
5/29/14

Ordered By
Cody Thompson

McMaster-Carr Number
4436990

Line		Product	Ordered	Ships	Price	Total
1	2636A81	Long-Life General Purpose Tap, 3 Piece Set, 4-40 Thread Size	1 set	today	21.30 per set	21.30
2	27575A67	High-Speed-Steel Clog-Resistant Jobbers' Drill Bit, Black-Oxide, Wire Gauge 43, 2-1/4" Oal, 1.07" Drill Depth	2 each	today	2.75 each	5.50
3	2636A118	Long-Life General Purpose Tap, 3 Piece Set, 2-56 Thread Size	1 set	today	31.21 per set	31.21
4	27575A75	High-Speed-Steel Clog-Resistant Jobbers' Drill Bit, Black-Oxide, Wire Gauge 50, 2" Oal, .86" Drill Depth	2 each	today	2.75 each	5.50
5	3163A54	Double End High-Speed-Steel Drill Bit for Sheet Metal, 1/8", 1-15/16" Overall Length, 9/16" Drill Depth	1 each	today	1.91 each	1.91
6	3063A115	Cobalt Steel Extended Reach Drill Bit, 1/8", 5-1/8" Overall Length, 2.5" Drill Depth	2 each	today	9.34 each	18.68
7	90945A705	300 Series Stainless Steel NAS 620 Flat Washer, No. 2 Size, .15" OD, .01"-.02" Thickness, Dash No. C2, packs of 500	1 pack	today	11.14 per pack	11.14
8	90945A711	300 Series Stainless Steel NAS 620 Flat Washer, No. 4 Size, .21" OD, .02"-.04" Thickness, Dash No. C4, packs of 500	1 pack	today	13.57 per pack	13.57
9	3196K2	Pressure Transmitter, Standard, 0-10 V, 1/4 NPT, 3000 PSI	5 each	today (1 from our Chicago warehouse)	181.40 each	907.00
10	4034K5	Pulsation-Damping Snubber with Filtering Disc, Type 303 Stainless Steel, 1/4 NPT, 0.5 Micron, 15000 PSI	1 each	today	15.07 each	15.07
11	6628K47	High Strength 1144 Medium Carbon Steel Rod, Extra-Strength, 2-1/2" Diameter, 3' Length	1 each	today (from our Chicago warehouse)	175.34 each	175.34
12	8966K381	Multipurpose 110 Copper, Rod, 2-1/2" Diameter, 1' Long	1 each	today	185.63 each	185.63
13	91251A115	Black-Oxide Alloy Steel Socket Head Cap Screw, 4-40 Thread, 1" Length, packs of 50	1 pack	today	5.31 per pack	5.31
14	91251A103	Black-Oxide Alloy Steel Socket Head Cap Screw, 2-56 Thread, 3/4" Length, packs of 50	1 pack	today	13.00 per pack	13.00

McMaster-Carr Supply Company

Page 1 of 2

McMASTER-CARR

Order Confirmation

562-692-5911
562-695-2323 (fax)
la.sales@mcmaster.com

Ship to

California Polytechnic State University
1 Grand Ave
San Luis Obispo CA 93407-9000

Attention Cody
Aerospace Engineering

Order Date
5/29/14

Ordered By
Cody Thompson

McMaster-Carr Number
4436990

Line		Product	Ordered	Ships	Price	Total
15	6677A13	High-Pressure Gas Regulator, for Argon & Helium, CGA #580 Inlet, 200-3000 PSI	1 each	today	361.36 each	361.36
16	5665K14	Hose for Nitrogen Gas, Argon, and Oxygen, Brass Female Fittings, PTFE Hose, 4' L, 1/4" ID, 3600 PSI	2 each	today	89.05 each	178.10
17	29745A31	Chip-Clearing High-Speed-Steel Extended-Reach Drill Bit, 1/8", 8" Overall Length, 5.8" Drill Depth	2 each	today	15.96 each	31.92

Merchandise $1,981.54

Notes

Your order is subject only to our terms and conditions, available at www.mcmaster.com.

Applicable shipping charges and tax will be added.

Swagelok
Los Angeles\Ventura
Bakersfield\Hawaii

Make Payable to:
CCFST
325 Balboa Circle
Camarillo, CA 93012
PHONE: (800) 252-7087
FAX: (805) 383-2046
info@la.swagelok.com

INVOICE
483114

Cust Order No: VERBAL CRCD
Requisition Number:
Our Order No: 98478470

Sold To: SBPHONE
CAL POLY S.U.
1 GRAND AVE

SAN LUIS OBISPO CA 93407

Ship To: SBPHONE
ALLEN CAPATINA
CAL POLY AEROSPACE ENG.
1 GRAND AVE
BLDG 41B ROOM 140
SAN LOUIS OBISPO CA 93407

FOB Shipping Point

We Accept

Date Shipped	Shipping Instructions	Territory	Order Date	Sales Tax Code	Invoice Date	Invoice Number
11/04/14	OUR DELIVERY	99	10/16/14	065	11/04/14	483114

Item	Description	QUANTITY Ordered	Balance Due	Shipped	Unit Price	Disc	Amount
1	SS-43GF4-SC11-31C-CH-ASY 40G SERIES BALL VALVE 1/4" FNPT, NORM CLOSED AC 1 PSIG CRACK CHECK VLV ON OUTLET SC-11 CLEANED(NO LONGER APPLICABLE AFTER ASSEMBLY) ***NON-CANCELABLE/NON-RETURNABLE*** SUBJECT TO PRIOR SALE DELIVERY: 2 WEEKS + TRANSIT ARO Contact us or visit the Swagelok web site at www.swagelok.com for Swagelok product warranty information. NO OTHER WARRANTIES APPLY AND IN NO EVENT SHALL SELLER OR MANUFACTURER BE LIABLE FOR ANY CONSEQUENTIAL OR INCIDENTAL DAMAGES. U.N. Convention on Contracts for the Sale of International Goods is specifically excluded.	1		1	464.63		464.63
2	SS-MB-43G 43G/43GX SERIES BALL VALV MOUNTING BRACKET KIT (131 STOCK SUBJECT TO PRIOR SALE	1		1	35.83		35.83

Customer Copy

Swagelok
Los Angeles\Ventura
Bakersfield\Hawaii

Make Payable to:
CCFST
325 Balboa Circle
Camarillo, CA 93012
PHONE: (800) 252-7087
FAX: (805) 383-2046
info@la.swagelok.com

INVOICE
483114

Cust Order No: VERBAL CRCD
Requisition Number:
Our Order No: 98478470

Sold To: SBPHONE
CAL POLY S.U.
1 GRAND AVE
SAN LUIS OBISPO CA 93407

Ship To: SBPHONE
ALLEN CAPATINA
CAL POLY AEROSPACE ENG.
1 GRAND AVE
BLDG 41B ROOM 140
SAN LOUIS OBISPO CA 93407

FOB Shipping Point

We Accept

Date Shipped	Shipping Instructions	Territory	Order Date	Sales Tax Code	Invoice Date	Invoice Number
11/04/14	OUR DELIVERY	99	10/16/14	065	11/04/14	483114

Item	Description	QUANTITY Ordered	Balance Due	Shipped	Unit Price	Disc	Amount
3	MS-131-SR 131 SERIES PNEUMATIC SPRING-RETURN ACTUATOR STOCK SUBJECT TO PRIOR SALE	1		1	224.47		224.47
4	SS-400-R-6 REDUCER 1/4" TUBE x 3/8" TUBE ADA STOCK SUBJECT TO PRIOR SALE	1		1	9.61		9.61
5	SS-T6-S-049-10 3/8" x .049 TUBING 10FT NON-CANCELABLE, NON-RETURNABLE FOB CLEVELAND, OHIO SUBJECT TO PRIOR SALE **** THERE IS AN ADDITIONAL FREIGHT CHARGE WHEN SHIPPING TUBING OVER 7FT LENGTHS **** TUBING MAY BE CUT DOWN AT AN ADDITIONAL CHARGE OF $3.00 PER CUT STOCK SUBJECT TO PRIOR SALE	10		10	3.82		38.20

Customer Copy

Swagelok
Los Angeles\Ventura
Bakersfield\Hawaii

Make Payable to:
CCFST
325 Balboa Circle
Camarillo, CA 93012
PHONE: (800) 252-7087
FAX: (805) 383-2046
info@la.swagelok.com

INVOICE
483114

Cust Order No: VERBAL CRCD
Requisition Number:
Our Order No: 98478470

Sold To: SBPHONE
CAL POLY S.U.
1 GRAND AVE
SAN LUIS OBISPO CA 93407

Ship To: SBPHONE
ALLEN CAPATINA
CAL POLY AEROSPACE ENG.
1 GRAND AVE
BLDG 41B ROOM 140
SAN LOUIS OBISPO CA 93407

FOB Shipping Point

We Accept

Date Shipped	Shipping Instructions	Territory	Order Date	Sales Tax Code	Invoice Date	Invoice Number
11/04/14	OUR DELIVERY	99	10/16/14	065	11/04/14	483114

Item	Description	QUANTITY Ordered	Balance Due	Shipped	Unit Price	Disc	Amount
6	SS-43GF4-SC11-31C-CH-ASY	1		0			
		*** CANCELLED ***					
	OUR DELIVERY GIVE ORDER TO PHIL TO TAKE UP TO MARC FOR OD						
	Contact us or visit the Swagelok Web site at www.swagelok.com for Swagelok product warranty information. NO OTHER WARRANTIES APPLY AND IN NO EVENT SHALL SELLER OR MANUFACTURER BE LIABLE FOR ANY CONSEQUENTIAL OR INCIDENTAL DAMAGES. U.N. Convention on Contracts for the Sale of International Goods is specifically excluded.						

Terms	Sub Total	Sales Tax Rate	Sales Tax	Shipping & Handling	TOTAL
PREPAY-CASH/CREDIT CARD	772.74	8.0000%	61.82	.00	834.56

RETURN POLICY: No returns will be accepted without written authorization. All returns are subject to a restocking charge. Orders for special non-price listed items are non-cancelable and non-returnable. All returns are subject to inspection and approval. All claims and shortages must be reported by telephone immediately. Hold all materials and packing slip for our immediate inspection.
ALL ORDERS WILL SHIP VIA UPS GROUND UNLESS OTHERWISE SPECIFIED.
ALL ITEMS WILL BE PACKAGED TO PREVENT ANY REASONABLY FORSEEABLE DAMAGE DURING TRANSIT.

Customer Contact & Phone Number
ALLEN CAPATINA
562-686-5701

Customer Copy

Tax Exemption Number
004 100.00

McMASTER-CARR

Receipt

562-692-5911
562-695-2323 (fax)
la.sales@mcmaster.com

Purchase Order	SEPTEMBER 2014
Paid	$368.64
Invoice	17816871
Invoice Date	11/24/14

Billed to
ATTENTION: ALLEN CAPATINA
CALIFORNIA POLYTECHNIC STATE UNIVERSITY
1 GRAND AVE
SAN LUIS OBISPO CA 93407-9000

Shipped to
Attention: Allen Capatina
California Polytechnic State University
Aerospace Engineering Dept
1 Grand Ave Bldg 41-143
San Luis Obispo CA 93407-9000

Information About Your Payment

Credit Card	Visa Ending- 8464
Date	11/25/14
Name on Card	Allen Capatina
Your Account	171690100

Allen Capatina placed this order.

Line		Product	Ordered	Shipped	Balance	Price	Total
1	7453K83	Electrical-Insulating Sleeving, High-Temperature Silicone Rubber, 0.09" ID, 10' Long, White, Each of 10	1 Each	1	0	4.57 Each	4.57
2	3096A365	High-Speed Steel Extended-Reach Drill Bit, Black Finish, Wire Gauge #50, 1.89" Drill Depth	1 Each	1	0	4.39 Each	4.39
3	61975K41	Solenoid Air Directional Control Valve, with 3 Ports, Single Solenoid, 1/4 NPT, 110V AC	2 Each	2	0	26.72 Each	53.44
4	7457K643	Long-Life Surface-Mount Timer Relay, Single Shot, 120V AC Control, 1 Amp, .5 to 10 Second	2 Each	2	0	34.75 Each	69.50
5	7457K36	Long-Life Surface-Mount Timer Relay, Delay-on-Break, 120V AC Control, 1 Amp, 3-60 Second	1 Each	1	0	32.39 Each	32.39
6	4416T63	Very Easy-to-Machine 1215 Carbon Steel, Hex Bar, 3/8" Hex Size, 6' Length	1 Each	1	0	7.58 Each	7.58
7	5929K22	Steel Yor-Lok Tube Fitting, Straight Adapter for 3/8" Tube OD X 1/4 NPT Male	2 Each	2	0	5.56 Each	11.12
8	3096A198	High-Speed Steel Extended-Reach Drill Bit, Black Oxide, Wire Gauge #80, .29" Drill Depth	1 Each	1	0	5.45 Each	5.45
9	50925K131	Compact Extreme-Pressure Steel Thread Fitting, 1/4 Male X 1/4 Male Pipe Size, 1-29/64" L, Hex Nipple	10 Each	10	0	1.29 Each	12.90
10	9171K214	Precision High-Pressure Brass Thread Pipe Fitting, 1/4 X 1/4 Pipe Size X 1-7/16" Length, Hex Nipple	3 Each	3	0	5.64 Each	16.92
11	8955K112	Multipurpose Copper Tubing, 1/8" Tube Size, 1/4" OD, .152" ID, .049" Wall, 10' Coil	1 Each	1	0	31.78 Each	31.78
12	5272K221	Brass Yor-Lok Tube Fitting, Straight Connector for 1/4" Tube OD	3 Each	3	0	4.71 Each	14.13

McMASTER-CARR

562-692-5911
562-695-2323 (fax)
la.sales@mcmaster.com

Receipt

Purchase Order	**SEPTEMBER 2014**
Invoice	**17816871**
Invoice Date	**11/24/14**

Line		Product	Ordered	Shipped	Balance	Price	Total
13	5929K22	Steel Yor-Lok Tube Fitting, Straight Adapter for 3/8" Tube OD X 1/4 NPT Male	2 Each	2	0	5.56 Each	11.12
14	4757T152	High-Pressure Brass Threaded Pipe Fitting, 1/4 Pipe Size, Male Tee	2 Each	2	0	13.28 Each	26.56
15	4757T92	High-Pressure Brass Threaded Pipe Fitting, 3/8 Male X 1/4 Female, Hex Reducing Bushing	1 Each	1	0	3.98 Each	3.98
16	5929K52	Steel Yor-Lok Tube Fitting, Straight Adapter for 3/8" Tube OD X 1/4 NPT Female	1 Each	1	0	7.66 Each	7.66
17	50785K24	Medium-Pressure Brass Threaded Pipe Fitting, 1/2 Pipe Size, Hollow Hex-Head Plug	2 Each	2	0	2.81 Each	5.62

Merchandise	319.11
Sales Tax	23.92
Shipping	25.61
Total	$368.64
Payment Received 11/25/14	(368.64)
Balance Due	$0.00

Packing List	Shipped	Weight	Carrier	Tracking
4079799-02	11/24/14	5 lb	UPS Ground	1Z9293810341020515
4079799-01	11/24/14	1 lb	FedEx Standard	624095560172
4079799-03	11/24/14	8 lb	UPS Ground	1Z9293810341020524

Engineering solutions, product research & development

MY ACCOUNT (HTTPS://TACUNASYSTEMS.COM/ZC/INDEX.PHP?MAIN_PAGE=ACCOUNT&ZENID=CAC8CAF8225B6E3CF3297A0275FD86F9)

LOG OUT (HTTPS://TACUNASYSTEMS.COM/ZC/INDEX.PHP?MAIN_PAGE=LOGOFF&ZENID=CAC8CAF8225B6E3CF3297A0275FD86F9)

CUSTOMER SERVICE (INDEX.PHP?MAIN_PAGE=CONTACT_US)

CART (HTTP://TACUNASYSTEMS.COM/ZC/INDEX.PHP?MAIN_PAGE=SHOPPING_CART&ZENID=CAC8CAF8225B6E3CF3297A0275FD86F9)

Tacuna Systems (http://tacunasystems.com/zc/)

1-800-550-0280

Search

MENU

You are here : Home (http://tacunasystems.com/zc/) / My Account (https://tacunasystems.com/zc/index.php?main_page=account&zenid=cac8caf8225b6e3cf3297a0275fd86f9) / History (https://tacunasystems.com/zc/index.php?main_page=account_history&zenid=cac8caf8225b6e3cf3297a0275fd86f9) / Order #352

Order Date: Monday 24 November, 2014

Order Information - Order #352

Qty.	Products	Total
1 ea.	AmCells STL-25 S-Type/S-Beam Alloy Steel Load Cell 25Lb	$129.95
1 ea.	AmCells STL-200 S-Type/S-Beam Alloy Steel Load Cell 200Lb	$129.95
2 ea.	6 Pin Detachable Screw Terminal	$8.38

Sub-Total:	$268.28
United States Postal Service (Priority Mail™):	$19.74
Sales Tax:	$0.00
Total:	$288.02

Status History & Comments

WESTERN SWITCHES & CONTROLS, INC.

PLEASE REMIT TO: Western Switches & Controls
750 Challenger Street
Brea, CA 92821
wscsa@westernswitches.com
(800) 454-8144

INVOICE
118853
CC011

P.O. NUMBER	BUYER	S.O. NUMBER	AREA	DATE
	ALLEN CAPATINA	44301A	T11	06/12/14

CREDIT CARD SALE FOR TERR 011
CREDIT CARD
,

CAL POLY
1 GRAND AVE
SAN LUIS OBISPO, CA 93407

Part Number	Ordered	Backordered	Shipped	Price	U/I	Total
*653135	24	0	24	4.59000		110.16
651141	64	0	64	1.57000	EA	100.48
	5/16-18X11/16" FBHSCS&DOUBLE ECON T-NUT					
*653203	6	0	6	6.92000		41.52
*651205	16	0	16	0.57000		9.12
651129	40	0	40	0.65000	EA	26.00
	5/16-18 X 11/16" FBHSCS & ECONOMY T-NUT					

Total of all parts this order = $	287.28
Total sales tax on this order = $	25.85
Total freight on this order = $	11.16
Invoice total = $	324.29

Ship Dte	Shipped Via	Tracking No.	Wght	F.O.B.	Terms
06/12/14	DIRECT	1Z16R4X40360447275		MFG WHSE	CREDIT CARD

* * * We accept VISA, MasterCard and American Express * * *

TOTAL FREIGHT INCLUDES SHIPPING AND HANDLING AND F.O.B. FACTORY

www.westernswitches.com

NO STATEMENT WILL BE SENT - PLEASE PAY FROM THIS INVOICE
WE RESERVE THE RIGHT TO BILL AT THE PRICE IN EFFECT AT THE TIME OF SHIPMENT
NO GOODS RETURNED WITHOUT WRITTEN PERMISSION
A Service Charge of 1.5% (18% per annum) will be charged on all credits past 30 days.
Purchaser agrees to pay all collection costs and attorney's fees necessary to collect past due amounts, as permitted by law.

WESTERN SWITCHES & CONTROLS, INC.

PLEASE REMIT TO: Western Switches & Controls
750 Challenger Street
Brea, CA 92821
wscsa@westernswitches.com
(800) 454-8144

INVOICE
118958
CC011

P.O. NUMBER	BUYER	S.O. NUMBER	AREA	DATE
	ALLEN CAPATINA	44301B	T11	06/17/14

CREDIT CARD SALE FOR TERR 011
CREDIT CARD
,

CAL POLY
1 GRAND AVE
SAN LUIS OBISPO, CA 93407

Part Number	Ordered	Backordered	Shipped	Price	U/I	Total
*653135	6	0	6	4.59000		27.54
651141	16	0	16	1.57000	EA	25.12
	5/16-18X11/16" FBHSCS&DOUBLE ECON T-NUT					
*653203	4	0	4	6.92000		27.68
*651205	4	0	4	0.57000		2.28

Total of all parts this order	= $	82.62
Total sales tax on this order	= $	7.44
Total freight on this order	= $	9.37
Invoice total	= $	99.43

Ship Dte	Shipped Via	Tracking No.	Wght	F.O.B.	Terms
06/17/14	DIRECT	1Z16R4X40360393216		MFG WHSE	CREDIT CARD

* * * We accept VISA, MasterCard and American Express * * *

TOTAL FREIGHT INCLUDES SHIPPING AND HANDLING AND F.O.B. FACTORY

www.westernswitches.com

NO STATEMENT WILL BE SENT - PLEASE PAY FROM THIS INVOICE
WE RESERVE THE RIGHT TO BILL AT THE PRICE IN EFFECT AT THE TIME OF SHIPMENT
NO GOODS RETURNED WITHOUT WRITTEN PERMISSION
A Service Charge of 1.5% (18% per annum) will be charged on all credits past 30 days.
Purchaser agrees to pay all collection costs and attorney's fees necessary to collect past due amounts, as permitted by law.

Appendix N: Test Matrices

The data collected in all the relevant tests was assembled in Table 10 through Table 13 on the following pages. The four tables were helpful for fast lookup of the average values and standard deviations of the mixture ratio, total mass flow rate, combustion chamber pressure, total thrust, duct thrust, and total specific impulse. With the values in the tables all other values could be calculated, for example the individual mass flow rates for ethanol and oxygen could be calculated from the total mass flow rate and the mixture ratio. Also the engine's thrust could be calculated by subtracting the duct thrust from the total thrust. The data in the tables was what was referenced by all the plots presented throughout Section 3 and 4. The standard deviations were used as the error bar values of the means and were included in some of the presented plots.

The tables were organized with the duct configuration along the horizontal and ring configuration along the vertical. The average values for each respective category were bolded and the standard deviations were not bolded. The number of significant figures displayed was limited to a reasonable amount for each category to be understandable even though the data collected during testing went out to many significant figures because the NI USB-6210 DAQ was 16-bit.

Table 10: Selected cold flow test data, chamber pressure approximately $100\ psi$.

	Values to report:	No Mixing Duct	Long Duct
No Ring	**Test #**	**1cold**	**12cold**
	Mixture Ratio $[r]$ $(unitless)$	**Ave = 4.23;** Stdev = 0.044	**Ave = 4.12;** Stdev = 0.039
	Primary Mass Flow Rate $[\dot{m}]$ $\left(\frac{slug}{s}\right)$	**Ave = 0.00681;** Stdev = 0.000046	**Ave = 0.00647;** Stdev = 0.000062
	Chamber Pressure $[P_c]$ (psi)	**Ave = 102.8;** Stdev = 4.24	**Ave = 95.7;** Stdev = 3.73
	Total Thrust $[F_{tot}]$ (lbf)	**Ave = 8.89;** Stdev = 0.030	**Ave = 8.30;** Stdev = 0.019
	Mixing Duct Thrust $[F_{duct}]$ (lbf)	**Ave = -0.014;** Stdev = 0.002	**Ave = 3.35;** Stdev = 0.022
	Total Specific Impulse $[I_{sp}]$ (s)	**Ave = 40.6;** Stdev = 0.31	**Ave = 39.8;** Stdev = 0.36
Solid Ring	**Test #**		**6cold**
	Mixture Ratio $[r]$ $(unitless)$		**Ave = 4.21;** Stdev = 0.038
	Primary Mass Flow Rate $[\dot{m}]$ $\left(\frac{slug}{s}\right)$		**Ave = 0.00669;** Stdev = 0.000058
	Chamber Pressure $[P_c]$ (psi)		**Ave = 100.4;** Stdev = 3.47
	Total Thrust $[F_{tot}]$ (lbf)		**Ave = 7.91;** Stdev = 0.055
	Mixing Duct Thrust $[F_{duct}]$ (lbf)		**Ave = 4.06;** Stdev = 0.028
	Total Specific Impulse $[I_{sp}]$ (s)		**Ave = 36.7;** Stdev = 0.41
C-Ring	**Test #**		**7cold**
	Mixture Ratio $[r]$ $(unitless)$		**Ave = 4.18;** Stdev = 0.031
	Primary Mass Flow Rate $[\dot{m}]$ $\left(\frac{slug}{s}\right)$		**Ave = 0.00665;** Stdev = 0.000051
	Chamber Pressure $[P_c]$ (psi)		**Ave = 99.7;** Stdev = 3.79
	Total Thrust $[F_{tot}]$ (lbf)		**Ave = 7.77;** Stdev = 0.037
	Mixing Duct Thrust $[F_{duct}]$ (lbf)		**Ave = 3.97;** Stdev = 0.021
	Total Specific Impulse $[I_{sp}]$ (s)		**Ave = 36. 3;** Stdev = 0.34

Table 11: Nominally $400\ psi$ chamber pressure test data.

	Values to report:	No Mixing Duct		Diverging Duct		Short Duct		Long Duct	
No Ring	**Test #**	**1**	**13**	**10**	**22**	**11**	**23**	**12**	**24**
	Mixture Ratio $[r]$ $(unitless)$	**Ave = 0.724;** Stdev = 0.015	**Ave = 0.846;** Stdev = 0.017	**Ave = 0.709;** Stdev = 0.010	**Ave = 0.728;** Stdev = 0.012	**Ave = 0.710;** Stdev = 0.010	**Ave = 0.720;** Stdev = 0.012	**Ave = 0.712;** Stdev = 0.012	**Ave = 0.721;** Stdev = 0.011
	Primary Mass Flow Rate $[\dot{m}]$ $\left(\frac{slug}{s}\right)$	**Ave = 0.00682;** Stdev = 0.00003	**Ave = 0.00670;** Stdev = 0.00002	**Ave = 0.00680;** Stdev = 0.00002	**Ave = 0.00673;** Stdev = 0.00002	**Ave = 0.00682;** Stdev = 0.00002	**Ave = 0.00672;** Stdev = 0.00003	**Ave = 0.00682;** Stdev = 0.00003	**Ave = 0.00674;** Stdev = 0.00003
	Chamber Pressure $[P_c]$ (psi)	**Ave = 391.9;** Stdev = 5.34	**Ave = 418.7;** Stdev = 7.50	**Ave = 385.2;** Stdev = 5.65	**Ave = 394.0;** Stdev = 5.92	**Ave = 385.1;** Stdev = 5.22	**Ave = 391.9;** Stdev = 6.34	**Ave = 383.7;** Stdev = 6.21	**Ave = 389.9;** Stdev = 6.12
	Total Thrust $[F_{tot}]$ (lbf)	**Ave = 36.18;** Stdev = 0.16	**Ave = 38.37;** Stdev = 0.48	**Ave = 34.45;** Stdev = 0.14	**Ave = 35.60;** Stdev = 0.12	**Ave = 34.93;** Stdev = 0.31	**Ave = 35.62;** Stdev = 0.08	**Ave = 35.53;** Stdev = 0.19	**Ave = 35.74;** Stdev = 0.15
	Mixing Duct Thrust $[F_{duct}]$ (lbf)	**Ave = -0.012;** Stdev = 0.002	**Ave = -0.008;** Stdev = 0.030	**Ave = -0.257;** Stdev = 0.024	**Ave = -0.231;** Stdev = 0.023	**Ave = 0.632;** Stdev = 0.061	**Ave = 0.650;** Stdev = 0.017	**Ave = 2.717;** Stdev = 0.377	**Ave = 2.234;** Stdev = 0.235
	Total Specific Impulse $[I_{sp}]$ (s)	**Ave = 163.7;** Stdev = 0.95	**Ave = 175.9;** Stdev = 4.00	**Ave = 156.8;** Stdev = 2.13	**Ave = 163.7;** Stdev = 1.97	**Ave = 159.1;** Stdev = 2.03	**Ave = 164.2;** Stdev = 2.24	**Ave = 161.3;** Stdev = 1.60	**Ave = 164.5;** Stdev = 1.51
Solid Ring	**Test #**	**2**	**14**	**4**	**15**	**3**	**16**	**5**	**17**
	Mixture Ratio $[r]$ $(unitless)$	**Ave = 0.723;** Stdev = 0.012	**Ave = 0.780;** Stdev = 0.011	**Ave = 0.725;** Stdev = 0.012	**Ave = 0.761;** Stdev = 0.010	**Ave = 0.721;** Stdev = 0.013	**Ave = 0.763;** Stdev = 0.012	**Ave = 0.720;** Stdev = 0.009	**Ave = 0.751;** Stdev = 0.011
	Primary Mass Flow Rate $[\dot{m}]$ $\left(\frac{slug}{s}\right)$	**Ave = 0.00680;** Stdev = 0.00002	**Ave = 0.00679;** Stdev = 0.00002	**Ave = 0.00682;** Stdev = 0.00002	**Ave = 0.00681;** Stdev = 0.00002	**Ave = 0.00681;** Stdev = 0.00002	**Ave = 0.00679;** Stdev = 0.00002	**Ave = 0.00682;** Stdev = 0.00002	**Ave = 0.00679;** Stdev = 0.00002
	Chamber Pressure $[P_c]$ (psi)	**Ave = 391.5;** Stdev = 5.80	**Ave = 408.3;** Stdev = 6.30	**Ave = 390.5;** Stdev = 6.06	**Ave = 406.8;** Stdev = 7.05	**Ave = 390.8;** Stdev = 6.78	**Ave = 406.2;** Stdev = 5.71	**Ave = 388.4;** Stdev = 5.45	**Ave = 402. 7;** Stdev = 6.49
	Total Thrust $[F_{tot}]$ (lbf)	**Ave = 35.71;** Stdev = 0.17	**Ave = 37.78;** Stdev = 0.18	**Ave = 34.20;** Stdev = 0.21	**Ave = 35.95;** Stdev = 0.24	**Ave = 35.19;** Stdev = 0.24	**Ave = 36.56;** Stdev = 0.14	**Ave = 34.55;** Stdev = 0.32	**Ave = 36.22;** Stdev = 0.14
	Mixing Duct Thrust $[F_{duct}]$ (lbf)	**Ave = -0.011;** Stdev = 0.003	**Ave = 0.009;** Stdev = 0.003	**Ave = -0.608;** Stdev = 0.036	**Ave = -0.468;** Stdev = 0.033	**Ave = 0.551;** Stdev = 0.030	**Ave = 0.475;** Stdev = 0.017	**Ave = 3.25;** Stdev = 0.301	**Ave = 2.76;** Stdev = 0.153
	Total Specific Impulse $[I_{sp}]$ (s)	**Ave = 162.2;** Stdev = 2.51	**Ave = 172.1;** Stdev = 1.03	**Ave = 154.7;** Stdev = 1.95	**Ave = 163.1;** Stdev = 2.16	**Ave = 159.5;** Stdev = 2.44	**Ave = 166.8;** Stdev = 1.53	**Ave = 157.3;** Stdev = 2.03	**Ave = 165.3;** Stdev = 1.83
C-Ring	**Test #**	**6**	**18**	**8**	**19**	**7**	**20**	**9**	**21**
	Mixture Ratio $[r]$ $(unitless)$	**Ave = 0.718;** Stdev = 0.010	**Ave = 0.749;** Stdev = 0.012	**Ave = 0.715;** Stdev = 0.010	**Ave = 0.741;** Stdev = 0.011	**Ave = 0.715;** Stdev = 0.013	**Ave = 0.742;** Stdev = 0.011	**Ave = 0.715;** Stdev = 0.011	**Ave = 0.738;** Stdev = 0.012
	Primary Mass Flow Rate $[\dot{m}]$ $\left(\frac{slug}{s}\right)$	**Ave = 0.00682;** Stdev = 0.00002	**Ave = 0.00678;** Stdev = 0.00003	**Ave = 0.00682;** Stdev = 0.00002	**Ave = 0.00677;** Stdev = 0.00002	**Ave = 0.00681;** Stdev = 0.00003	**Ave = 0.00675;** Stdev = 0.00002	**Ave = 0.00683;** Stdev = 0.00002	**Ave = 0.00675;** Stdev = 0.00002
	Chamber Pressure $[P_c]$ (psi)	**Ave = 387.9;** Stdev = 6.26	**Ave = 400.7;** Stdev = 6.42	**Ave = 387.4;** Stdev = 5.87	**Ave = 399.9;** Stdev = 5.79	**Ave = 388.7;** Stdev = 5.11	**Ave = 396.9;** Stdev = 6.35	**Ave = 386.2;** Stdev = 6.40	**Ave = 397.0;** Stdev = 4.55
	Total Thrust $[F_{tot}]$ (lbf)	**Ave = 35.33;** Stdev = 0.14	**Ave = 36.21;** Stdev = 0.14	**Ave = 33.80;** Stdev = 0.23	**Ave = 34.76;** Stdev = 0.16	**Ave = 34.74;** Stdev = 0.22	**Ave = 35.39;** Stdev = 0.11	**Ave = 34.46;** Stdev = 0.22	**Ave = 35.39;** Stdev = 0.09
	Mixing Duct Thrust $[F_{duct}]$ (lbf)	**Ave = -0.010;** Stdev = 0.14	**Ave = -0.007;** Stdev = 0.003	**Ave = -0.542;** Stdev = 0.042	**Ave = -0.455;** Stdev = 0.052	**Ave = 0.485;** Stdev = 0.014	**Ave = 0.481;** Stdev = 0.019	**Ave = 3.36;** Stdev = 0.273	**Ave = 2.83;** Stdev = 0.294
	Total Specific Impulse $[I_{sp}]$ (s)	**Ave = 159.8;** Stdev = 2.27	**Ave = 165.6;** Stdev = 1.99	**Ave = 152.3;** Stdev = 3.47	**Ave = 158.9;** Stdev = 2.10	**Ave = 157.2;** Stdev = 2.88	**Ave = 162.3;** Stdev = 1.71	**Ave = 155.2;** Stdev = 3.73	**Ave = 162.5;** Stdev = 1.84

Table 12: Nominally $550\ psi$ chamber pressure test data.

	Values to report:	No Mixing Duct		Diverging Duct		Short Duct		Long Duct	
No Ring	**Test #**	**25**	**40**	**34**	**39**	**35**	**38**	**36**	**37**
	Mixture Ratio $[r]$ $(unitless)$	**Ave = 1.01;** Stdev = 0.010	**Ave = 0.765;** Stdev = 0.005	**Ave = 0.873;** Stdev = 0.005	**Ave = 0.773;** Stdev = 0.008	**Ave = 0.866;** Stdev = 0.007	**Ave = 0.784;** Stdev = 0.007	**Ave = 0.861;** Stdev = 0.006	**Ave = 0.789;** Stdev = 0.007
	Primary Mass Flow Rate $[\dot{m}]$ $\left(\frac{slug}{s}\right)$	**Ave = 0.00839;** Stdev = 0.00002	**Ave = 0.00834;** Stdev = 0.00001	**Ave = 0.00850;** Stdev = 0.00001	**Ave = 0.00838;** Stdev = 0.00002	**Ave = 0.00852;** Stdev = 0.00002	**Ave = 0.00839;** Stdev = 0.00001	**Ave = 0.00845;** Stdev = 0.00002	**Ave = 0.00838;** Stdev = 0.00002
	Chamber Pressure $[P_c]$ (psi)	**Ave = 581.2;** Stdev = 8.12	**Ave = 501.7;** Stdev = 5.48	**Ave = 547.0;** Stdev = 5.19	**Ave = 503.9;** Stdev = 6.58	**Ave = 544.9;** Stdev = 5.70	**Ave = 508.3;** Stdev = 7.14	**Ave = 537.8;** Stdev = 7.79	**Ave = 513.3;** Stdev = 5.12
	Total Thrust $[F_{tot}]$ (lbf)	**Ave = 54.95;** Stdev = 0.23	**Ave = 47.01;** Stdev = 0.15	**Ave = 50.76;** Stdev = 0.13	**Ave = 46.48;** Stdev = 0.24	**Ave = 50.91;** Stdev = 0.14	**Ave = 47.43;** Stdev = 0.11	**Ave = 50.96;** Stdev = 0.21	**Ave = 48.33;** Stdev = 0.18
	Mixing Duct Thrust $[F_{duct}]$ (lbf)	**Ave = -0.011;** Stdev = 0.003	**Ave = -0.031;** Stdev = 0.008	**Ave = -0.250;** Stdev = 0.010	**Ave = -0.349;** Stdev = 0.028	**Ave = 0.725;** Stdev = 0.056	**Ave = 0.696;** Stdev = 0.053	**Ave = 1.927;** Stdev = 0.148	**Ave = 2.618;** Stdev = 0.213
	Total Specific Impulse $[I_{sp}]$ (s)	**Ave = 202.8;** Stdev = 0.66	**Ave = 174.9;** Stdev = 1.41	**Ave = 185.4;** Stdev = 1.01	**Ave = 173.1;** Stdev = 1.23	**Ave = 185.3;** Stdev = 1.03	**Ave = 175.0;** Stdev = 0.74	**Ave = 187.0;** Stdev = 1.51	**Ave = 178.7;** Stdev = 1.04
Solid Ring	**Test #**	**26**	**41**	**31**	**46**	**32**	**47**	**33**	**48**
	Mixture Ratio $[r]$ $(unitless)$	**Ave = 0.968;** Stdev = 0.010	**Ave = 0.761;** Stdev = 0.005	**Ave = 0.931;** Stdev = 0.003	**Ave = 0.887;** Stdev = 0.004	**Ave = 0.892;** Stdev = 0.003	**Ave = 0.883;** Stdev = 0.005	**Ave = 0.884;** Stdev = 0.006	**Ave = 0.881;** Stdev = 0.007
	Primary Mass Flow Rate $[\dot{m}]$ $\left(\frac{slug}{s}\right)$	**Ave = 0.00853;** Stdev = 0.00003	**Ave = 0.00829;** Stdev = 0.00001	**Ave = 0.00855;** Stdev = 0.00002	**Ave = 0.00847;** Stdev = 0.00001	**Ave = 0.00852;** Stdev = 0.00002	**Ave = 0.00844;** Stdev = 0.00001	**Ave = 0.00853;** Stdev = 0.00002	**Ave = 0.00843;** Stdev = 0.00001
	Chamber Pressure $[P_c]$ (psi)	**Ave = 579.3;** Stdev = 7.97	**Ave = 497.0;** Stdev = 4.33	**Ave = 564.8;** Stdev = 8.29	**Ave = 554.4;** Stdev = 7.03	**Ave = 549.4;** Stdev = 7.58	**Ave = 551.4;** Stdev = 7.92	**Ave = 549.9;** Stdev = 6.23	**Ave = 549.1;** Stdev = 8.65
	Total Thrust $[F_{tot}]$ (lbf)	**Ave = 54.30;** Stdev = 0.21	**Ave = 45.76;** Stdev = 0.28	**Ave = 53.11;** Stdev = 0.20	**Ave = 51.55;** Stdev = 0.20	**Ave = 51.36;** Stdev = 0.14	**Ave = 51.58;** Stdev = 0.20	**Ave = 51.36;** Stdev = 0.28	**Ave = 51.46;** Stdev = 0.28
	Mixing Duct Thrust $[F_{duct}]$ (lbf)	**Ave = -0.010;** Stdev = 0.003	**Ave = -0.017;** Stdev = 0.010	**Ave = -0.165;** Stdev = 0.014	**Ave = -0.191;** Stdev = 0.020	**Ave = 0.265;** Stdev = 0.018	**Ave = 0.409;** Stdev = 0.024	**Ave = 2.369;** Stdev = 0.081	**Ave = 2.291;** Stdev = 0.109
	Total Specific Impulse $[I_{sp}]$ (s)	**Ave = 197.1;** Stdev = 2.18	**Ave = 172.4;** Stdev = 1.49	**Ave = 192.2;** Stdev = 2.03	**Ave = 188.4;** Stdev = 0.36	**Ave = 186.7;** Stdev = 0.75	**Ave = 189.0;** Stdev = 0.68	**Ave = 186.7;** Stdev = 1.06	**Ave = 188.7;** Stdev = 1.40
C-Ring	**Test #**	**27**	**42**	**28**	**43**	**29**	**44**	**30**	**45**
	Mixture Ratio $[r]$ $(unitless)$	**Ave = 0.955;** Stdev = 0.003	**Ave = 0.747;** Stdev = 0.009	**Ave = 0.957;** Stdev = 0.006	**Ave = 0.886;** Stdev = 0.003	**Ave = 0.948;** Stdev = 0.004	**Ave = 0.886;** Stdev = 0.005	**Ave = 0.936;** Stdev = 0.006	**Ave = 0.883;** Stdev = 0.006
	Primary Mass Flow Rate $[\dot{m}]$ $\left(\frac{slug}{s}\right)$	**Ave = 0.00854;** Stdev = 0.00003	**Ave = 0.00831;** Stdev = 0.00002	**Ave = 0.00860;** Stdev = 0.00003	**Ave = 0.00845;** Stdev = 0.00001	**Ave = 0.00856;** Stdev = 0.00003	**Ave = 0.00845;** Stdev = 0.00001	**Ave = 0.00859;** Stdev = 0.00002	**Ave = 0.00847;** Stdev = 0.00001
	Chamber Pressure $[P_c]$ (psi)	**Ave = 576.3;** Stdev = 6.13	**Ave = 492.8;** Stdev = 4.56	**Ave = 568.5;** Stdev = 8.96	**Ave = 559.7;** Stdev = 6.71	**Ave = 570.6;** Stdev = 8.20	**Ave = 559.6;** Stdev = 5.44	**Ave = 567.5;** Stdev = 6.92	**Ave = 558.3;** Stdev = 6.18
	Total Thrust $[F_{tot}]$ (lbf)	**Ave = 53.87;** Stdev = 0.16	**Ave = 45.24;** Stdev = 0.32	**Ave = 53.13;** Stdev = 0.14	**Ave = 51.73;** Stdev = 0.15	**Ave = 53.43;** Stdev = 0.17	**Ave = 51.66;** Stdev = 0.20	**Ave = 53.42;** Stdev = 0.19	**Ave = 51.76;** Stdev = 0.24
	Mixing Duct Thrust $[F_{duct}]$ (lbf)	**Ave = -0.013;** Stdev = 0.005	**Ave = -0.020;** Stdev = 0.005	**Ave = -0.184;** Stdev = 0.013	**Ave = -0.167;** Stdev = 0.020	**Ave = 0.393;** Stdev = 0.019	**Ave = 0.383;** Stdev = 0.028	**Ave = 1.85;** Stdev = 0.086	**Ave = 2.31;** Stdev = 0.106
	Total Specific Impulse $[I_{sp}]$ (s)	**Ave = 195.1;** Stdev = 2.34	**Ave = 168.9;** Stdev = 2.25	**Ave = 191.2;** Stdev = 2.08	**Ave = 189.4;** Stdev = 1.07	**Ave = 193.3;** Stdev = 2.17	**Ave = 189.1;** Stdev = 0.61	**Ave = 192.4;** Stdev = 1.81	**Ave = 189.1;** Stdev = 0.43

Table 13: Nominally $680\ psi$ chamber pressure test data.

	Values to report:	No Mixing Duct	Long Duct	
No Ring	**Test #**	**55**	**53**	**54**
	Mixture Ratio $[r]$ $(unitless)$	**Ave = 0.973;** Stdev = 0.006	**Ave = 0.975;** Stdev = 0.016	**Ave = 0.941;** Stdev = 0.010
	Primary Mass Flow Rate $[\dot{m}]$ $\left(\frac{slug}{s}\right)$	**Ave = 0.00995;** Stdev = 0.00001	**Ave = 0.0101;** Stdev = 0.00003	**Ave = 0.0100;** Stdev = 0.00002
	Chamber Pressure $[P_c]$ (psi)	**Ave = 673.5;** Stdev = 5.04	**Ave = 687.3;** Stdev = 6.18	**Ave = 674.7;** Stdev = 6.11
	Total Thrust $[F_{tot}]$ (lbf)	**Ave = 64.83;** Stdev = 0.16	**Ave = 66.16;** Stdev = 0.11	**Ave = 64.79;** Stdev = 0.16
	Mixing Duct Thrust $[F_{duct}]$ (lbf)	**Ave = -0.026;** Stdev = 0.002	**Ave = 1.620;** Stdev = 0.054	**Ave = 1.569;** Stdev = 0.052
	Total Specific Impulse $[I_{sp}]$ (s)	**Ave = 202.7;** Stdev = 0.66	**Ave = 202.8;** Stdev = 1.08	**Ave = 200.8;** Stdev = 1.11
Solid Ring	**Test #**		**51**	**50**
	Mixture Ratio $[r]$ $(unitless)$		**Ave = 0.993;** Stdev = 0.010	**Ave = 0.951;** Stdev = 0.015
	Primary Mass Flow Rate $[\dot{m}]$ $\left(\frac{slug}{s}\right)$		**Ave = 0.0101;** Stdev = 0.00002	**Ave = 0.0100;** Stdev = 0.00003
	Chamber Pressure $[P_c]$ (psi)		**Ave = 696.3;** Stdev = 5.94	**Ave = 678.3;** Stdev = 6.14
	Total Thrust $[F_{tot}]$ (lbf)		**Ave = 65.90;** Stdev = 0.12	**Ave = 64.27;** Stdev = 0.13
	Mixing Duct Thrust $[F_{duct}]$ (lbf)		**Ave = 1.926;** Stdev = 0.073	**Ave = 2.167;** Stdev = 0.060
	Total Specific Impulse $[I_{sp}]$ (s)		**Ave = 201.9;** Stdev = 0.67	**Ave = 199.3;** Stdev = 0.94
C-Ring	**Test #**		**52**	**49**
	Mixture Ratio $[r]$ $(unitless)$		**Ave = 0.984;** Stdev = 0.010	**Ave = 0.952;** Stdev = 0.012
	Primary Mass Flow Rate $[\dot{m}]$ $\left(\frac{slug}{s}\right)$		**Ave = 0.0101;** Stdev = 0.00002	**Ave = 0.0100;** Stdev = 0.00003
	Chamber Pressure $[P_c]$ (psi)		**Ave = 693.2;** Stdev = 5.08	**Ave = 677.3;** Stdev = 5.93
	Total Thrust $[F_{tot}]$ (lbf)		**Ave = 65.28;** Stdev = 0.12	**Ave = 64.75;** Stdev = 0.14
	Mixing Duct Thrust $[F_{duct}]$ (lbf)		**Ave = 1.985;** Stdev = 0.039	**Ave = 2.122;** Stdev = 0.048
	Total Specific Impulse $[I_{sp}]$ (s)		**Ave = 199.8;** Stdev = 0.67	**Ave = 199.8;** Stdev = 0.93

Appendix O: AARLITE Firing

The combustion pressure was approximately 700 psi, no mixing duct, no annular cavity. Beautiful view of the mach diamonds and two testing personel can be seen in the background inside the bullet resistant (perfectly safe) testing control room.